Glycolytic Flux Control of Glyceraldehyde 3-Phosphate Dehydrogenase in Yeast

by

Christoff Odendaal

Thesis presented in partial fulfilment of the requirements for the degree of Master of Science (Biochemistry) in the Faculty of Science at Stellenbosch University

Supervisor: Prof. J.L. Snoep
Co-supervisor: Dr. D.D. Van Niekerk

December 2019

Declaration

By submitting this thesis electronically, I declare that the entirety of the work contained therein is my own, original work, that I am the sole author thereof (save to the extent explicitly otherwise stated), that reproduction and publication thereof by Stellenbosch University will not infringe any third party rights and that I have not previously in its entirety or in part submitted it for obtaining any qualification.

Date: December 2019

Abstract

Glycolytic Flux Control of Glyceraldehyde 3-Phosphate Dehydrogenase in Yeast

J.C.W. Odendaal

Department of Biochemistry,
University of Stellenbosch,
Private Bag X1, Matieland 7602, South Africa.

Thesis: MSc (Biochemistry)

December 2019

To save precious experimental time and resources and to gain a deeper understanding of living systems, modelling approaches and systems biological tools like Metabolic Control Analysis (MCA) offer the opportunity to analyse these systems at the level of integrated reaction networks. These tools can aid in the discovery of promising industrial and pharmaceutical metabolic targets.

In addition, modelling promises to reduce duplication of work by allowing for the integration of existing models into larger networks that have extended predictive capacity. This is known as the modular approach to model construction.

A cornerstone of the modular approach to metabolic modelling is that model expansion increases the predictive abilities of a given model instead of just changing it to describe a new, narrow set of behaviours. Glycolysis - a ubiquitous pathway responsible for glucose catabolism - was probably the first metabolic pathway to be modelled and a history of iterative model expansion is now starting to take shape based on this model.

The model by Teusink *et al.* [1] and its descendent by Du Preez *et al.* [2] are two existing glycolytic models of *Saccharomyces cerevisiae* that represent such an expansion. Du Preez and colleagues adapted the steady-state Teusink model *in silico* to describe glycolytic oscillations. This presents a good opportunity to test whether the adjustment expanded the model's predictive capacity or just changed it to a new, narrow set of behaviours.

Iodoacetic acid (IAA), a specific, irreversible inhibitor of glyceraldehyde 3-phosphate dehydrogenase (GAPDH), was used to perturb yeast glycolysis for the calculation of the glycolytic flux control coefficient of GAPDH. The

ability of the model to correctly predict the flux control of GAPDH would be a validation of the model.

We found that both the Teusink and the Du Preez models predicted the glycolytic control of GAPDH to be close to zero, which was in good agreement with our experimental finding. Furthermore, the models could predict the effect of larger perturbations of GAPDH reasonably well. This finding is also exciting as it validates the usefulness of IAA as a chemical perturbant that can be used to experimentally measure GAPDH's glycolytic flux control, which can be reapplied to other metabolic systems where it might have clinical or industrial significance.

Uittreksel

Glikolise-fluksiekontrole van Gliseraldehied-3-fosfaat-dehidrogenase in Gis

(" Glycolytic Flux Control of Glyceraldehyde 3-Phosphate Dehydrogenase in Yeast")

J.C.W. Odendaal

Departement Biochemie,
Universiteit van Stellenbosch,
Privaatsak X1, Matieland 7602, Suid-Afrika.

Tesis: MSc (Biochemie)

Desember 2019

Om kosbare eksperimentele tyd en hulpbronne te bespaar en om 'n dieper begrip van lewende sisteme te bekom, bied modellering en sisteembiologiese middele die geleentheid om lewende sisteme op die vlak van geïntegreede-reaksienetwerke te analiseer. Dit kan help om belowende nywerheids- en farmaseutiese teikens in die metabolisme uit te lig.

Verder beloof modellering om herhaling van werk te verminder deur vir die integrasie van bestaande modelle in groter netwerke toe te laat - hierdie uitgebreide netwerke het dan ook uitgebreide voorspellingsvermoë. Dit staan bekend as die modulêre benadering tot modelkonstruksie.

'n Hoeksteen van die modulêre benadering to metabolismemodellering is dat modeluitbreiding die voorspellingsvermoë van 'n gegewe model verbeter en nie bloot aanpas tot 'n nuwe, noue stel metaboliese gedrag nie. Glikolise - 'n algemene padweg verantwoordelik vir glukoseafbraak - was waarskynlik die eerste gemodelleerde padweg en 'n geskiedenis van herhaalde modeluitbreiding is aan't groei gebaseer op hierdie padweg..

Die model deur Teusink *et al.* [1] en sy afstammeling deur Du Preez *et al.* [2] is twee bestaande glikolisemodelle van *Saccharomyces cerevisiae* wat só 'n uitbreiding verteenwoordig. Du Preez en kollegas het die bestendige-toestand-model deur Teusink aangepas *in silico* om glikolitiese ossillasies te kan beskryf. Dit bied 'n goeie geleentheid vir 'n toets: is die model se voorspellingsvermoë uitgebrei, of bloot verstel na 'n nuwe, noue gedragsrepertoire?

Jodoasynsuur (IAA), 'n spesifieke, onomkeerbare inhibitor van gliseraldehied-3-fosfaat dehidrogenase (GAPDH), is gebruik om gisglikolise te perturbeer vir die berekening van die glikoliseﬂuksie-kontrokontolekoëffisiënt van GAPDH. Die vermoë om die fluksiekontrole van GAPDH akkuraat te voorspel, sal 'n validering van die model wees.

Ons het bevind dat beide die Teusink- and die Du Preez-modelle voorspel het dat die glikolisekontrole van GAPDH byna nul is, wat goed met ons eksperimentele data ooreenstem. Verder, kon die modelle die effek van groter perturbasies van GAPDH-aktiwiteit redelik goed voorspel. Dit is 'n belowende bevinding, want dit valideer ook die nut van IAA as 'n chemiese perturbasiemiddel wat eksperimenteel aangewend kan word om GAPDH se glikolitieseﬂuksie-beheer te bepaal. Dít kan nou gebruik word in ander metaboliese stelsels wat van kliniese of industriële belang is.

Acknowledgements

I would like to express my sincere gratitude to the following people and organisations:

The *National Research Foundation (NRF)* and the *South African Centre for Epidemiological Modelling and Analysis (SACEMA)*, whose financial contributions directly and indirectly have made all of my work possible.

The Molecular Systems Biology Group, Stellenbosch University. Specifically,

Mr Arrie Arends,

Prof. Jacky Snoep,

Dr Dawie van Niekerk,

Clara van Schalkwyk, who shared a project with me for two years,

Stefan Kühn, *Cobus van Dyk*, *Klarissa Shaw*, and *Dr Theresa Kouril*, who all contributed to this project in their various capacities, be it fruitful conversation or working their magic in the lab,

and *Julian Wissing*, who was a great source of support in this undertaking.

My Parents, *Hanli* and *Bernard Odendaal*, without whom none of this would be possible.

Finally, my beloved *Jana van Schalkwyk*, my constant source of inspiration.

Dedications

Hierdie tesis word opgedra aan my ouers, Hanli en Bernard, sonder wie se ondersteuning niks hiervan moontlik sou wees nie
&
My geliefde Jana, wat altyd 'n groter bron van hoop is as wat sy besef
&
Mevrou Nolingo Lisa Glass, met wie ek hierdie so graag sou deel.

Contents

List of Figures

List of Tables

Nomenclature

Enzymes

ADH	alcohol dehydrogenase
GTr	glucose transporter
$GAPDH$	glyceraldehyde 3-phosphate dehydrogenase
PGK	phosphoglycerate kinase

Metabolites

ADP	adenosine diphosphate
AMP	adenosine monophosphate
ATP	adenosine triphosphate
$DHAP$	dihydroxy acetone phosphate
$ETOH$	ethanol
$ETOHo$	extracellular ethanol
GAP	glyceraldehyde 3-phosphate
GLC	glucose
$GLCo$	extracellular glucose
NAD^+	nicotinamide adenine dinucleotide (oxidised)
$NADH$	nicotinamide adenine dinucleotide (reduced)
P_i	inorganic phosphate
PGA	phosphoglyceric acid

Enzyme Kinetics

K_{eq}	equilibrium constant
K_i	dissociation constant of a ligand, i
K_m	Michaelis constant (substrate concentration at half-maximal reaction rate)
v_i	reaction rate through enzyme i
V_{max}	maximal rate of an enzyme-catalysed reaction

Metabolic Control Analysis

$C^J_{v_i}$	control coefficient of reaction rate v_i (catalysed by an enzyme, i) over the flux, J, through a pathway
$\epsilon^{v_i}_{x_j}$	elasticity coefficient of the reaction between enzyme i (v_i) and a change in the concentration of effector j of magnitude x_j
J_{v_i}	steady-state flux through the enzyme, i
$R^J_{x_j}$	response coefficient of flux, J, due to a concentration change of effector j of magnitude x_j.

General

DTT	dithiothreitol
IAA	iodoacetic acid
λ	wavelength of light
OD_x	optical density at a wavelength of x
P_x	permeability constant of a substance, x, across a membrane
R^2	coefficient of determination (goodness-of-fit metric)

Chapter 1

Introduction

Computational models offer biologists the ability to integrate component-level knowledge into networks, elucidating systemic properties that might otherwise have been hidden from view [4]. Metabolic models, especially, show promise as helpful research tools, given that metabolic enzymes are readily isolated and characterised, and that high flux rates are seen *in vivo* - these properties allow us to easily measure their activity in the laboratory [5].

Glycolysis occupies a particularly relevant position within metabolism, given its ubiquity and its position as the initial pathway in carbohydrate catabolism in most organisms [6]. Accurate kinetic models of glycolysis have historically been very important to the endeavour of molecular systems biology as a model pathway for the development of the theoretical tools for bottom-up systems biology: for instance, it was probably the first pathway to be kinetically modelled [7] and the whole framework of Metabolic Control Analysis (MCA) has, in large part, red blood-cell glycolysis to thank for its existence [8].

Beyond its status as a model pathway, a better understanding of glycolysis also has many important practical implications, for instance as the industrially important pathway in alcoholic fermentation [9], and as drug target in the blood-borne stages of *Plasmodium falciparum* (the causal agent of malaria; 10) and *Tryposonoma brucei* (responsible for African sleeping sickness; 11).

A major use of kinetic modelling and analysis tools, like MCA, is to direct research and to avoid wasteful experimenting by, for instance, indicating where to intervene in the metabolic network of a pathogen [12]. Fundamental to the success of these predictions, is having models that are valid descriptors of metabolism in the relevant cell, pathogenic or otherwise.

The process of validating computational models - within the Silicon Cell paradigm [13] - lies beyond just investigating a model's ability to simulate the behaviour on which it was trained [14]. It is important that models are tested for their ability to predict behaviour that they have not seen before, so that "model construction and validation are completely separate" [5].

To avoid unnecessary duplication of modelling work, it is important to

construct models that are re-usable, accurate representations of what is truly happening in a cell. One of the advantages of re-using models is that the process of adjusting them to new behaviours allows one to refine and improve them with each new study, leading to complementary instead of duplicative work [13]. The alternative is the construction of very specific models that predict only a narrow range of behaviour for a particular organism at particular conditions, which - even though this approach might be useful in certain circumstances - would exponentially increase the amount of modelling work that must be done [15].

One attempt to not duplicate glycolytic modelling work but rather to iteratively refine an existing model, was the work of Du Preez *et al.* [2] on glycolytic oscillations. They computationally adjusted an existing model of glycolysis in *S. cerevisiae* which was originally constructed to predict steady-state behaviour [1]. The adjusted model was then validated for its ability to predict glycolytic oscillatory behaviour, implicitly verifying the original model as flexible enough to describe at least one qualitatively new behaviour without the need for complete re-parameterisation.

One of the ways of determining how accurate the models are, is to test their ability to make correct predictions about metabolic behaviour to which they have not been exposed before [16]. Core predictions (predictions that implicate not just a single parameter but the entire set of parameters in a model) are a powerful way of doing this [17]. Usually, models are adjusted to predict the new behaviour, as was the case for Du Preez *et al.* [2]. If the process of model expansion is carried out according to the Silicon Cell approach, each new iteration of the model should improve on the ability of the original to describe *in vivo* behaviour [18].

It is important, however, that the expansion of a model's predictive capacity does not strip the original model of its ability to predict the behaviours for which it was designed - doing that would amount to the same duplicative, *ad hoc* modelling approach that bottom-up systems biology strives to avoid [15]. It is important that models, through the process of refinement, retain some important network characteristics that relate the individual enzyme to each other.

MCA offers a good framework for testing this. MCA allows systems biologists to link observed systems-level metabolic phenomena directly to component-level reactions [19]. The flux control coefficient, for instance, quantifies the importance of a single step in maintaining the flux through a pathway. The summation theorem - which states that all of the metabolic flux control coefficients have a additive value of 1 - necessarily implicates the entire pathway in a prediction about the flux control of a single step [20], rendering it an effective core prediction for testing model validity [17].

In this study, we wanted to test whether the model by Du Preez *et al.* [2] retained (or improved on) the ability of the original Teusink *et al.* [1] model to predict the control of GAPDH over glycolytic flux. We used a

specific, irreversible inhibitor of glyceraldehyde 3-phosphate dehydrogenase (GAPDH) to determine the glycolytic flux control coefficient of GAPDH in Baker's yeast. Iodoacetic acid (IAA) - known as one of the classical examples of specific and irreversible enzyme inhibition [21–24] - allows us to incrementally inhibit GAPDH activity. The relative change in flux over the relative change in GAPDH activity is the flux control of GAPDH [25].

Beyond this, the irreversibility of IAA offers another opportunity. If an inhibitor is administered to whole-cells and cell-free extract separately, the observed inhibition might be confounded by additional unknowns, e.g. the differences in intracellular availability of the inhibitor to the enzyme [26]. Since we lack clear kinetics describing this disparity, model simulations cannot be adjusted to compensated for this difference. An irreversible inhibitor, however, allows one to expose whole-cells to IAA and to use those same cells for flux measurements and for making cell-free extract for enzyme activity measurement. This hypothetically eliminates disparities in inhibitor availability between flux and enzyme activity data.

The aims (each with their objectives sub-listed below them) of this study were:

1. Optimise IAA administration conditions and method
    a) confirm the irreversibility of IAA
    b) determine the difference in measured activity in prelytically inhibited cell-free extract *versus* extract that received IAA *in vitro*
    c) test whether differences in intracellular en cell-extract redox conditions can account for any disparities in measured activity
2. Experimentally determine the glycolytic flux control of GAPDH
    a) independently measure the effect of a IAA titration on GAPDH activity and glycolytic flux in yeast
    b) determine the glycolytic flux control coefficient of GAPDH at [IAA] = 0 μM
3. Analyse Du Preez and Teusink models for GAPDH flux control predictions
    a) adapt both models to simulate the conditions and the inhibition mechanism used in the experiments
    b) calculate glycolytic flux control of GAPDH as the relative inhibition of glycolytic flux as a fraction of relative inhibition of GAPDH
    c) compare the flux control predictions of both models to each other and to the experimental data

The aims listed above were constructed to test hypotheses about IAA as a useful chemical perturbant for flux control coefficient calculation, and on the success of Du Preez *et al.* [2] in their model expansion. The hypotheses tested, in summary, will be:

- incubating cells in IAA before cell lysis allows the experimenter to disregard the unknown variables contributing to IAA availability involved when comparing flux perturbations and GAPDH activity perturbations;
- the Du Preez and Teusink models both accurately predict the glycolytic flux control that is seen experimentally;
- [2] succeeded in refining the Teusink model [1] for description of glycolytic oscillations without seriously compromising its predictive ability with regards to steady-state flux control.

Chapter 2

Literature Review

2.1 What Does Systems Biology Do?

Systems biology aspires to understand how the interaction of molecules inside cells can give rise to phenomena like metabolic rhythms, drug resistance, and coordinated behaviour [27]. Understanding living organisms at this level would open doors to several medical and biotechnological possibilities: the cell that is understood at the molecular level can, potentially, also be manipulated at the molecular level [28]. To understand systems at this level, however, large amounts of reaction-level data need to be integrated: data which, for the best part of the history of molecular biology, were arduous to come by [4].

The past quarter century, however, has seen a rapid expansion in the data-generating capacity of molecular biology. The first fully sequenced genome - that of the bacterium *Haemophilus influenzae* [29] - marked a leap forward in our analytical abilities, culminating quickly in the complete sequencing of the human genome in 2001 [30]. Long-standing investigations into other levels of cellular organisation and function soon underwent accelerations of their own, e.g. with the developments in proteomics [31], metabolomics [32], and fluxomics [28].

The emergence of high-throughput experimental techniques have made molecular biology a data-rich field. This has necessitated a move towards modelling, theory, and simulation to make sense of the rapidly growing pool of knowledge [4]. These modelling approaches can save valuable laboratory time and resources (e.g. 33) and hold much promise as tools for accelerating the discovery of mechanisms in cell functioning that can be engineered for the benefit of humankind. Flux and concentration control distributions (see Section 2.3), for instance, pinpoint targets that can be of medical value (as potential drug targets in parasites and tumour cells) and of industrial value (as control mechanisms to yield economically valuable metabolites more quickly and in greater volumes; 25).

As it currently stands, modelling approaches can be loosely divided into

the "top-down" and the "bottom-up" sort [4]. Both approaches provide a means of integrating knowledge about biochemical components and their structures, interactions, and functions, with a spatio-temporal description of their behaviour. Top-down modelling (also known as "inverse modelling"; 26) starts at the phenomenological level and attempts to infer responsible mechanisms lower down in the causal chain. In contrast to this, bottom-up modelling (or "forward modelling") tries to deductively infer functional properties from detailed mechanistic descriptions of biochemical components and their interactions [15].

Despite its labour-intensiveness and intolerance to unknowns, bottom-up modelling is a powerful approach in that detailed knowledge about the mechanistic properties of a system are the point of departure. Systemic properties are then predicted from what is discovered about the building blocks and their interactions, clearly linking the physiological phenomenology to defined molecular mechanisms [34]. Top-down modelling, if left entirely to its own devices, runs the risk of inventing parameter sets that perfectly describe emergent phenomena under very specific conditions but translate not at all to other milieus, resulting in a form of biological "stamp collecting" [15].

Another drawback of top-down models is that they are often very small (due to the challenge of independently perturbing intracellular conditions) and that the limited range of perturbations leads to very similar model construction and validation data-sets - begging the question: "What is being validated?". (16; also see Subsection 2.2.2 for more on model validation). The focus of systems biology, after all, is not on merely being descriptive of biological systems at given conditions but on allowing extrapolation to general principles and qualitatively different behaviours [4]. Computational models based on detailed mechanistic data are very useful in this regard, insofar as they serve not only as an end point for model construction studies but often also as sources of testable hypotheses for subsequent investigations [15]. Beyond that, an integrative and iterative modelling approach has been shown to be a valuable quality control tool for experimental data: an advantage that is unavailable to purely experimental studies [35]. Such models then also have the advantage of being available for integration into models of larger networks [13], as described in Subsection 2.2.1.

2.2 The Silicon Cell

"Bioinformatic and computational approaches offer a means of obtaining full value from experimentally acquired data, extending their interpretation, suggesting novel hypotheses for future experiments, and guiding the experimentalist towards potentially rewarding investigations but away from likely fruitless ones" - Pritchard and Kell [33].

2.2.1 Parameterising the Silicon Cell

The Silicon Cell initiative [5] aspires to create ever more inclusive replicas of cellular systems based on detailed reaction kinetics. It builds on the idea of bottom-up modelling [26] in that it is aimed at describing the "whole" (metabolic phenotypes) by independently specifying the properties of the "parts" (enzyme kinetics). The holy grail of this project is the eventual construction of an accurate computational simulation of an organism's complete inner workings from accumulated experimentally determined parameters [36]. Even if completion is not attainable, however, incremental progress towards more and more comprehensive dynamic descriptions of biological function provides a useful way of summarizing the "state of the art" [27]. Models that are incomplete or not fully correct, mechanistically speaking, can still have valuable predictive power: this predictive ability constitutes the intermediate milestones on the way to the Silicon Cell [37].

Because of the number of individual reactions that constitute a cell's behaviour at a given metabolic state, individual research groups can, realistically, only study small subsets of reactions at a time [13]. As complex behaviours can often arise from collections of simple parts interacting non-linearly, the impact of the parameters of a system can lead to non-obvious system behaviour [38]. The independent measurement of *in vitro* enzyme kinetics under standardised conditions is suggested to avoid interpretive bias until the system is assembled [1].

Morohashi *et al.* [39] define two types of parameter: (A) those that vary within an organism over the duration of its lifetime (e.g. regulated gene-activity level, temperature, substrate and product concentrations) and (B) those that remain constant within an organism but vary across individuals or species (e.g. reaction rate constants). Parameters from class (B) are the constants that are sought during parameterisation studies.

What do these parameters mean, however? It is very important, when building a model, to choose the right level of detail at which to describe the system. Top-down modelling approaches might infer phenomenological descriptions (e.g. parameters that describe the collective behaviour of sets of reactions as a single value) [15], while the bottom-up approach to metabolic modelling requires more mechanistic parameters (i.e. parameters describing actual physico-chemical properties of an enzyme).

Simplified, phenomenological descriptors of system behaviour often lead to a restricted range of applicability, describing a property of an enzyme that is only relevant under, for instance, starvation conditions, and is actually a product of more fundamental, mechanistic characteristics [26]; detailed, mechanistic parameters, on the other hand, are often experimentally inaccessible or excessively laborious to measure [10].

Phenomenological approximations of enzymatic properties provide a useful way of circumventing overly stringent reductionistic requirements while still

translating well between varying research questions [26]. "Convenience kinetics", for instance, offers a biochemically justified way of approximating mechanistic properties of enzymatic reactions when binding order is inconsequential [40], while Rohwer *et al.* [41] posit a generic bi-substrate rate equation with fewer, more easily determinable parameters but which still have operational meaning.

Parameterisation approaches are also being facilitated by the development of software tools for simulation and modelling. As the field of systems biology matures, tools like these are becoming increasingly available: COPASI (COmplex PAthway SImulator; 42), for instance, a biochemical simulator, offers a user friendly parameter estimation functionality, which can accelerate the process of determining, from experimental data, the Michaelis-Menten parameters that form a part of many kinetic models (e.g. [1]).

Phenomenological approximations are useful and biochemically meaningful descriptions of enzyme responses to changes in substrate and product concentrations [41]. These parameters might not, however, be direct descriptions of an enzyme's mechanistic properties and might be subject to change based on variations in their environment, such as pH and temperature [6], ambient nutrient availability [43], or less intuitive intracellular factors like macromolecular crowding [44]. Standardised conditions for determining these parameters are, therefore, indispensable: differences in ambient conditions may well lead to discrepancies in the behaviour of different enzymes in a single model, or to disparity between different models of the same system [45].

Beyond standardisation, however, it is also necessary that the measured *in vitro* parameters are valid descriptions of the *in vivo* properties of a cell. The inside of a cell is a very complex environment, however: beyond the hundreds of metabolites, the cytosol of an organism is occupied by a variety of proteins, long-chain carbohydrates, nucleic acids, and much more [46]. García-Contreras *et al.* [46] stated that mimicking the intracellular environment exactly would be "very difficult, if not impossible", confirming the need for an approximation of the intracellular environment. Pragmatically, therefore, physiological buffers are always inexact replications of the intracellular environment but parameterisation studies in these buffers have yielded encouraging predictions of *in vivo* phenomena so far [3, 46]. The use of physiological buffer conditions then has the added advantage that models constructed in an *in vivo*-like, standardised buffer can be reapplied to different contexts and in describing behaviours that is has not seen before, e.g. [2].

A further goal of the Silicon Cell project and advantage of paramaterisation in physiologically accurate buffers, is to allow for later integration of models: both vertical merging (the integration of models at different levels of organisation, e.g. the combined expression of genetics and kinetics by Bruck *et al.* [47]) and horizontal merging (integration of adjacent pathways to increase the coverage of a model, e.g. the integration of a glycolytic and two branching pathways in yeast by Snoep *et al.* [13]) will form part of this modular model

expansion [37].

Integration exposes the models to more opportunity for the effect of erroneous parameters to be magnified by an expanded interconnectivity [15]. If properties of enzymes are described accurately by parameters, however, there is no reason why models should not be re-usable or integratable [16]. This further justifies the requirement for the standardisation of experimental conditions so that the integrated models have parameters sets that were measured in similar buffer conditions, so the relationship between adjacent parts of an integrated metabolic model are not an artefact of differences in assay buffer [13]. Bruck *et al.* [47], for instance, incorporated transcriptional regulation into a computational model of yeast glycolysis [1]. The expanded model did manage to more closely predict experimental results but still failed to accurately simulate them in many ways. Since the experimental conditions used for the determination of the kinetic parameters of the original model differed from those used for determination of adjusted parameters for the new study, fitting had to be used to find parameters that could otherwise have been empirically determined [47]; this potentially hid the scrutinising effect of model integration.

2.2.1.1 Model Management as a Path to the Silicon Cell

Beyond the construction of models using standardised experimental conditions and the need for the standardised conditions to reflect, as closely as possible, the *in vivo* conditions of the cells, standardised model description and central accessibility are also necessary steps towards the construction of the Silicon Cell [5]. Efforts at model management hope to reduce duplicative work by curating models, ensuring that they have been properly validated, and presenting them in a centrally available database. CellML [48] and SBML [49] are examples of standardised model description formats that allow for better collaboration by presenting models in an accessible way. In addition, a group of systems biologists proposed, in 2005, a set of annotation criteria (MIRIAM: "minimum information requested in the annotation of biochemical models"; 50) which ensure that network components and properties are defined consistently and in a machine-readable format. Presentation of models in recognised formats according to accepted annotation criteria allows for greater ease of use: for example, the modelling and simulation tool COPASI [42] allows users to analyse models that are available in the SBML format much more conveniently.

Biomodels [50] and JWS Online [51] are examples of curated model repositories that aim to make them centrally available. JWS Online, for instance, provides an on-line interface on which users can interact with existing, curated models. Beyond the avoidance of duplication, such central repositories also provide the opportunity to identify models describing adjacent subsets of

reactions. These models can then be linked, in line with the aspiration of the Silicon Cell project's modular approach [13].

2.2.2 Validating the Silicon Cell

As smaller models are integrated into ever more complete networks, parameters will often have to be refitted to reconcile strain or other experimental differences, (e.g. Bruck *et al.* 47 nneded to refit many parameters to be able to combine the gene expression and flux data from the work of Wiebe *et al.* [52] with the parameters from the Teusink model [1]). This might amplify the uncertainty in the parameters that were hidden in the smaller models (see Subsection 2.2.1). Mechanistic models that are interrogated in isolation may very well survive scrutiny as some level of fitting or assumption is usually required; however as models are expanded and integrated (eventually intending to include all of the the almost 2000 reactions in the yeast metabolome 53), incorrect parameter sets will - while hiding in plain site - fail to describe new levels of complexity [15]. Expanded models might also necessitate a reintepretation of the original model construction data in the light of new observations [37]: this is a natural part of model integration and refinement and will require more credible and more sophisticated model recalibration and validation tools.

Traditionally, validation studies have focused on the identification of biologically plausible parameter sets for which experimental observations and model simulations match [14]. For instance, the ability of a model to predict the steady-state fluxes when provided only with initial rate kinetics is seen as good initial evidence of model validity [10]. As quantitative models grow in scope and in complexity, however, the possible parameter space of more models will become large enough to contain multiple plausible parameter combinations with conceptually irreconcilable implications [14]. Parameter estimation strategies, furthermore, open up the risk of disguising gaps in our knowledge by fitting incorrect parameters that cover up anomalies - a phenomenon known as "over-fitting" [15].

Most validation assays look for consistency between model predictions and observed systemic behaviour [54]. Model predictions can take various shapes, from single-value predictions of variables to so-called "core predictions" [17]. Single-variable predictions can confirm the parameter values associated with single nodes or edges in the modelled network. Comparing these predictions to experimental data can be strong validations of single parameter values, but would impose an impractical experimental burden on researchers. Core predictions, on the other hand, implicate the full range of parameters and constitute a much more general validation or invalidation of a proposed computational model [17]. Since models are inherently an attempt to "zoom out" from a component-level view to a systems-level view, the ultimate test of a model lies in evaluating its ability to provide a higher-level perspective

on a problem [38], rather than in independent confirmation of each individual predicted variable.

Core predictions can be tested by presenting a model with data that is qualitatively different from the "training data" used during construction: for instance, metabolic behaviour that it has not seen before [16]. This addresses the blind spot of over-fitting as it presents the model with phenomena to which it could not have been artificially adjusted. In this way, the construction and validation of the model are kept separate in a very strict sense [5]. The ultimate result of such an attempted validation can form a useful part of the model development cycle, as - in the absence of total invalidation or confirmation of the proposed model - useful refinements can be suggested [18].

In principle, it is impossible to fully verify a model, as this would require independent confirmation of each one of its possible predictions and invalidation of each possible alternative set of biochemically plausible parameters [54]. Cvijovic *et al.* [37] stress the importance of making optimal use of the available data since "empirical data will [n]ever cover the entire possible state space". To To address this issue, tests of model validity are constructed as *invalidation* assays, aimed at identifying experimental data that an inaccurate model could not have predicted by chance [18]. Combined with the use of core predictions that implicate more than a single parameter, this type of validation assay is much more feasible for systems biologists to implement. Each failed attempt at *invalidation* adds to the credibility of a model [18].

Du Preez *et al.*'s repurposing [2] of an established model to describe an unfamiliar behaviour (glycolytic oscillations in *S. cerevisiae*), is an example of a core prediction about the original model's flexibility: it posed the question whether relatively minimal changes in the original parameter values could be applied to describe qualitatively novel behaviour. The original model [1] could be minimally adjusted to describe an entirely new behaviour - strong evidence for the validity of the calculated parameters (see Sub-subsection 2.2.4.2).

2.2.3 Glycolysis *in silico*

Evolving experimental repertoires and analytic techniques are allowing ever greater forays to be made into bottom-up modelling of a variety of cellular processes, from signal transduction networks operating in human cancer cells [55] to autophagosome flux in murine liver cells [56]. These advances will, without a doubt, open up more avenues for integration across different modelled cell functions. Metabolic networks, however, remain by far the easiest networks to study, owing to ease with which their enzymes are isolatable and characterisable, and exhibit high flux *in vivo* [13].

Amongst these metabolic networks, glycolysis ranks as the classic example of a biochemical pathway. Its near-universality and long history of being studied [6] have made glycolysis an ideal candidate for some of the earliest

attempts at computationally modelling metabolic flux. The first iteration of this probably saw the light of day in the early 1960s with the work of Chance *et al.* [7]. Some other early pioneers, Heinrich *et al.* [8], did seminal work in the construction of a kinetic model of red blood-cell glycolysis, on which they would base their work on Metabolic Control Analysis (see Section 2.3).

Despite almost 70 years of research, much remains to be discovered about glycolysis [57]. In keeping with its significance as a model pathway for biochemists, glycolysis has led to a number of detailed, kinetic models in the spirit of the Silicon Cell (see 5) which have tried to make sense of the complexity of glycolytic flux in multiple contexts. This central pathway in the breakdown of glucose is embedded in a complex network of regulatory pathways, and feedback and -forward loops [58], the modelling of which has been a staple of molecular systems biology over the past two decades.

The work of Bakker *et al.* [11], for instance, on the pathogen responsible for African sleeping sickness in humans and nagana in animals, *Trypsonoma brucei*, yielded a kinetic model of glycolysis which held up well when tested for its ability to predict steady-state behaviour (11, 59). This model of the slender, blood-borne form of the parasite has undergone multiple subsequent updates (59–61) and serves as an example of model re-use and iterative expansion - an embodiment of the Silicon Cell approach [5]. This model and its descendants will, for simplicity, not be discussed in detail but will collectively be referred to as the *Bakker model*. Important to mention, however, is that the bloodstream-inhabiting phase of this parasite has no Krebs cycle, oxidative phosphorylation, or carbohydrate-storage abilities and is killed by a 50% inhibition of its glycolytic flux [34]. This makes the Bakker model not only valuable as an object of academic interest, but as a promising route to drug-target identification.

The glycolytic pathway of *Plasmodium falciparum*, the causal agent of malaria, was also kinetically modelled [10]. The central carbon metabolism of the asexual, blood-borne phase of this organism consists only of glycolysis and a low-flux pentose-phosphate pathway [62]. Intraerythrocytic *P. falciparum* relies on glycolysis for ATP production [63] and does not have any carbon stores [62]. Simulations of steady state fluxes made using this model - henceforward referred to as the *Penkler model* - also proved surprisingly robust under experimental interrogation (10, 64). Multiple potential drug targets were uncovered, with the glucose transporter being the most potent target suggested, as experimentally validated in a subsequent study [64].

2.2.4 The Silicon Yeast Cell

For largely economic reasons, Baker's yeast (*Saccharomyces cerevisiae*) glycolysis has been the subject of scientific study for over a century [33]. This organism has been the model for a number of systems biological studies that hope to standardise the tool kit for use in other organisms, for instance being

the first subject for a consensus metabolic network reconstruction [53]. Yeast was specifically chosen due to its long history of being studied and the fact that its metabolic network is relatively well characterised. In its glycolysis, all of the enzymes are localised in a single compartment and have been functionally and structurally characterised [1], providing present-day researchers with a sturdy foundation of knowledge to inform further investigations. For the systems biologist interested in glycolysis, this advantage extends further to the history of models and model refinements available for *S. cerevisiae*: multiple models of yeast glycolysis have now been constructed (e.g. the models of Hynne *et al.* 65 and Teusink *et al.* 1) and can serve as the point of departure for comparative studies.

2.2.4.1 The Teusink model

Teusink *et al.* [1] addressed a central question of biochemistry: do *in vitro* kinetics suffice to describe and explain *in vivo* behaviour? To answer this question, a kinetic model based on *in vitro* experimental data was constructed without artificially fitting parameters to *in vivo* data. After model construction, an analysis was done to determine the minimum parameter adjustment that would be necessary to predict a steady-state fluxes and metabolite concentrations. All but three of the *in vivo* steady-state metabolite concentrations were predicted to within a factor of two and about half of the enzymes. V_{max} values needed adjustment (all adjustments smaller than a factor of two) to accurately predict the *in vivo* fluxes. For the majority of the concentrations and fluxes that weren't accurately predicted, suggestions could be made about how to subsequently resolve the discrepancy [1].

Subsequent iterations of the model have yielded insight into its usefulness as a starting point for studies of yeast glycolysis. For example, Bruck *et al.* [47] attempted, with some success, to test whether the inclusion of enzyme expression data (which is subsumed under V_{max}) could predict glycolytic flux at changing oxygenation conditions; additionally, Pritchard and Kell [33] simulated various alternative combinations of V_{max} values and calculated, by simulation, how changes in the rate-limits (V_{max} values) of the enzymes (which is a proxy for transcriptional up- or down-regulation) would redistribute flux control.

The original model, on which the subsequent studies were based, will be referred to as the *Teusink model* and will be regarded as an initial attempt at describing systemic behaviour in yeast glycolysis in terms of *in vitro* kinetics.

2.2.4.2 The Du Preez model

Du Preez *et al.* [2] constructed a new model, based on the work of Teusink *et al.* [1], wherein the original model was adapted to predict qualitatively different behaviour: glycolytic oscillations. Glycolytic oscillations

are repetitive fluctuations in glycolytic metabolite concentrations and reaction rates, classically observed in Baker's yeast [66].

The overarching goal of the work was to explore the potential of re-using an existing kinetic models to predict behaviour which it was not originally trained to predict (Subsection 2.2.2). To this end, a stepwise adjustment of the Teusink model was undertaken [2]:

1. first, the Teusink model was adapted to express of the trehalose and glycogen synthesis branches in terms of mass-action kinetics instead of fixed fluxes. Additionally, they rewrote adenylate kinase using rapid mass-action kinetics in lieu of the existing equilibrium assumption of the Teusink model. Adenosine phosphates were expressed not as a single variable but explicitly as ATP and AMP, with ADP calculated by means of a moiety conservation ratio; ATPase was also rewritten with saturation kinetics instead of linear kinetics. This was a key change in the computational simulation of glycolytic oscillations [2]. Glycerol 3-phosphate (G3P) formation was explicitly modelled as an intermediate step between dihydroxy acetone-phosphate (DHAP, expressed in the model as part of a triose phosphate pool, together with GAP) and glycerol. Finally, Du Preez and colleagues also included an acetaldehyde transport step. None of these structural adjustments altered the steady-state fluxes by more than a factor of 1.4% (*dupreez1)*;

2. next, a search algorithm looked for the minimal adjustments that are needed to be made to the V_{max} values for oscillations to be simulated (*dupreez2*);

3. then the model's V_{max} values and some K_m values were adjusted to yield oscillations that were similar in phase and amplitude to experimentally observed oscillations of a yeast X2180 strain; all parameters (except for the glycerol synthesis branch) were adjusted by factors of between 0.6 and 1.4 (*dupreez3*);

4. finally, the inclusion of biomass terms and terms allowing for synchronisation of oscillations (e.g. acetaldehyde export and removal) yielded *dupreez4*, which was used in the present study.

Earlier iterations of the model by Du Preez *et al.* [2] could qualitatively predict glycolytic oscillations without having ever seen glycolytic oscillations before (*dupreez2*) and could describe them quite accurately after exposure to a small set of training data (*dupreez3*). On top of this, the training data for parameter recalibrations were from a different strain of yeast (X2180) than what was used for the construction of the Teusink model (Koningsgist from DSM Bakery Ingredients, Heerlen, The Netherlands). It is informative to note that the changes necessary to get from the Teusink model to *dupreez4* (which

will be referred to as the *Du Preez model*, for simplicity) included a considerable downward adjustment of most of the V_{max} values of the Teusink model, among others lowering the V_{max} of glyceraldehyde 3-phosphate dehydrogenase (GAPDH) by a factor of four. These changes are relatively small, however, if the lower temperature of the oscillation experiments for the construction of the *dupreez3* model are considered: a difference of about 10°C would lead to a lower measured *in vitro* activity [2].

An additional set of validation experiments were performed by simulating oscillatory behaviour in a variety of different contexts and comparing the model predictions to experimental observations [16, 67]. Further derivatives of the *dupreez4* model (named *dupreez5* to *7* and *gustavsson1* to *4*) - in which the experimental conditions of the assays were mimicked (by, for instance, removing the transport steps for cell-free extract) were able to successfully predict systemic behaviour for a number of oscillation-related phenotypes. These results all confer a relatively high degree of confidence on the Du Preez model.

Having been adjusted and reconfigured to describe the behaviour of a new strain of yeast (X2180, as opposed to Koningsgist) at new experimental conditions, it should be interesting to investigate to what degree the two models predict similar systemic properties. The summation theorems suggest that the recalibration of the V_{max} values to scale the magnitude of the oscillations to fit experimental data would not change systemic phenotypes [16]. Since, however, parameters were changed asymmetrically, and the structure of the network was adjusted at some sites, systemic behaviour cannot be concluded to remain unaltered without experimental confirmation.

Glycolysis in *S. cerevisiae*, though subject to inter-strain variation in enzyme expression [68], has a consistent layout and stoichiometry for the two strains concerned in this study (X2180 and Koningsgist; [1, 2]). The parameter scan by Pritchard and Kell [33] suggested that a variation of parameter values should not, under physiologically relevant conditions, significantly change the control profile of the model by Teusink *et al.* [1]. From these premises, one would expect the distribution of metabolic control (Section 2.3) to remain more or less consistent under the changes effected to get from the Teusink model to the Du Preez model.

One of the pillars of the bottom-up approach to systems biology is that modules of metabolism can be studied in isolation and integrated later-on [13]. The assumption related to this approach is that the modules can be reduced to characteristics that are context-independent and do not radically change each time the model is expanded or adapted. The adaptation of the Teusink model [1] to yield the Du Preez model [2] entailed a refinement of reaction maps for yeast glycolysis and a recalibration of some parameters to more closely resemble the oscillatory behaviour of yeast cells as observed experimentally. Both models were developed for very specific purposes, as is common in metabolic modelling [37]. If they do describe the same pathway under different

conditions, however, some characteristics should remain conserved during model adaptation (see Subsection 2.2.2). Validation of both models using the same data set could shed light on whether the model adjustment truly conserved important pathway properties.

2.2.4.3 Model availability

Note that all of the discussed models are available for viewing and simulation on the JWS Online model database ([51]; available at https://jjj.bio.vu.nl/).

2.3 Metabolic Control Analysis

Concurrent with advances in experimental biology, the second half of the 20th century also saw a theoretical shift in the way living organisms were viewed: a shift from "component thinking" to "systems thinking" [4]. Important in this "systems thinking" paradigm was the development of Metabolic Control Analysis (MCA) in the 1970s. Foundational work was done by Kascer and Burns [69] in Scotland and Heinrich and Rapoport [70] in East Germany. The resulting theoretical framework would prove very useful for the relation of steady-state network properties to the component reactions [19]. These approaches would allow for models to contribute to our understanding beyond just precise prediction based on a set of prior conditions [26].

Much work has been done to refine the theoretical basis of MCA, and at present it can describe most metabolic networks in terms of the distributed metabolic control of its component reactions. For brevity, a detailed discussion of MCA will not be undertaken, but the mathematically inclined reader is referred to Reder [71], Hofmeyr [19], and Visser and Heijnen [72] for overviews of the underlying theory.

MCA can be thought of as a sensitivity analysis, structured according to the stoichiometry of the component reactions [19]. It allows systems biologists to quantify the contribution of one enzymatic step (or a defined module of steps; 73) to the control of steady-state metabolic flux or metabolite concentration in a pathway. This is defined as the *control coefficient*, which, conceptually, can be expressed as follows:

$$C_j^f \equiv \frac{\partial f}{\partial \lambda_j} \tag{2.3.1}$$

where C_j^f is the control of any process j over any system function f; λ_j represents a modulation of process j; and the partial derivative indicates that the control coefficient is a function of multiple potential variables (like temperature, enzyme concentrations, etc.) but that perturbation in its parameter space is reserved, in this instance, to a modulation of process j [26].

Written more explicitly with regard to the interaction of the reaction rate of one enzymatic step, v_i, with the steady-state flux through the pathway, J, this can be reformulated as follows [20]:

$$C^J_{v_i} = \frac{dJ/J}{dv_i/v_i} \tag{2.3.2}$$

where $C^f_{v_i}$ is the control of the rate of reaction i, namely v_i, to the flux through the system, J; dJ/J is the change in the flux normalised to the wild-type flux; and dv_i/v_i is the change in the rate of the reaction in question, normalised to its wild-type value.

To understand the relevance of such a control coefficient, it is first of all important to understand that metabolic steps add up non-linearly. For instance, while the mass of the cell is the sum of the masses of its components, the rate of flux through a metabolic pathway is related to its component steps in a more complex way: the different steps influence each other in various combinations and to various magnitudes, resulting in non-obvious pathway characteristics [26].

The *summation theorem* posits that the sum of all of the individual flux control coefficients in pathway up to unity [20]:

$$C^J_{v_1} + C^J_{v_2} + C^J_{v_3} + ... + C^J_{v_i} = 1 \tag{2.3.3}$$

It can be understood from Eq. 2.3.3 that if the full magnitude of a change in steady state flux were 100%, the various individual reactions that constitute that pathway flux would be responsible for various smaller chunks of the full change, providing that the full 100% of change is ultimately accounted for. For example, v_1 could be responsible for 30% of the change, v_2 for 20%, and v_3 for 50%:

$$C^J_{v_1} + C^J_{v_2} + C^J_{v_3} = 0.3 + 0.2 + 0.5 = 1$$

Metabolic control coefficients are systems level properties that are determined mechanistically by an enzyme's sensitivity to changes in the concentrations of any of its ligands or of itself [25]. This sensitivity (known in MCA as *elasticity* and described by the *elasticity coefficient*), in turn, is determined by the physicochemical properties of the enzyme. Elasticity is a local property that is defined as the change in reaction rate in response to a change in metabolite concentration, or in the enzyme level, or the concentration of an external effector [72]:

$$\epsilon^{v_i}_{x_j} = \frac{x^0_j}{v^0_i}\frac{\partial v_i}{\partial x_j} \tag{2.3.4}$$

In Eq. 2.3.4, $\frac{x^0_j}{v^0_i}$ is the steady-state (pre-perturbation) concentration of metabolite, enzyme, or effector j, divided by the unperturbed activity of

enzyme i. $\frac{\partial v_i}{\partial x_j}$ is the partial derivative of the reaction rate of through enzyme i (v_i) with respect to the new concentration of metabolite, enzyme, or effector j. If we were to rewrite this equation to represent the change in the reaction rate as catalysed by specific enzyme j, for example, in response to the addition of an inhibitor, one would say:

$$\epsilon_{I_j}^{v_i} = \frac{I_j^0}{v_i^0}\frac{\partial v_i}{\partial I_j}$$

where I_j^0 is the concentration of the specific inhibitor, j, before perturbation and I_j its concentration after perturbation.

The elasticity coefficient only describes the local effects of perturbations, while the control coefficient can relate these effects to behaviour at a systems-level. The product of these two terms offers a powerful description of the overall effect of a perturbation as the combination of local and systemic properties [25]:

$$R_{x_k}^{J_i} = C_{v_j}^{J_i} \cdot \epsilon_{x_k}^{v_j} \tag{2.3.5}$$

Expanding this equation gives us:

$$R_{x_k}^{J_i} = \frac{x_k^0}{J_i^0}\frac{J_i}{dx_k} \tag{2.3.6}$$

This is known as the *response coefficient*, and it quantifies the response of steady-state flux to a perturbation in a parameter (e.g. x_k^0 in Eq. 2.3.6). It can be seen that the response of a systemic property (such as a steady-state flux) is dependent on both systemic (*control coefficient*) and local (*elasticity coefficient*) properties.

The control-matrix equation (omitted here for simplicity) is a direct mathematical relation of control and elasticity, since it expresses flux as a function of elasticity. This direct relation of control to elasticity is arguably the most powerful feature of metabolic control analysis, as it provides the theoretical grounding for direct experimental measurement of systemic properties as a function of component properties [19].

2.3.1 MCA and the Silicon Cell

Validation of mechanistic, kinetic models of glycolysis can benefit enormously from MCA as a paradigm for making predictions about the link between component properties and systems phenotypes (see Section 2.3). This has value both as a validation technique in the development of metabolic models (see Subsection 2.2.2) and as a direct route to rational drug design (see Subsection 2.3.2). Control coefficients can be experimentally measured by perturbing single enzymes and then measuring the perturbed property and the resultant systemic change independently (e.g. 74).

Control coefficients are subject to change in response to altered environments. Hence, control coefficients are at their most useful as systemic predictions if standard experimental conditions are adhered to (see Subsection 2.2.1 for more on standardisation). The distribution of glycolytic control can vary, for instance, depending on active enzyme concentration (33, 47) or substrate availability [43]. The latter can be experimentally fixed but the former, being a function of, among other things, growth phase [43], is bound to lead to some error. Growth phase, though it cannot be directly manipulated, can be indirectly standardised by consistently adhering to one culturing and harvesting protocol, for instance by growing up yeast cultures to the point of glucose depletion, or diauxic shift [43].

MCA, then, provides a framework within which systems-level predictions can be made in an attempt to invalidate an existing model (see Subsection 2.2.2). The summation theorem [20] implicates the entire system in the prediction of individual control coefficients. Control coefficients can therefore be seen as network-based properties [4], since a discrepancy in the prediction of flux control implicate all other control coefficients as well, and a discrepancy system's control distribution would imply a change throughout the rest of the distribution, hence casting doubt on the whole set of model parameters [17].

2.3.2 MCA and Disease

Beyond the fact that MCA has utility as a model validation tool, determining the control coefficient distribution in a parasite's metabolism offers a double advantage as it "gives us the initial assessment of where to intervene in a network" [12]. This is becoming increasingly important as the (re-)emergence of resistance is threatening the efficacy of existing treatments. This tendency calls for the development of new treatments and can be accelerated by rational approaches to drug target identification [75].

The first thing a drug target needs to be, is essential. Differential gene expression assays - a mainstay of disease-aetiology determination - suffer from myopia to the multiple layers of regulatory networks that confer robustness on a parasite's pathways [12]. MCA gives us the ability to evaluate which nodes are more crucial to systemic integrity than others, at the functional level of organisation (e.g. metabolism; 25).

MCA is useful, for instance, as a means of identifying the site(s) and relative importance of an effector for controlling certain physiological functions. This application of MCA to whole-body regulatory networks has been used to determine the importance of various effectors for controlling their surrounding pathway. These effectors can then be modulated for therapeutic effect. The group of M.D. Brand, for example (76–78), investigated the control of glucagon, phylogeny, and anaesthetics, respectively, over mitochondrial function by using an MCA approach.

A second application of MCA to medicine pertains to drug selectivity. The ability to understand which steps in metabolic pathways are least tolerant to change can be instrumental in identifying targets for therapies [25]. One of the big issues with current treatments is that they often come paired with severe side-effects [75]. Differential metabolic control analysis can aid researchers in addressing this: a comparison of metabolic control profiles of the parasite and the host can potentially expose loci of selective drug action (12, 75). Notably, the use of MCA as a drug-target identification tool can also unveil so-called "network-based selectivity", where selective action on parasitic enzymes is a function not of the physicochemical properties of the enzyme directly but of the distribution of flux control throughout the network [79].

We support the idea of MCA as a tool for drug-target identification, and it is useful to interrogate the description of "selectivity" by Haanstra *et al.* [80]:

$$Selectivity \equiv \frac{(dJ/J)_{pathogen}}{(dJ/J)_{host}} \tag{2.3.7}$$

and

$$\frac{(dJ/J)_{pathogen}}{(dJ/J)_{host}} = \frac{(C_I^J)_{pathogen}}{(C_I^J)_{host}} \cdot \frac{(\varepsilon^I_{[I]_T/K_t})_{pathogen}}{(\varepsilon^I_{[I]_T/K_t})_{host}} \cdot \frac{(K_I)_{host}}{(K_I)_{pathogen}} \cdot \frac{(P_I)_{pathogen}}{(P_I)_{host}} \tag{2.3.8}$$

In Eq. 2.3.7, "selectivity" pertains to the heightened effect of an inhibitor, I, on the glycolytic flux of the parasite as opposed to the host. dJ/J expresses the change in flux, normalised over the wild-type flux (effectively "% change in flux"). The expression $\frac{(dJ/J)_{pathogen}}{(dJ/J)_{host}}$ is therefore a comparison of the percentage change in flux experienced by the pathogen *versus* that of the host.

To zoom in on this expression, selectivity can then be expanded into its contingent terms, as in Eq. 2.3.8. In this equation, C_I^J refers to the flux control of the inhibitor and $\varepsilon^I_{[I]_T/K_t}$ refers to the sensitivity of the enzyme to either an increase in inhibitor concentration or an increase in the enzyme's affinity for the inhibitor - these terms are both network-based determinants of selectivity. K_I is inversely proportional to the binding affinity of the inhibitor to the enzyme and captures the structure-based selectivity of the inhibitor. Finally, P_I is known as the "partition coefficient" and is a measure of the pharmacokinetics of the inhibitor, i.e. the propensity of the inhibitor to reach its target in the cell after being administered extracellularly.

Of the four determinants of selectivity, therefore, two are network-based, one is structure-based, and the last one is pharmacokinetic [80]. The fact that two of the four terms that contribute to the selectivity of a drug target are network-based, offers a strong argument for the further investigation of these relational generators of selectivity as a route to drug-target discovery [79].

Important differences in the control distributions within the essential network, glycolysis, between pathogens and human hosts have already been reported, e.g. the observed high differential control of the glucose transporter (GTr) and GAPDH in the malaria parasite and *T. brucei* compared to human red blood cells [59, 81].

In descendants of the Penkler and Bakker models, MCA-based experimental validations of some key properties have been undertaken. In the case of the Penkler model, GTr was competitively blocked with the inhibitor, cytochalasin B, and the differential effects on glucose import and lactate export calculated as control coefficients [64]; in the Bakker model, phloretin, also a competitive inhibitor of the GTr, was added in erythrocyte-trypanosome co-cultures and the differential effect on glycolytic flux between the parasite and the red blood cells determined [80].

In both of the above-mentioned cases, glycolysis is the principal source of energy in the blood-borne stages of the parasite (10, 11) and, in both cases, GTr showed considerable network-based selectivity (59, 81). Intuitively, one can understand the high control of GTr as being due to its unique position as the gateway-enzyme to the pathway: by restricting the amount of glucose that can even enter the pathway, it strongly controls glycolytic flux whenever external glucose concentrations are not fully saturating [82]. This is not the case in cells that can make use of alternative energy sources, like red blood cells. It is, however, useful to open up multiple channels of enquiry after potential drug targets, not just because this increases the chances of finding a suitable treatment more quickly, but also because the threat of resistance to treatments can be more strongly mitigated by combined-drug therapy [12]. GAPDH offers such a possibility, as it has a unique position as the first enzyme after the branch point in glycolysis (see Section 2.4).

Differential control analysis also goes beyond host-pathogen comparisons, even showing promise in the identification of drug targets in cancer cells, where the disease cells are genetically identical to the healthy cells and few structural differences can be expected. Non-oxidative ribose synthesis via the pentose-phosphate pathway, for example, is almost unique to tumours and an analysis of metabolic control identified glucose 6-phosphate dehydrogenase as a site of high control over tumour growth [83], opening up very useful paths of network-based enquiry [84].

2.3.3 Control Coefficient Determination: Transporters and Intracellular Enzymes

As mentioned, selective perturbation of reaction-level parameters is necessary to connect systems-level phenomena to molecular causes [74]. Perturbation studies are often undertaken as gene knock-out studies; this method suffers from the limitation, however, that it can determine, experimentally, the

consequences of complete abrogation of activity but not intermediate phases of partial inhibition, as would be required in clinical settings [75]. Chemical perturbation is therefore more suited to the aims of rational drug design.

Typically, the kinetics of glycolytic enzymes are measured *in vitro* in cell-free extracts. A cell-free extract is not, however, an exact reconstruction of the complexity of a living cell: regulatory effects of very specific intracellular conditions, like compartmentalisation and co-localisation, might lead to a considerable level of heterogeneity within a single cell (28, 85). The process of creating cell-free extract usually homogenises the lysate, destroying any internal complexity that is present *in vivo*.

Addressing the differences between the *in vivo* and *in vitro* environments has, to a certain extent, been circumvented by keeping *in vitro* parameterisation limited to mechanistic or approximate phenomenological properties of an enzyme [26]. This was the case in the Teusink, Penkler, and Bakker models (1, 11, 81): all three models were validated for the ability of the *in vitro* kinetics to predict *in vivo* steady-state metabolite concentrations (2, 64, 80), bolstering the "phenomenologically approximate" approach to *in vitro* parameterisation [26].

The obstacle of *in vitro* kinetics, however, becomes somewhat harder to ignore when model validation is in question. The ability of *in vitro* kinetics to make accurate core predictions about *in vivo* systemic behaviour serves as a general validation that the parameters measured *in vitro* translate well to a model of a living system (see Subsection 2.2.2; 17). Those *in vivo* measurements to which the model is compared, are measured in intact cells [28].

The mismatch between the *in vitro* environment of the enzyme activity titrations and the whole-cell environment of the flux perturbations can, hypothetically, be circumvented by keeping the *in vitro* conditions in which enzyme activity is assayed, constant [22]. If the effects of an inhibitor on whole-cell flux and *in vitro* enzyme kinetics are to be compared, though, one cannot know for sure that the inhibitor is affecting the same target in the same way [46]. A work-around for this problem would be to perturb enzymes of which the activity can be measured without cell lysis, e.g. transporter enzymes. Much more convincing MCA-based model validations could be carried out, however, if the flux control of both membrane-bound and intracellular enzymes could be determined. Refer to Section 3.2 for further elaboration on this problem.

Control coefficients are not constants, however, but vary with changes in their environment [22], e.g. at different glucose concentrations [57, 59]. This has already been discussed as a variable affecting control distribution (see Subsection 2.3.2; "MCA and Disease").

Flux control is a non-linear function of the enzyme levels [25]. Our discussion of an increase in IAA being comparable to a decrease in "free GAPDH" (see Subsection 5.1.2) then implies that as GAPDH activity is

decreased, every subsequent further decrease might have a different effect. Flux control coefficients are conventionally referred to as the ratio between the relative change in flux and the relative change in enzyme activity at zero inhibitor [25]. Since control changes in response to enzyme activity titration, the change in flux control over the range of IAA used, can also be compared for experimental results and model predictions [75].

2.4 GAPDH: A Fork in the Road

GAPDH has been computationally identified as a possible target for rational drug design in both *Plasmodium falciparum* and *Trypsonoma brucei*, due to the high control exerted by GAPDH in the parasites' glycolytic pathway *versus* its control over erythrocyte glycolysis (see Subsection 2.3.2; [10, 59]).

Shestov *et al.* [86] also found recurring high control of GAPDH over glycolysis in human colon cancer cells undergoing aerobic glycolysis. "Aerobic glycolysis" (also known as the "Warburg effect" in oncology and plant physiology) refers to the tendency of proliferating cancer cells to upregulate glucose consumption and produce lactate at an increased rate rather than using the more efficient oxidative pathway [87]. Unlike blood-borne *P. falciparum* and *T. brucei*, substrate-level phosphorylation is not usually the main source of energy for mammalian cells under aerobic conditions. The high control of GAPDH over glycolysis in cells undergoing the Warburg effect coincides with the increased production of lactate via glycolysis, which is also accompanied by an increased expression of the enzymes of lower glycolysis, particularly GAPDH [86]. This is called the "Crabtree effect" in *S. cerevisiae* cells [9].

GAPDH is positioned just after the branching point of the pathway, where a 6-carbon sugar phosphate has been converted to two 3-carbon sugar phosphates [6]. The high glycolytic control of this enzyme in certain organisms can be ascribed to its reversible reduction of NAD^+ to NADH and its close interaction with phosphoglycerate kinase (PGK) - which reversibly converts ADP to ATP [86]. Both ATP consumption and NAD^+ regeneration have been shown to be important in regulating glycolytic flux [88], and it is reasonable to expect some of these regulatory effects to be exerted via GAPDH. On these grounds, Shestov *et al.* [86] suggest GAPDH as a potential target for cancer treatment.

Even in organisms purported to have low GAPDH-driven glycolytic flux control, like *S. cerevisiae* [2], GAPDH is repeatedly mentioned for its importance in controlling certain cellular events. Van Heerden *et al.* [82], for example, emphasise GAPDH as a point of control allowing yeast cells to thermodynamically drive glycolysis in the forward direction by the liberation of high levels of P_i via the trehalose synthesis pathway. The extensive validation study on the Du Preez model also identified GAPDH as an important site in the aetiology of phenotypes associated with cofactor imbalances, e.g. the

transduction of the effects of acetaldehyde capture by cyanide to PFK via its ATP sensitivity is ascribed to the GAPDH-PGK module [16].

It appears from these data that GAPDH is an important enzyme where glycolysis is very active - a phenotype often associated with disease conditions - qualifying it as an enzyme worthy of investigation.

2.4.1 Iodoacetic Acid: Specific GAPDH Inhibitor

The activity of GAPDH is mediated by an active-site cysteine residue that acts as a nucleophile during the conversion of glyceraldehyde 3-phosphate (GAP) to 1,3-bosphosphoglycerate (BPG) [89]. Cysteine is important in the catalytic mechanisms of many enzymes. Apart from being one of the least abundant amino acids in the proteome, cysteine also has the most extreme distibution of abundance and locality among the amino acid residues [90]: typically either very highly conserved (higher than the expected rate of random mutation) or very degenerated (much less conserved than random mutation would yield). This, combined with the tendency of cysteine to be conserved in functional positions but to degenerate quickly when positioned randomly, is a consequence of cysteine's high reactivity. This reactivity - resulting from two unpaired electrons in the its outer valence shell and the lowered electronegativity of sulphur compared to oxygen - are two key characteristics of cysteinyl sulphur [91]. The wide range of biological functions that can be facilitated by cysteine (catalysis, cofactor binding, regulation), arises from this unique reactivity.

Haloalkenes have been used as irreversible enzyme inhibitors since the 1930s [92]. They principally act on on enzymes by alkylating cysteine residues, forming a covalent bond with the thiol in the cysteine residue's side-chain [93]. Iodoacetate (IAA) and iodoacetamide (IAM) are two examples of such alkenes. Embden and Meyerhof suggested as early as 1933 that the site of glycolytic inhibition by IAA lies at the oxidation of triose phosphates [21]. Glycolysis has been targeted for inhibition via alkylation by IAA in prokatyotes, such as *Streptococcus lactis* [94], in unicellular eukaryotes, such as *Trypsonoma cruzi* [23], as well as in tissues from multicellular eukaryotes [95]. The inactivation of GAPDH by IAA is often used as a textbook example of irreversible enzyme inhibition [93].

The number of enzymes that are known to be affected by IAA counts in the hundreds [96]. It is not surprising that a simple compound such as IAA, which acts as a covalent modifier of the functionally important cysteine residue, is an inhibitor of multiple enzyme-catalysed processes. At relatively low concentrations, however, (<1 mM) and over short exposure times (< 1 hour), IAA appears to bind almost exclusively to protein thiols [97], specifically to the catalytic cysteine residue of GAPDH (though alkylation of other nucleophilic side-chains are known to occur, but are thought to be innocuous for most analytical applications; 92). For instance, both Jones *et al.* [98] and Whitehead and Rabin [99] used IAA as an alkylating agent

of cysteine groups in hexokinase and alcohol dehydrogenase, but made use of millimolar concentrations of the compound. According to the method of Poolman *et al.* [22], specificity can be assumed at very low concentrations of IAA, as this compound only significantly reduces the activity of other glycolytic enzymes at millimolar concentrations, whereas GAPDH can lose as much as 90% of its activity by being exposed to only 100 μM of IAA. GAPDH seems to have the highest affinity for IAA and an inhibited glycolysis has been repeatedly ascribed to irreversible, specific active-site blocking of GAPDH by this haloalkene [21–24, 93–95, 100].

Webb [21] indicated that 1 mM could significantly inhibit GAPDH, but also certain alcohol dehydrogenases (ADH), succinate dehydrogenases, and proteolytic enzymes. A later study investigated this claim and showed that IAA targets GAPDH selectively in *S. cerevisiae* at IAA concentrations below 0.5 mM [101].

It has been suggested that IAA is inappropriate as a thiol-alkylating agent, due to its negative charge. This charge could lead to substantially reduced reaction rate when the target site is located in a hydrophobic environment; furthermore, IAA's negative charge might also render it membrane-impermeable [102]. Despite these concerns, however, IAA has been used successfully as an inhibitor of GAPDH activity *in vivo* in multiple studies [22, 24, 86, 93–95, 100, 101, 103, 104].

2.4.1.1 Iodoacetic acid and GAPDH protection

Taking a step back, it must first be mentioned that the possible structural differences in the enzymes are particularly relevant in case of IAA as inhibitor. Brodie and Reed [105] showed, using human lung carcinoma cells (A549), that cells that were oxidatively stressed by the exposure to non-toxic or mildly toxic concentrations of hydrogen peroxide (H_2O_2), were protected from IAA-binding in a dose-dependent way. The formation of disulphide bridges between otherwise catalytically active thiol groups likely contributes to this protection against IAA [102]. This dose-dependent protection has been shown to be alleviated by the addition of dithiothreitol (DTT; 106), suggesting that oxidative damage in cell-free extract might lead to quantitative differences in the inhibition profile [105]. The intracellular redox environment is very flexible and is used as a regulatory mechanism to respond to ambient conditions [107–109].

Work by Segal and Boyer [110], furthermore, has suggested that GAPDH is protected from IAA alkylation in the presence of its substrates.

Cell lysis will immediately interrupt these ambient factors and lead to possible differences in the environments in which glycolytic flux and specific activity are measured, respectively.

2.4.1.2 Iodoacetic acid and pharmacokinetics

S. cerevisiae cells are enveloped in both a cell wall and a cell membrane [6]. Hansen and Winther [102] suggested, due to the negative charge of iodoacetate (the conjugate base of IAA, which is more common at the physiological pH characteristic of yeast; 21), it is membrane-impermeable. Many researchers who have worked with IAA in a variety of different cell types, have worked from - and succeeded under - the assumption that extracellular administration of the inhibitor leads to glycolytic inhibition (including, to name but a few: 22, 86, 93, 101, 103). None of the studies of which we are aware, however, have quantified the pharmacokinetic properties that define the bioavailability of IAA at the inhibitory site in GAPDH.

In the next chapter, we outline our approach to addressing this issue (Chapter 3).

2.4.2 *S. cerevisiae* and GAPDH Control

From existing literature, it seems that GAPDH has very little control over glycolysis in yeast. The computational work of Pritchard and Kell [33] and the experimental work of Bruck *et al.* [47] looked at the behaviour of glycolysis at varying possible and even purely hypothetical combinations of enzyme expression levels. In all cases, lower glycolysis was almost devoid of flux control. Glycolysis in yeast appears to be almost entirely controlled by the hexose transporter with some (probably unrealistic) simulated conditions yielding PFK as the principal site of glycolytic control [33].

The predictions of glycolytic flux control by the existing models can be tested against experimental data as a way to determine the models' validity. Flux control in the models can be simulated as a changing parameter as the activity of the perturbed enzyme decreases, yielding not a single control coefficient, but a more complete *control profile* (see Fig. 5.8). This is an even stronger model validation, as it tests the ability of the model to track changes in this systemic property over a range of inhibition [25]. Control profiles are also useful in pharmaceutical studies, as a sudden precipitous change in the flux control of an enzyme might have clinical use where this change renders a pathogen more vulnerable to inhibition at a certain enzyme than its human host [12].

Chapter 3

Materials and Methods

In this study, we experimentally determine the control of GAPDH over glycolytic flux as a validation of the model by Teusink *et al.* [1] and its descendent, the model by Du Preez *et al.* [2].

We use the same laboratory strain as Du Preez *et al.* [2, 16] and the predictions of metabolic flux control that we test are core predictions and qualitatively different from anything either model was trained on: in this sense, the model construction and model validation data are kept strictly separate [5].

3.1 Cell Cultivation and Preparation

S. cerevisiae X2180 cells were grown in a yeast growth medium consisting of 10 g.L^{-1} glucose, 6.7 g.L^{-1} yeast nitrogen base (Sigma-Aldrich, St Louis, MO, USA), and 100 mM potassium phthalate (Sigma-Aldrich, St Louis, MO, USA) at a pH of 5.0, shaking on a rotary shaker at 140 rpm (30°C) as in Gustavsson *et al.* [67]. The optical density of two standard cultures was monitored with spectrophotometric readings at regular intervals at a wavelength of 600 nm. These cultures were not, themselves, harvested, but served to determine the growth conditions at which harvesting would take place. The readings were taken using a SPECTROstar^{nano} spectrophotometer (BMG Labtech, Cape Town, South Africa). Optical density data were plotted as a function of time to visualise growth. Concurrent optical density and glucose concentration readings (obtained using Medi-Test Combi 4/6 Urine Test Strips; Product Code 4020, Humor Diagnostica, Hermanstad, Pretoria) confirmed that the point of glucose exhaustion reproducibly coincided with a plateau in the OD_{600} readings. We isolated our cells at this point, known as diauxic shift [111].

The cells were pelleted by centrifugation at a relative centrifugal force of 4500×g for 5 minutes at 4°C in an Eppendorf 5804 R Centrifuge (Eppendorf, Hamburg, Germany). They were then washed twice with a volume of 1:10 wash buffer (g cells : mL wash buffer). The wash buffer consisted of 100

mM potassium phthalate and 2 mM ethylenediaminetetraacetic acid (EDTA) according to the method of Van Eunen *et al.* [3]. Three independent biological samples were grown and harvested in this way. The cells were weighed after the first centrifugation step and a consistent yield in approximate dry weight (between 0.4 and 0.6 g per 50 mL of culture) was obtained.

After harvesting, the cells were exposed to known concentrations of a GAPDH inhibitor, iodoacetic acid (IAA). The precise details of the inhibition method are discussed at length in Subsection 3.4.1. First we turn to the underlying theory.

3.2 Inhibiting Intracellular Enzymes: The Problem

Subsection 2.3.3 of the literature review briefly referred to the problem of perturbing intracellular enzymes and credibly measuring the the effect of these perturbations. A good way to understand the problem, lies in the description of inhibitor-selectivity by Haanstra *et al.* [80] in Eq 2.3.8. Dividing selectivity into four categories - inhibitor control, enzyme elasticity, structural differences, and pharmacokinetic differences [80] - yields useful insight into the issue of intracellular perturbation. If Eq. 2.3.8 is adjusted to express the difference not between a host and a pathogen, but between the intracellular environment and a cell-free extract, then one can see that selectivity of an inhibitor for a target might also occur when the same enzyme is exposed to the inhibitor in different contexts:

$$\frac{(dJ/J)_{cell}}{(dJ/J)_{extract}} = \frac{(C_I^J)_{cell}}{(C_I^J)_{extract}} \cdot \frac{(\varepsilon^I_{[I]_T/K_t})_{cell}}{(\varepsilon^I_{[I]_T/K_t})_{extract}} \cdot \frac{(K_I)_{extract}}{(K_I)_{cell}} \cdot \frac{(P_I)_{cell}}{(P_I)_{extract}} \tag{3.2.1}$$

where the flux control of the inhibitor (C_I^J), the sensitivity of the enzyme to an increase in the inhibitor or an increase in the inhibitor's affinity for the enzyme ($\varepsilon^I_{[I]_T/K_t}$), the binding affinity (K_I), and the partition coefficient (P_I) all contribute to a "selectivity" of the inhibitor for its target enzyme in whole cells ("cell") *versus* cell-free extract ("extract").

The challenge for an experimenter that will measure the effect of an inhibitor on an enzyme *in vitro* and the effect on flux *in vivo* is to ensure that the effects are not obscured by an enhanced selectivity of the enzyme for the inhibitor in one environment as opposed to another.

Since the enzymes in cells and in cell extract originate from the same organism and strain, it is tempting to posit that there will be no selectivity as all terms remain the same, but this is not so. Smallbone *et al.* [35], for example, mention unknown effectors, intracellular crowding, and channelling as potential causes of differences in *in vivo* and *in vitro* enzyme activities.

This might also apply to the mechanism of inhibition: if the reaction-level kinetics and the systemic phenotypes are assayed in different contexts, one might be combining data from two experimental environments that affect inhibitor action in different ways (Eq. 3.2.1).

The flux control term in Eq. 3.2.1 can be disregarded, as the networks originate from the same organism, hence will be identical. Terms elasticity, structural selectivity, and pharmacokinetics (terms 2 to 4 in Eq. 3.2.1), however, cannot be ignored. By measuring enzyme activity in standardised, physiologically relevant buffer conditions and extrapolating biochemically operative phenomenological parameters from measurements (e.g. 40, 41), like V_{max} or K_m (see Subsection 2.2.1; 3, 26) one can attempt to minimise the mismatch between the inhibition contexts, but the sheer number of factors for which one would need to compensate, render a perfect recreation of the intracellular environment inconceivable [46].

Ambient conditions can lead to lower affinity of the inhibitor for its target, like the formation of disulphide bridges in a more oxidised environment [112] or competition in high substrate concentrations [12]. Conformation changes might also be brought about by changes in medium ionic strength and might lead to decreased structural affinity for the inhibitor [6].

Since the elasticity coefficient in Eq. 3.2.1 is also partially determined by the enzyme-inhibitor affinity, this term is also implicated in contributing towards possible context-specific selectivity.

The fourth term - the pharmacokinetic term, expressing the availability of the inhibitor to the enzyme - can also not be assumed to be equal for whole cells and cell-free extract. Most obviously, the presence of cell envelopes and intracellular compartments, can lead to to differences in inhibitor concentrations when administered to incubations containing whole-cells *versus* to cell-free extracts [113]. Additionally, something like localised hydrophobicity in certain parts inside a cell could lead to poor access of a charged inhibitor, like the conjugate base of IAA, to certain enzymes [102].

The failure of standardised buffers to fully compensate for these factors complicates the task of determining the flux control of intracellular enzymes. This complexity can be resolved by *in vivo* measurement of intracellular kinetics, something that is becoming increasingly viable thanks to high-resolution imaging techniques [15]. These techniques are still comparatively expensive, however, and not readily accessible in all laboratories.

As has been mentioned, previous model validations have largely escaped this complexity by focusing on the perturbation of the glucose transporter (see Subsection 2.3.3): inhibiting the transporter and measuring the effect on glucose uptake and glycolytic flux does not require cell lysis, as the inhibitor acts on the cell-surface and both the enzyme-level effect and the flux effect can be measured on whole cells. The activity of intracellular enzymes, however, cannot easily be measured *in vivo* [15]. At the same time, measurements of

glycolytic flux on cell-free extract will disregard vital intracellular dynamics that might contribute to the ultimate effect on the flux [28]. The important task of validating metabolic control distribution predictions for intracellular enzymes remains hitherto largely unaddressed. In the following sections, we describe our approach to resolving this problem.

3.3 IAA as a Specific Inhibitor of GAPDH

For the present study, GAPDH was chosen as the target enzyme for experimental determination of its flux control coefficient. As was mentioned in Subsection 2.3.2, this enzyme has been computationally identified as a possible target for rational drug design in both *Plasmodium falciparum* and *Trypsonoma brucei*, due to the high control exerted by GAPDH in the parasites' glycolytic pathway compared to red blood cells' (10, 59).

Besides its purported high glycolytic flux control, GAPDH is a promising enzyme for our purposes because it has an irreversible, selective inhibitor (IAA; see Subsection 2.4.1). Succinate dehydrogenase and alcohol dehydrogenase (ADH) were reported to be susceptible to IAA inhibition, but only at concentrations above 1 mM [21]. Campbell-Burk *et al.* [101] investigated this by measuring anaerobic energy production by ^{31}P NMR: they found a marked change in the ^{31}P NMR spectrum 15 minutes of incubating *S. cerevisiae* cells in 0.25 mM IAA, consistent with the inhibition of GAPDH. In aerobic, ethanol-fed *S. cerevisiae* cultures, however, no change in O_2 consumption rate was observed at IAA concentrations below 0.5 mM, consistent with an absence of inhibition of succinate dehydrogenase and ADH. At concentrations above this, however, O_2 consumption rate quickly decreases, indicating that GAPDH specificity can no longer be assumed at these concentrations. For the purposes of this study, then, only IAA concentrations lower than 400 μM are used.

3.4 Prelytic Inhibition

In Subsection 3.2 we explain why pharmacokinetic properties and the effect of differing ambient conditions on inhibitor affinity cannot be merely disregarded when measuring whole-cell glycolytic flux as a factor of perturbed *in vitro* kinetics. This problem is exacerbated by the usual measurement of intracellular V_{max} values in supraphysiological substrate concentrations: work by Segal and Boyer [110] suggested a protective effect of substrate against IAA alkylation - something that will likely differ greatly between the *in vitro* and whole-cell assays. Despite our best efforts at imitating *in vivo* conditions [3], pharmacokinetic discrepancies will not be accounted for by mere manipulation of *in vitro* assay conditions [46].

The irreversibility of IAA in its effect on GAPDH, however, coupled with the specificity of this effect in the context of glycolysis [21, 22, 86], offers a good opportunity to circumvent these issues.

The cells in question can be exposed to IAA for a given duration before lysis, after which further inhibition can be stopped by washing the cells: this will remove the extracellular IAA and, considering that the diffusion gradient of IAA will now be towards the much larger extracellular volume, subsequent IAA binding to GAPDH can be regarded as negligible. Furthemore, since inhibition is irreversible, what has taken place in terms of active-site cysteine alkylation by IAA can be assumed to remain constant from this point. From this same batch of inhibitor-exposed cells, both whole-cell incubations for flux determination and production of cell-free extract for measurement of specific activity can be performed. Under the assumption that the IAA-binding profile does not change upon cell lysis or transferral to the *in vivo*-like medium proposed by Van Eunen *et al.* [3], any measured specific activity in this study expresses the maximal remaining catalytic capacity of the enzyme pool [26], or $V^{app}_{max,GAPDH}$.

Comparison between cell-free extract made from prelytically inhibited cells and cell-free extract to which the inhibitor was administered directly will be done to quantify the difference between administering the inhibitor before *versus* after cell lysis. We hypothesise that IAA should have a significantly larger effect when administered directly to the cell-free extract, as fewer barriers to accessing the inhibitory site on GAPDH exist *in vitro*.

3.4.1 Inhibition of GAPDH: Procedure

The yeast cells harvested in Section 3.1 were split into two batches (Fig. 3.1), one of which would be prelytically incubated in IAA and another which would be lysed and only exposed to IAA *in vitro*: these are referred to as the *preinh-batch* (prelytically inhibited) batch and the *in-vitro-batch* (*in vitro* inhibited) batch, respectively (importantly, *preinh-batch* later subdivides into *preinh-flux* and *preinh-activity*: they were lysed and used for GAPDH activity measurement and kept whole and used for flux measurement, respectively). The cells were kept on ice or frozen at -20°C until further use.

Prelytic inhibition: the isolated yeast cells from *preinh-batch* were resuspended in a preheated (30°C) growth medium identical to the culturing medium used by Gustavsson *et al.* [67], but with a lowered glucose content (20 mM). This suspension was then divided into identical smaller volumes that were each administered with a known concentration of iodoacetic acid (IAA) within the range: $0\mu M \leq [IAA] \leq 400\mu M$. This method of administering IAA is based on the method of Poolman *et al.* [22]. The concentrations administered to the three biological repeats (termed *I*, *II*, and *III*, respectively) were:

- *I*: 0 μM , 25 μM , 50 μM , 100 μM , 200 μM , 400 μM
- *II*: 0 μM , 18.75 μM , 37.5 μM , 75 μM , 150 μM , 300 μM
- *III*: 0 μM , 15.625 μM , 31.25 μM , 62.5 μM , 125 μM , 250 μM

A *wild-type* (zero IAA) sample was included for each biological repeat. The IAA-containing cell suspensions were incubated at 30°C on a rotary shaker for 60 minutes. The cells were then pelleted by centrifugation at 2700×g for 5 minutes at 4°C . They were resuspended in a wash buffer containing 100 mM potassium phthalate at a pH of 5.0, and centrifuged again at 2700×g for 5 minutes at 4°C . This wash step was repeated once more. Half the cells were then kept on ice and used immediately for flux incubations (called

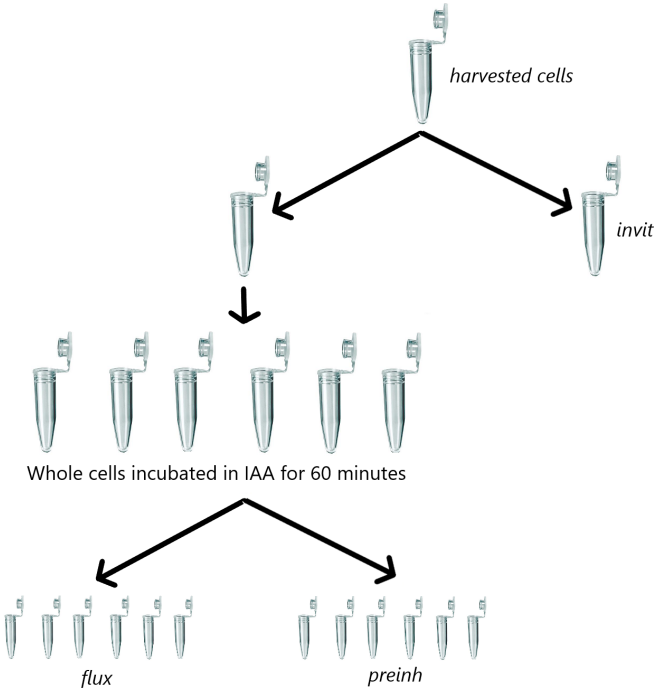

Figure 3.1: Division of a harvested culture into various batches. A single harvested culture is split into two batches of equal volume: one which will be lysed and used for GAPDH activity determination in the presence of IAA *in vitro* (called *in-vitro-batch*), and one which will be split into six batches of equal volume that will be incubated for 60 minutes in varying concentrations of IAA (*preinh-batch*). The prelytically inhibited cells will then each be further split into two batches of equal volume: one destined for lysis and GAPDH activity titration (*preinh-activity*) and one of which the flux will be determined by assaying the production and consumption rates of whole cells (the *preinh-flux* batch).

preinh-flux), while the other half was frozen at -20°C for later lysis and use during GAPDH activity measurements (*preinh-activity*). Since the flux measurements and the GAPDH activity measurements are from the same inhibitor incubation, all pharmacokinetic and structural differences that can contribute to a context-specific selectivity and which result from differences in ambient conditions, are eliminated.

In vitro inhibition: the cells from the *in-vitro-batch* batch were not treated any further after harvesting. The were stored at -20°C until cell extract was produced (see Section 3.5). IAA was administered to the cell-free extract directly and the mixture incubated at 30°C for 60 minutes before being transferred to and kept on ice until GAPDH activity measurements were performed. The time between transfer to ice and activity measurement was kept as short as possible to avoid time-dependent artefacts when comparing the prelytic and *in vitro* inhibition techniques - in the end, the extra incubation time for the *in-vitro-batch* samples never exceeded 5 minutes. *In vitro* inhibited GAPDH enzymes were therefore allowed at least as much incubation time in IAA before activity was measured. IAA could not be removed from this mixture by washing like with the prelytic inhibition.

3.5 Cell Extraction

Cell-free *S. cerevisiae* extract was produced for GAPDH activity measurement *in vitro* and for protein determination. For this, harvested cells were resuspended in the *in vivo*-like buffer of Van Eunen *et al.* [3]. The extract was then produced by means of a glass-bead extraction protocol, according to the method of Teusink *et al.* [1]. The isolated cells were placed in Eppendorf tubes, along with acid-washed glass beads (425 to 600 μm in diameter; Sigma-Aldrich, St Louis, MO, USA) in a ratio of 1 mg of glass beads per 1 mL of cell suspension. The glass-bead-containing suspensions were then fastened to a bench-top vortex (Vortex Genie2^{TM}, Scientific Industries, Bohemia, NY, USA) and shaken for 5 minutes, after which the tubes were placed on ice for 5 minutes. This was repeated for 10 cycles, or until no white layer of unlysed cells was visible in the tubes any more.

This process was independently carried out for each *preinh-batch* sample and for the *in-vitro-batch* lysate (see Fig. 3.1).

3.6 Flux Determination

Glycolytic flux was measured as the rate of extracellular product accumulation or substrate consumption by whole cells. Flux was only measured on whole cells, and these data used for both the *in vitro* and prelytically inhibited cell-free extracts.

3.6.1 Time Course Incubation

Cells that were harvested and incubated in IAA for 60 minutes were, as described in Section 3.1, split into two equal batches (*preinh-activity* and *preinh-flux*). One batch was subjected to a cell-extraction protocol (see Section 3.5) and the other was used for flux determination.

For the flux determination the cells were resuspended in 2 mL of an incubation buffer that had been preheated to 30°C (identical to the culture medium except for a lowered glucose concentration of 20 mM). The cell suspension was kept at 30°C for the duration of the incubation. A timer was immediately started (marking t_0) and an initial sample of 200 μL of the extracellular medium was taken. This sample was centrifuged at a relative centrifugal force of 2000×g using a benchtop picofuge (Labnet Prism Mini Centrifuge, Edison, NJ, USA). 180 μL supernatant was extracted (taking care to avoid pipetting up cells) with a pipette and flash-frozen in liquid nitrogen before storage at -20°C .

After the first sample was taken and stored, 200 μL aliquots of each incubation were distributed over 9 clearly marked 1.5 mL Eppendorf tubes to ease the process of sampling: at each interval, one of these aliquots from each sample would be centrifuged and the supernatant stored. Sampling was done every 10 minutes over a duration of 90 minutes, yielding 10 time-points tracking the changes in extracellular medium composition. After all the time-points had been extracted, the samples were allowed to thaw at room temperature and centrifuged again at 2700×g in an Eppendorf 5804 R Centrifuge (Eppendorf, Hamburg, Germany), and the top 160 μL of the sample supernatant transferred to new 1.5 mL Eppendorf tubes. The samples were then flash-frozen in liquid nitrogen and stored at -20°C for ethanol and glucose determination at a later stage.

3.6.2 Ethanol Determination

The samples collected during the time-course incubation of yeast cells were assayed for ethanol content according to the method of Bergmeyer [114]. A buffer of 0.33% (g/mL) $Na_4P_2O_7{\cdot}10H_2O$, 0.016% (g/mL) glycine, and 0.83% (g/mL) semicarbazide was made up with milliQ H_2O and set to pH = 8.8. After making up the buffer, it was filter-sterilised using a sterile syringe filter with a pore size of 0.2 μm (Biosmart, Cape Town, South Africa).

Aliquots of the samples were diluted 1:19 into the assay buffer. The addition of 1 U.μL $^{-1}$ alcohol dehydrogenase and 10 mM NAD^+ thermodynamically drove the conversion of ethanol to acetaldehyde. The absorbance at λ = 340 nm was tracked for 10 minutes when all reagents but NAD^+ had been added (E1) and then again after NAD^+ had been added until the reaction reached equilibrium (E2). NADH concentration was tracked spectrophotometrically (SPECTROstar^{nano}, BMG Labtech, Cape Town, South

Africa) at $\lambda = 340$ nm until plateaus were reached for all samples and standards. All readings were within the linear range of the spectrophotometer.

After this data was collected, a segment of the absorption increase curves were chosen as representative of the plateau (see Appendix H) and the mean of the chosen segment was treated as the end-point value. The absorbance increase from the end-point of E1 to that of E2 represented the detected ethanol concentration. The change in absorbance over this segment was converted to an ethanol concentration using a calibration curve with known ethanol concentrations assayed according to the same method.

3.6.3 Glucose Determination

Time-course incubation samples were assayed for glucose concentration according to the method of Ogawa *et al.* [115]. The assay was carried out in a buffer consisting of 100 mM triethanol amine hydrochloride (TEA-HCl) and 10 mM $MgCl_2$ at a pH of 8.2. This buffer was sterilised with a sterile syringe filter with a pore size of 0.2 μm (Biosmart, Cape Town, South Africa).

Samples were diluted 20 times into the assay buffer, along with NAD^+ to a concentration of 4 mM and ATP to a concentration of 2 mM. The absorbance of the assay cocktails was spectrophotometrically measured for 10 minutes at $\lambda = 340$ nm (SPECTROstar^{nano}, BMG Labtech, Cape Town, South Africa). This was reading G1. Glyceraldehyde 6-phosphate dehydrogenase from *Leuconostoc mesenteroides* was then added to a final concentration of 0.5 U.100 μL $^{-1}$. Another 10 minute spectrophotometric reading was performed at $\lambda = 340$ nm (reading G2). Finally, hexokinase from *S. cerevisiae* was added to a final concentration of 32.5 U.100 μL $^{-1}$. The final absorbance reading at 340 nm was then taken for 10 minutes (G3).

The difference between the readings of G2 and G1 is a control for glucose 6-phosphate (G6P) to see if intracellular metabolites somehow get into the supernatant samples - nothing like this was observed. G3 minus G2 then yielded the absorbance change due to glucose detection. This absorbance change was converted to a glucose concentration using a calibration curve set up using known standard glucose concentrations.

3.7 Protein Determination

Protein determinations were performed on each sample after IAA incubation and lysis. This was done according to the method of Bradford [116] as adapted by Ernst and Zor [117]: the ratio of the measured absorbance at $\lambda = 595$ nm to the measured absorbance at $\lambda = 450$ nm was calculated, which extends the range of absorbance values to which protein concentration relates linearly. This was successfully done for a serial dilution of bovine serum albumin, which served as standards (see Appendix A).

This permitted determinations of the total protein content for each prelytically inhibited sample (collectively called *preinh-batch*) as well as for the cells from *in-vitro-batch* that were only exposed to inhibitor after lysis. The measured activity of GAPDH and the flux through the whole cells were then both normalised to their relevant total protein concentrations.

3.8 GAPDH Activity Measurements

The activity of GAPDH was measured *in vitro* for the determination of the relative effect of IAA on the enzyme. The relative effect of IAA on GAPDH in standard conditions is necessary for the calculation of a control coefficient using specific inhibition [22]. We opted for the *in vivo*-like conditions of Van Eunen *et al.* [3] as a standardised physiological buffer for the determination of glycolytic enzyme activities in yeast: 300 mM K^+, 20 mM Na^+, 1.0 mM Ca^{2+}, 1.0 mM Cl^-, 245 mM glutamate, 50 mM phosphate, and 10 mM $MgSO_4$, at a final pH of 6.8.

The reagent concentrations of the reverse GAPDH activity assay were adapted from Van Eunen *et al.* [3], themselves having adapted the concentrations from Van Hoek *et al.* [118]. The composition of our reverse assay cocktail was: 0.6 mM NADH, 50 μM NAD^+ (suggested by Byers [119] to abrogate the initial lag in reverse activity measurements), 1 mM ATP, 5 U.μL $^{-1}$ phosphoglycerate kinase (PGK), and 5 mM 3-phosphoglycerate (3-PGA).

The reverse assay assumes that PGK is in equilibrium as a coupling enzyme and that it converts 3-PGA to 1,3-BPG quickly enough to saturate the reverse GAPDH reaction. It is unlikely that this is the case, but this assumption does allow reasonable measurements of GAPDH activity in reverse to be made (see 81 for a more detailed discussion on this assumption).

No forward assay was suggested by Van Eunen *et al.* [3] so we used - out of the assays discussed by Byers [119] - the one according to Ferdinand [120]. The final assay cocktail composition was: 0.8 mM NAD^+ , 10 mM ADP, 0.8 mM D-glyceraldehyde 3-phosphate (D-GAP), and 5 U.μL $^{-1}$ PGK. The thermodynamically unfavourable forward GAPDH reaction would be elicited by adding high concentrations of PGK to convert the product of GAPDH, 1,3-bisphosphoglycerate, to 3-PGA.

For both assays, the activity was measured as either the consumption (reverse assay) or production (forward assay) of NADH over time at λ = 340 nm using a spectrophotometer (SPECTROstar^{nano}, BMG Labtech, Cape Town, South Africa). As was done during the construction of the original model [1], enzyme activity was measured only where the protein concentration and the measured activity related to each other linearly.

The measured specific activities are approximate V_{max} values, as they were measured in conditions of substrate excess. The unperturbed specific

activities measured in this study were therefore treated as $V_{max,GAPDH}$ values for comparison to literature $V_{max,GAPDH}$ values.

We also wanted to determine the effect of oxidative damage in cell-free extract as a contributing factor to the binding efficacy of IAA to the cysteinyl thiolate of GAPDH. For this, activity titrations were all performed in assay cocktails that contain 5 mM of the moderate reducing agent dithiothritol (DTT) and cocktails that have no external reducing agent. Comparison of these data sets would yield insight into the effect of the redox environment on IAA binding.

3.8.1 Compensating for the Redox Environment

The reader is reminded of Eq. 3.2.1, where the flux control of the inhibitor (C_I^J), the sensitivity of the enzyme to an increase in the inhibitor or an increase in the inhibitor's affinity for the enzyme ($\varepsilon^I_{[I]_T/K_t}$), the binding affinity (K_I), and the partition coefficient (P_I) all contribute to a "selectivity" of the inhibitor for its target enzyme in whole cells ("cell") *versus* cell-free extract ("extract").

Reports in the literature of GAPDH cysteine being protected from IAA action by being in a oxidised state suggest another important difference between the cell-free extract and whole-cell environments: outside of the regulated intracellular environment, enzymes often become oxidised [106]. Brodie and Reed [105] reported that an oxidised state reduces the affinity of the GAPDH cysteinyl thiol for IAA. This means that the binding affinity term (K_I) of Eq. 3.2.1 might differ when comparing inhibition *in vitro* and *in vivo*. In order to address this for a good comparison between prelytic and *in vitro* inhibitor administration, we needed to compensate for the impact of the redox environment on IAA effect.

The precise redox conditions of the intracellular environment is experimentally laborious to measure, and would - owing to the flexibility of the redox proteome - have to be redetermined for each extraction [107, 121]. In order to address the possibility of a changing redox environment leading to unaccounted-for variation in the inhibition profile, we will investigate whether oxidation of the enzyme in the lysate affects the observed effect of IAA: all specific activity measurements will be conducted in a moderate concentration of DTT and in the absence of DTT. Divergent results will be regarded as indicators that the redox environment is influencing the inhibition.

3.8.2 NADH Calibration Curve

Changes in absorbance measurements were converted to changes in NADH concentration by means of a calibration curve for NADH concentration *versus* absorbance at $\lambda = 340$ nm. This method compensates for experimental artefacts where mere calculation of concentrations using the Beer-Lambert law does not.

3.8.3 V_{max} Segment Selection

In both the forward and the reverse directions, the initial increase/decrease in NADH in the substrate-saturating assays (for calculation of approximate V_{max}) were selected manually. These segments of absorbance increase were linear and express GAPDH activity where substrate concentrations are not inhibitory. Figure D.1 shows some examples to illustrate the of segment selection.

The criteria that were applied during segment selection were:

1. selected initial segments were all 30 seconds (four readings) to a minute (seven readings) long, depending on the duration of the linear absorbance increase;

2. the segments were kept consistent within biological repeats for each reaction direction (forward *versus* reverse);

3. to avoid underestimation of V_{max} , the segments all started at the first time point, unless there was a clear initial lag in the reaction (e.g. at 31.25 μM and 62.5 μM in Fig. D.1*C*);

4. if the standard deviation of the data was unstable or large, the members of a technical triplicate were inspected and the most unstable member of the set dropped (*data cleaning*) - no more than one member of each triplicate was dropped (Fig. D.1*E* is an example data before *cleaning* and Fig. D.1*F* is an example of the same data after *cleaning*);

3.9 Data Analysis and Mathematical Modelling

Data analysis and mathematical modelling were both carried out using Mathematica 11.1 (Wolfram Research Inc., Champaign, IL, USA). The models analysed in this study are available on the JWS Online model repository as the teusink model and the dupreez4 models.

Detail about the model analysis procedure are located in the Model Analysis chapter (Chapter 5) as the modelling methods are best understood when presented together with their results.

3.10 Control Coefficient Calculation

The control of an enzyme over the flux through the pathway is defined in Eq. 2.3.2. In this equation, the derivative represents the change in pathway flux, J, as a function of an infinitesimal change in the rate of one of its steps, v_i. Experimentally, infinitesimal changes in a reaction rate would be undetectable, so the standard approach is to make noninfinitesimal, detectable perturbations

and to normalise the effect described by Eq. 2.3.2 using the ratio between the initial values for which the slope was calculated [25]:

$$C^J_{v_i} = \frac{dJ/J}{dv_i/v_i} \cdot \frac{v_i^0}{J_0} = \frac{J - J_0}{v_i - v_i^0} \cdot \frac{v_i^0}{J_0}$$

Flux measurements and GAPDH activity measurements were normalised to unperturbed flux or activity to yield a relative value. The change in relative flux or relative GAPDH activity over an IAA concentration change of 3.2 μM (from 0 μM) is taken as an infinitesimal perturbation. This was the size of the increment for which model behaviour was simulated in all cases. These increments were then used to calculate glycolytic flux control and regarded as equivalent to control at an inhibitor concentration of zero for both the model predictions and the mathematical fits to the experimental data.

3.10.1 IAA in Control Analysis

In Section 2.3 of the previous chapter, we describe some of the theory underlying Metabolic Control Analysis (MCA). Importantly, flux control is defined in Eq. 2.3.2, which we present again for convenience:

$$C^J_{v_i} = \frac{dJ/J}{dv_i/v_i}$$

As explained in Section 2.3, this parameter relates the change in flux through a pathway to the change in the rates of its component steps. To determine flux control experimentally, it is important to know that the chosen enzyme is the only component in the pathway that is being varied. To this end, one can either downregulate an enzyme's concentration, or administer a known specific inhibitor. IAA (administered in low concentrations) allows us to specifically inhibit GAPDH within glycolysis. Poolman *et al.* [22] present a derivation of Eq. 2.3.2 where an inhibitor is administered and the resulting change in pathway flux and enzyme activity expressed together:

$$C^J_{E_i} = \frac{(dJ/J)}{(dI/I)_{ss}} \div \frac{(dv_i/v_i)}{(dI/I)_{S_i,P_i}} \tag{3.10.1}$$

in which the flux through a pathway is controlled by its constituent enzyme, E_i; in this equation, $\frac{(dJ/J)}{(dI/I)_{ss}}$ expresses the change in steady-state (hence the subscript, *ss*) flux due to the inhibitor, I, while $\frac{(dv_i/v_i)}{(dI/I)_{S_i,P_i}}$ expresses the change in the reaction rate through enzyme E_i (at constant substrate and product concentrations,S_i and P_i), due to the same inhibitor concentration. Substrate excess is most useful as they allow the measurement of the inhibition effect without the decrease in substrate concentration also contributing to a decrease in enzyme activity. The ratio between these changes gives the flux control of E_i over the pathway.

This equation offers a simple way of using IAA as a means for determining the control coefficient of GAPDH over glycolysis: indeed this was what Poolman and colleagues [22] used it for.

Chapter 4

Experimental Results

It is important to note that three independent biological repeats were made. They are named chronologically, *I* having been grown and assayed first, *II* second, and *III* third, with a time span of 15 days between the first and the last biological repeat was grown up and harvested.

4.1 Growth Curve Construction

The optical density of two *S. cerevisiae* X2180 cultures was monitored with readings at regular intervals at a wavelength of 600 nm. This was done prior to the growth of repeats *I*, *II*, and *III*, on two cultures with identical growth medium composition and from the same strain as the cultures that would be assayed. These optical density data were plotted as a function of time to visualise the growth of a culture of this strain of yeast with defined starting conditions. Fig. 4.1 shows these curves. We concluded that the rate of biomass yield is reproducible and that an optical density measurement at a wavelength of 600 nm could be used to define the appropriate point in growth for cell harvesting, namely at diauxic shift, as in Du Preez *et al.* [2]. Glucose measurements with urine strips verified that the plateaus seen in the OD_{600} data coincide with glucose depletion.

4.2 Protein Determination

To convert enzyme activiy to specific enzyme activity, a protein determination according to the method of Bradford [116] was performed. The protein yield varied considerably between the different isolates but less so within each one. The cell-free extracts made from the *in-vitro-batch* (see Fig. 3.1) of isolate *I*, *II*, and *III* yielded approximately 1.0, 7.8 and 7.6 $mg.ml^{-1}$ protein, respectively, while the *preinh-batch* extracts contained approximately 0.22 (*I*), 0.64 (*II*), and 0.55 (*III*) $mg.ml^{-1}$ protein. We followed common practice and calculated the protein concentration from multiple dilutions of each sample. The standard

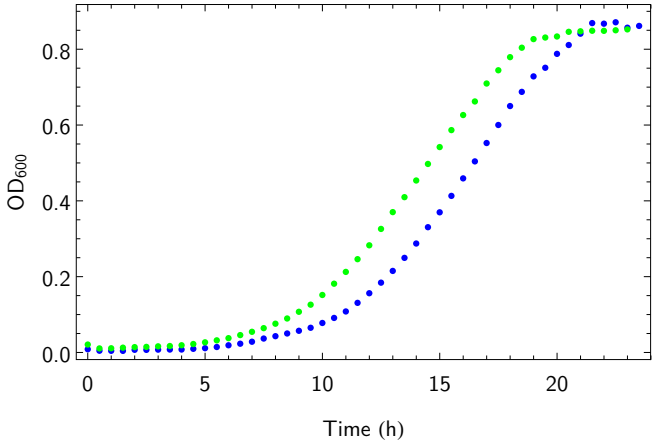

Figure 4.1: Growth of *Saccharomyces cerevisiae* X2180 on 1% (w/v) glucose containing growth media can be accurately tracked to diauxic shift using a spectrophotometer. The green and the blue data points represent the means of two independent duplicate sets of the growth curve data. Glucose measurements using urine strips confirmed that the plateau seen when measuring the OD_{600} of a culture coincides with glucose depletion.

deviation of the protein concentrations exceeded 20% in only one case, where it was close to 21% (see Appendix A). We found this variation acceptable and continued with the calculated values.

The difference in protein yield between isolates were significant. This is probably due to incomplete lysis of cells during glass-bead extraction (see Section 6.4 in the Discussion for more on this). Isolate *I* appeared to be an outlier with respect to *II* and *III*. Full detail of the protein determination results can be seen in Appendix A.

4.3 Measuring GAPDH Activity

GAPDH activity was measured as a function of IAA concentration in each different combination of inhibition methods (prelytic *versus in vitro*), compensation for oxidative damage (DTT *versus* no DTT), and assay direction (forward *versus* reverse). As described in the methodology chapter (Chapter 3), the incubation time in IAA was 60 minutes for whole-cells and for cell-free extract.

Before GAPDH measurements in the aforementioned combinations of conditions were carried out, we ran tests to confirm the irreversibility of IAA's effect on GAPDH (see Appendix B) and whether non-specific NADH oxidation contributes significantly to the observed absorbance change during the reverse GAPDH assays (see Appendix C). It was found that GAPDH inhibition was irreversible over the time scales relevant to our assays, and that non-specific

NADH oxidation was not responsible for any significant absorbance change.

4.3.1 Rate Data Inspection

Appropriate segments of absorbance change were selected (see Appendix D) and the gradients of those data were determined. The mean change in absorbance was taken as the reaction rate, and converted to a NADH concentration change rate (see Appendix E for the absorbance-NADH calibration curve). Specific activity was a clear function of IAA concentration. Appendix F contains more detailed information on the standard error in the data, but the trends were unambiguous in all cases.

The specific activities measured in our study were approximate V_{max} values according to the method of Van Eunen *et al.* [3]. The wild-type $V_{max,GAPDH}$ values that we measured were all lower than the $V_{max,GAPDH}$ paramaters determined by Teusink *et al.* (1; Table 4.2 presents the activities that we measured in all the different combinations of conditions). As will be discussed in this chapter, we chose DTT-containing, prelytically inhibited samples for comparison to the models. In those conditions, we measured approximate forward $V_{max,GAPDH}$ values of 4.15, 2.56, and 2.54 μmol.min^{-1}.mg protein^{-1} for repeats *I*, *II*, and *III*, respectively (Table 4.1). In reverse, we measured 6.96, 4.5, and 4.69 μmol.min^{-1}.mg protein^{-1} (*I*, *II*, and *III*, respectively).

Table 4.1: Simulated and experimentally determined $V_{max,GAPDH}$ values. The Teusink and Du Preez model fluxes are presented (prior to model adjustment) as well as the three independent experimental triplicates (bottom three rows, below the double line). The $V_{max,GAPDH}$ values are measured in μmol.min^{-1}.mg protein^{-1}.

	V_{maxf}	V_{maxr}
Teusink model	4.4	24.3
Du Preez model	1.04	*n/a*
I	4.15	6.96
II	2.56	4.5
III	2.54	4.69

Teusink and colleagues used a forward $V_{max,GAPDH}$ of 4.4 μmol.min^{-1}.mg protein^{-1} and, in the reverse direction, 24.3 μmol.min^{-1}.mg protein^{-1} (Table 4.1). Our measured forward $V_{max,GAPDH}$ is therefore no more than a factor of two removed from the Teusink value, but our measured reverse $V_{max,GAPDH}$ is up to a factor 6 lower than the Teusink values.

Van Eunen *et al.* report measuring an almost 50% lower V_{max} of GAPDH than was measured in so-called "optimised" conditions by Van Hoek *et al.* [118]. The Teusink and Van Hoek buffers are more similar to each other than either is to the Van Eunen buffer (see Chapter 6). One might speculate that the difference in measured V_{max} could be similarly large when comparing data

Table 4.2: Experimentally measured approximate $V_{max,GAPDH}$ values are consistently smaller than the V_{max} values used by Teusink *et al.* [1]. The Teusink V_{max} values were: 4.4 μmol.min^{-1}.mg protein^{-1} forward and 24.3 μmol.min^{-1}.mg protein^{-1} in reverse. All values in the top table are our approximate V_{max} values measured in μmol.min^{-1}.mg protein^{-1} measured in various assay combinations of assay conditions and inhibitor administration methods. The bottom table also gives our V_{max} measurements as a percentage of the corresponding value in the Teusink models.

Absolute $V_{max,GAPDH}$ Values in μmol.min^{-1}.mg protein^{-1}

Isolate	*In vitro* inhibition				Prelytic inhibition			
	Reverse		Forward		Reverse		Forward	
	−DTT	+DTT	−DTT	+DTT	−DTT	+DTT	−DTT	+DTT
I	4.995	6.955	2.869	4.15	5.662	6.941	3.334	3.506
II	3.998	4.497	2.151	2.563	4.059	3.716	2.593	2.719
III	3.732	4.689	1.873	2.536	3.735	5.51	1.984	2.68

%Size of our $V_{max,GAPDH}$ Values against $V_{max,GAPDH}$ Values in Teusink Model

Isolate	*In vitro* inhibition				Prelytic inhibition			
	Reverse		Forward		Reverse		Forward	
	−DTT	+DTT	−DTT	+DTT	−DTT	+DTT	−DTT	+DTT
I	20.56	28.62	65.2	94.32	23.3	28.56	75.77	79.68
II	16.45	18.51	48.89	58.25	16.7	15.29	58.93	61.8
III	15.36	19.3	42.57	57.64	15.37	22.67	45.09	60.91

from the Teusink and the Van Eunen buffers. Moreover, the use of this buffer might affect measured K_m values, too. In this way the forward $V_{max,GAPDH}$ could be affected less strongly than the reverse $V_{max,GAPDH}$ while maintaining the Haldane relationship intact. This matter is discussed in more detail in Section 6.2.

Another contributing factor to the differences in measured $V_{max,GAPDH}$ might be the use of a different strain in our experiments (X2180) than was used by Teusink *et al.* (Koningsgist; [1]). We used the same strain as Du Preez and colleagues [2]. They used a search function which suggested a forward V_{max} that was only 23.6% the size of the forward $V_{max,GAPDH}$ in the Teusink model: the final $V_{max,GAPDH}$ used in *dupreez4* was 1.02 μmol.min^{-1}.mg protein^{-1} in the forward direction (Table 4.1; they do not use an explicit reverse $V_{max,GAPDH}$). They go on to note that their oscillation experiments were performed at between 20°C and 25°C and "(a)ssuming a Q10 value of 2 (i.e. a 10°C decrease

in temperature leads to 1/2 the activity), this temperature would result in up to 50% lower enzyme activities" [2].

If, for argument's sake, one doubles the Du Preez parameters to get hypothetical values of their parameters at 30°C , one would obtain a forward $V_{max,GAPDH}$ of 2.08 μmol.min^{-1}.mg protein^{-1}. This lies close to the 2.56 and 2.54 μmol.min^{-1}.mg protein^{-1} of repeats *II* and *III*, respectively, in our assays.

Within the data sets generated for this study, no more than a factor two difference was observed between any of our our unperturbed, approximate $V_{max,GAPDH}$ values, indicating internal consistency in our experimental method. We did not further investigate the differences between our measured $V_{max,GAPDH}$ values and the literature values.

4.3.2 Addition of DTT

Oxidative inactivation of enzymes has been shown to introduce artefacts into enzymology [122]. The suggestion to reverse this by the addition of DTT [105] was included as a variable in our investigation. 5 mM of DTT was added to test its effect on the inhibition of GAPDH by IAA.

In Table 4.3 it can be seen that higher activities were observed in the presence of DTT in most cases. Only 14 of the 67 data sets had higher activity in the absence of DTT. In eleven of those fourteen cases, the activity of both the DTT-containing and non-DTT-containing reactions were close to zero and heavily influenced by residual noise in the data. The remaining three were the sole outliers to the observed pattern of DTT effects.

The effect of DTT on the percentage inhibition of GAPDH activity by IAA, however, was minimal. Reaction rates were expressed as a percentage of the wild-type (i.e. uninhibited) activity. Across all three biological repeats, DTT did not affect the relative inhibition of GAPDH activity, e.g. in Fig. 4.2 (complete data not shown).

It was decided that the data from DTT-containing assays would be authoritative when analysing other variables, as it represents a condition closer to that encountered *in vivo* (109; 123). For the sake of brevity, data sets without DTT are omitted from further reporting and analysis (see Chapter 6, Discussion, for more on this).

4.3.3 *In vitro* Addition of IAA vs. Prelytic Inhibition

In Fig. 4.3*IA* and *IB*, GAPDH activity was completely or nearly completely abrogated by an hour-long incubation even in small concentrations of IAA *in vitro*, while the GAPDH of prelytically inhibited cell extract remained active at all the assayed IAA concentrations. This data is from repeat *I*. For repeats *II* and *III*, however, the specific activities of cell extracts from *in vitro* and prelytic inhibitions were almost identical (Fig. 4.3). This is also true of normalised

Table 4.3: DTT predictably leads to higher absolute measured activity. The table compares the activity in the presence of DTT and activity in the absence of DTT (*DTT effect = activity(+DTT)/activity(-DTT)*). Wherever *DTT effect > 1*, the data are shown in black and indicate a higher activity in the presence of DTT. A *DTT effect < 1* indicates that higher activity was observed without DTT (in red). Empty cells indicate conditions where data were dropped due to excessive error (Table F.1) and comparisons could not be made. 66 comparisons were made of which 14 had a *DTT effect < 1*. *I*, *II*, and *III* represent the biological triplicates.

I

[IAA] in μM	*In vitro* inhibition		Prelytic inhibition	
	Reverse	Forward	Reverse	Forward
0	1.392	1.446	1.226	1.052
25	1.711	6.085	1.049	1.69
50	0.954	8.113	1.387	1.293
100	0.294	11.663	1.594	
200	-1.825	4.31	1.166	1.196
400	1.014	2.409	2.366	2.975

II

[IAA] in μM	*In vitro* inhibition		Prelytic inhibition	
	Reverse	Forward	Reverse	Forward
0	1.125	1.191	0.916	1.048
18.75	1.014	1.269	1.237	
37.5	1.299	1.264	1.115	0.982
75	1.856	1.207	1.545	3.091
150	1.501		0.	0.676
300	1.352	1.449	0.406	0.

III

[IAA] in μM	*In vitro* inhibition		Prelytic inhibition	
	Reverse	Forward	Reverse	Forward
0	1.256	1.354	1.475	1.351
15.625	1.461	1.424		0.75
31.25	1.71	2.86	1.386	1.007
62.5	1.495		1.725	
125	1.136	4.183	0.738	3.144
250	0.936	0.317	0.	30.424

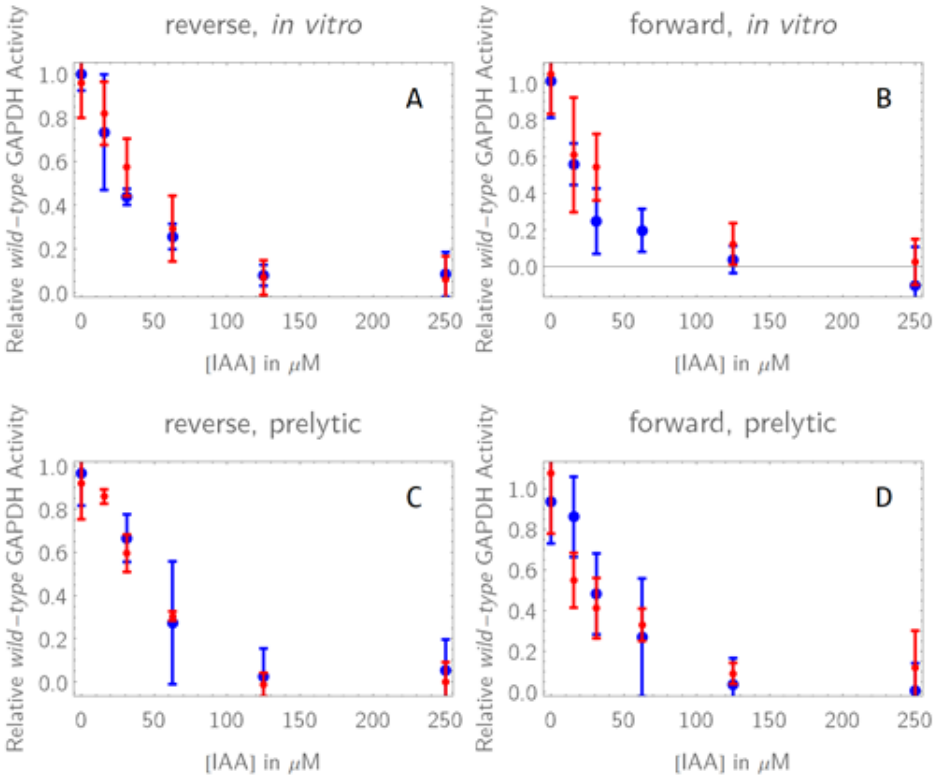

Figure 4.2: DTT did not significantly alter the percentage GAPDH inhibition by IAA. Specific activity was expressed as a percentage of the wild-type (uninhibited) activity at the same conditions. The blue data points indicate assays without DTT while the red points represent assays in the presence of DTT. The data in this figure are from only one biological repeat. *A*, *B*,*C*, and *D* represent the different reaction conditions (described in italicized labels above each graph: "*in vitro*" and "prelytic" referring to the method of inhibitor administration; see text for details). All normalised trends remain stable regardless of DTT addition.

rates, as seen in Fig. 4.4. Repeat *I* also had a significantly lower protein yield (see Section 4.2) and a higher measured $V_{max,GAPDH}$ (see Table 4.2).

The method of inhibitor administration seems to have made a big difference only in repeat *I*. Since a prelytic inhibition be used for both flux and GAPDH activity measurements (Section 3.4), it is a more consistent method for determining glycolytic control. For brevity, all GAPDH activity data presented in the following sections - unless explicitly stated otherwise - will be from the prelytically inhibited cell extract.

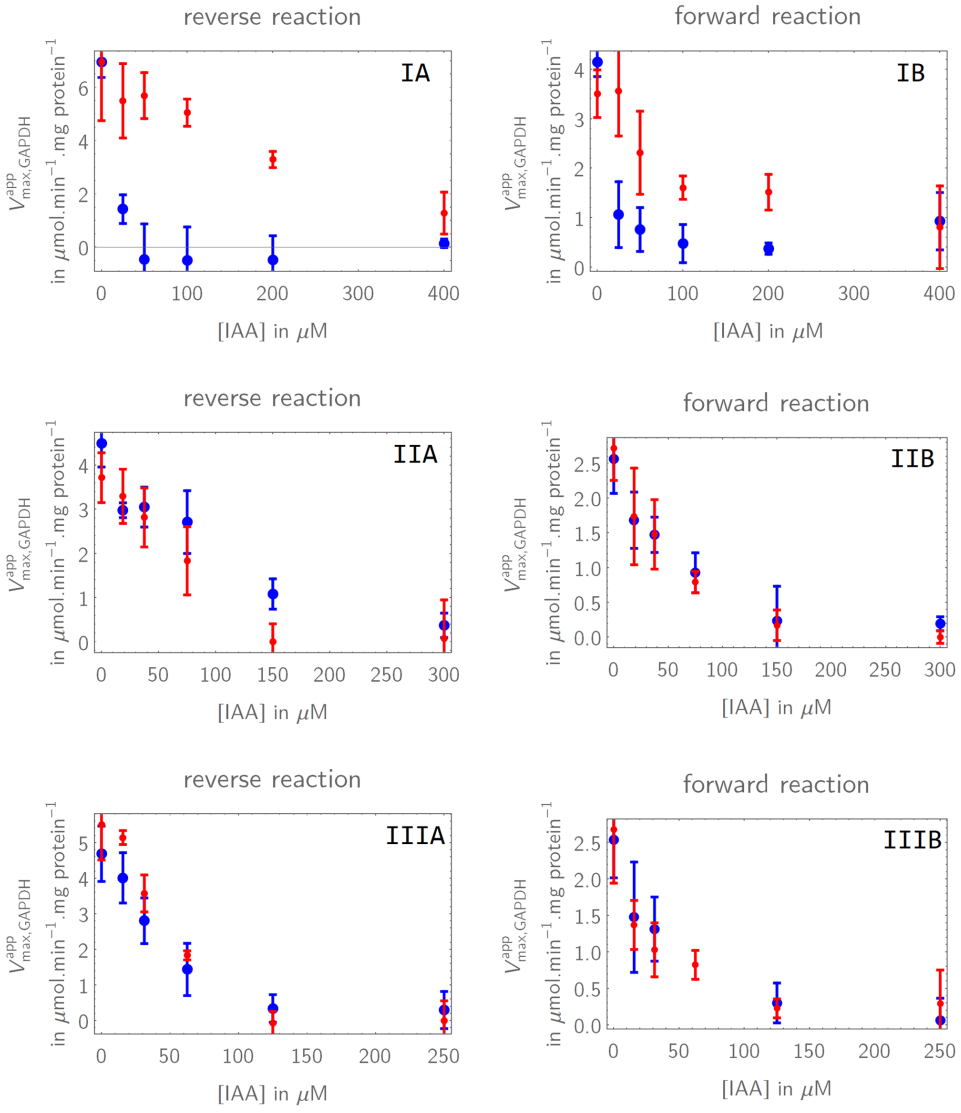

Figure 4.3: *In vitro* and prelytic inhibitor incubations have nearly identical effects in two out of three biological repeats. The data here are approximate measurements of the $V_{max,GAPDH}$ according to the method of Van Eunen *et al.* [3]. These graphics indicate the different consequences of exposing GAPDH to IAA after lysis, by adding it directly to the cell-free extract, *versus* incubating whole cells in a growth medium containing the inhibitor before cell lysis. *I*, *II*, and *III* represent three biological repeats. Those labelled *A* show GAPDH activity when assayed in the reverse direction while *B* shows the same activity when measured in the forward direction. Blue data points indicate the activity measured when IAA was added *in vitro* while the red points indicate the data from prelytically inhibited cell extract.

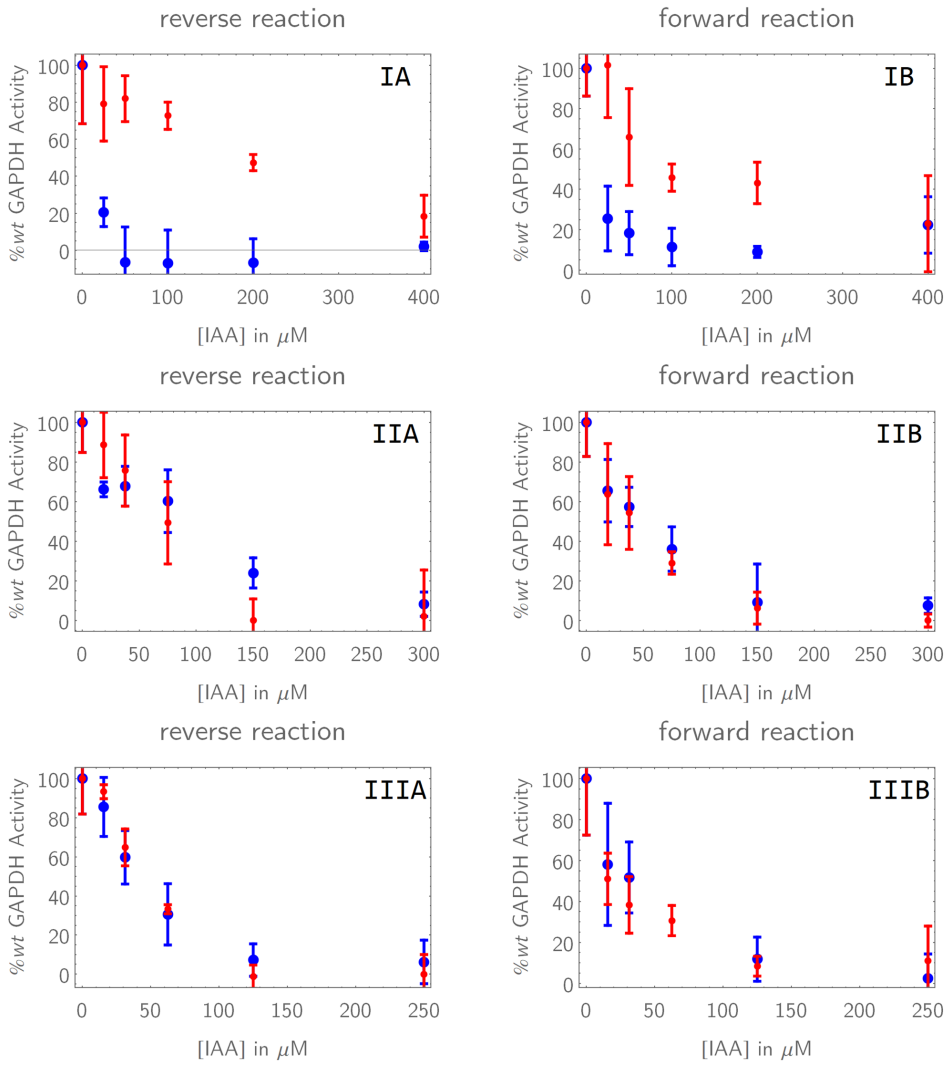

Figure 4.4: *In vitro* and prelytic inhibitor incubations have nearly identical effects in two out of three biological repeats when activity is expressed as a % of the wild-type (uninhibited) activity at the same conditions. These graphics indicate the different effects of administering IAA directly to cell-free extract *versus* incubating whole cells in a growth medium containing the inhibitor before cell lysis. *I*, *II*, and *III* represent the three different biological isolates. Those labelled *A* show reverse GAPDH activity and while *B* shows forward GAPDH activity. Blue data points are from *in vitro* inhibitions while the red points indicate the data from prelytically inhibited cell extract.

4.3.4 Forward and Reverse Activity

The wild-type forward rates were about half the size of the reverse rates (Fig. 4.5). There was also consistent dose-response within repeats but not between them: repeat *I* was especially divergent, particularly at higher [IAA]. This was a trend throughout this study and we return to it in Chapter 6.

Irreversible inhibition kinetics are best described using exponential decay functions [124], and lines were fitted to the absolute activity inhibition data from each biological repeat using the method of least squares (Fig. 4.5). It was striking that $R^2 \geq 0.96$ was obtained for all of these fits. All of the functions were constructed to pass through the y-axis, and this intercept represented the wild-type $V_{max,GAPDH}$ value of the relevant data set (see Subsection 5.2.2). The fitted lines and their functions are all shown in the caption of Fig. 4.5.

The dose-dependent % inhibition of GAPDH activity was almost identical in the forward and reverse directions (see Fig. 4.6). This was, again, true within repeats, but not between them. An exponential decay function was also fitted to these data. For fitting to the % inhibition data, we combined forward and reverse GAPDH activity inhibition data for each repeat (Fig. 4.6). This proved very useful during model analysis (see Subsection 5.2.2 on modelling IAA action on GAPDH). The fits all had $R^2 \geq 0.96$.

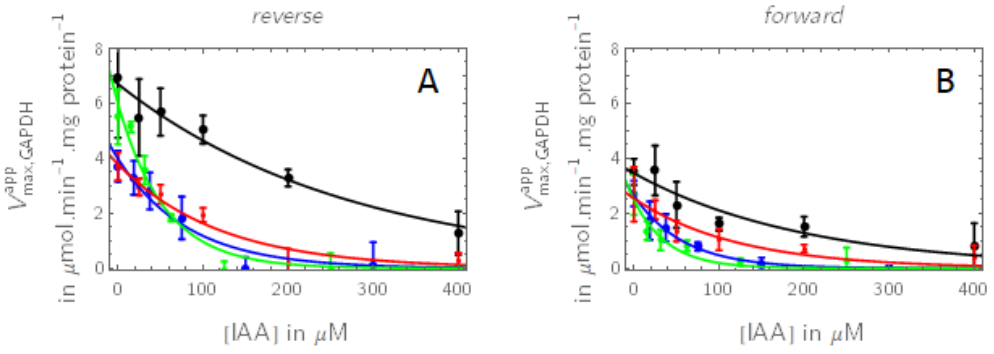

Figure 4.5: Forward and reverse GAPDH activity at substrate-saturating conditions is consistently related to IAA within repeats of the assay but not between repeats. The different colours represent the different biological isolates: the data from isolate I is presented in blue, II in green and III in red. *A* shows the reactions rates measured in the reverse direction while *B* presents the rates of the forward reactions. The fitted lines describe the data of the same colour and are defined by linear equations). They are (R^2 indicated in parentheses): in *A*, *I* in reverse: $V^{app}_{max,GAPDH} = e^{(1.9-0.0037[IAA])}$ (0.995); *II* in reverse: $V^{app}_{max,GAPDH} = e^{(1.4-0.012[IAA])}$ (0.98); *III* in reverse: $V^{app}_{max,GAPDH} = e^{(1.8-0.018[IAA])}$ (0.98). In *B*, *I* forward: $V^{app}_{max,GAPDH} = e^{(1.2-0.0050[IAA])}$ (0.98); *II* forward: $V^{app}_{max,GAPDH} = e^{(0.97-0.017[IAA])}$ (0.996); and *III* forward: $V^{app}_{max,GAPDH} = e^{(0.91-0.025[IAA])}$ (0.97).

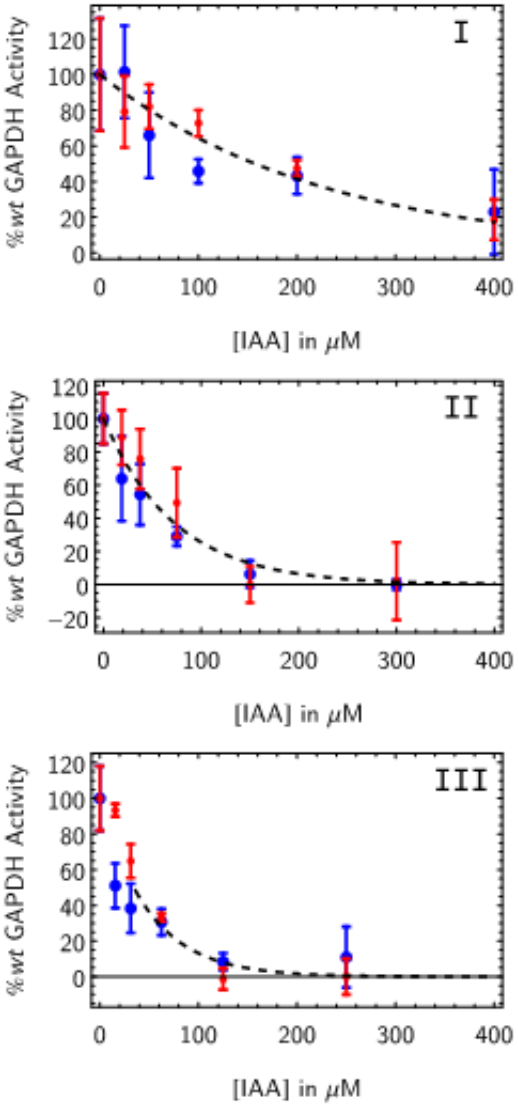

Figure 4.6: Forward and reverse normalised specific GAPDH activity form a single trend to which a function can be fit. The forward and reverse) reactions were each normalised over the measured wild-type GAPDH activity. The data sets of the forward (red) and reverse (blue reactions were then combined and an exponential decay function was fit to them according to the method of least squares. *I*, *II*, and *III* represent the three biological repeats, and yielded fits with the following equations (R^2 indicated in parentheses): *I*: $V^{app}_{max,GAPDH} = e^{(4.6-0.0044[IAA])}$ (0.98); *II* $V^{app}_{max,GAPDH} = e^{(4.6-0.014[IAA])}$ (0.98); and *III* $V^{app}_{max,GAPDH} = e^{(4.6-0.020[IAA])}$ (0.96).

4.4 Ethanol Production Rate

Glucose was not fixed during the incubations, hence what was measured was not technically steady-state fluxes. Substrate was added in excess, however, so the rates of glucose import and product formation are initially not substrate-limited and will be treated as equivalent to steady-state fluxes.

4.4.1 Ethanol Production Rate Determination

The ethanol concentrations (see Appendices G and H for more on their determination), were expressed as a function of time during sample incubation in 20 mM of glucose. The initial ethanol increase that would represent flux was selected by inspection (for example in Fig. 4.7). A linear model fit was done on each sample's initial segment: all fits had $R^2 > 0.95$, except where the gradients were near-zero (Table 4.4).

Near-zero gradients indicate very low ethanol production, and small standard deviations therefore had a disproportionate impact on their goodness-of-fit: these small R^2 values constituted only a fifth of all fits (see Fig. 4.8). Furthermore, of the 15 fits with R^2 values greater than 0.95, 13 had R^2 upwards of 0.99. The fits to the ethanol production data were therefore quite good. No fewer than six out of every data set's ten points (equal to 50 minutes of incubation) were used for fitting, so the trends were representative.

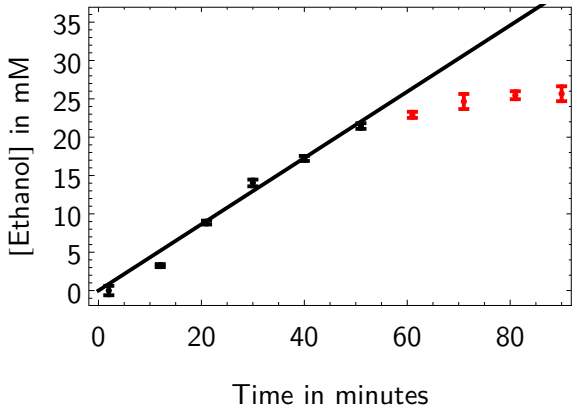

Figure 4.7: Example of ethanol production time-course. This sample was incubated in 18.75 μM of IAA for an hour. Ethanol concentration over time gave the production rate. Linear model fits through these data were forced through the origin and selected to reflect the substrate-saturating part of the incubation. The black points and black solid line represent the experimental data and the linear fit on those data, respectively. The red data points represent experimental data that were located at substrate-limiting conditions and excluded from the fit. The linear fit's equation was $y = 0.43x$ and had an $R^2 = 0.995$.

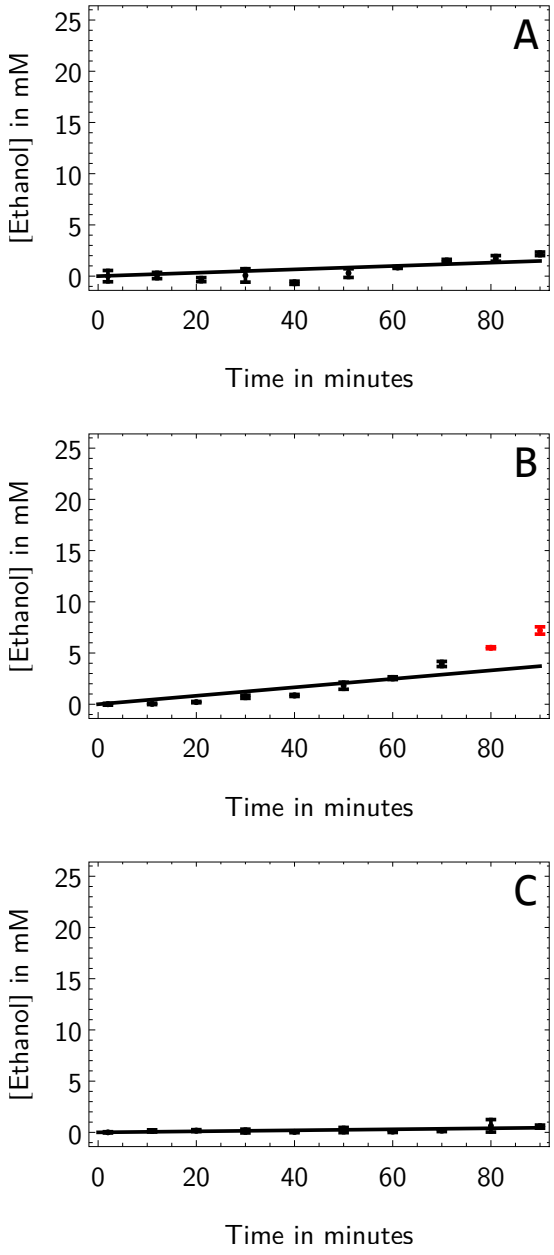

Figure 4.8: Fits with $R^2 \leq 0.95$. Low ethanol concentrations magnify the impact of slight standard deviations on the goodness-of-fit measure. The red points on B were not included in the calculation of the linear model fit. A was constructed with cells (from isolate II) that were inhibited with 300 μM IAA and had an $R^2 = 0.6955$. B (from isolate III) was inhibited with 125 μM and had an $R^2 = 0.9020$. C (also from III was inhibited with 250 μM and had an $R^2 = 0.8010$

Table 4.4: Coefficients of determination of linear model fits on ethanol production data show high goodness-of-fit. Only seven of the fifteen fits have $R^2 \leq 0.99$ (in red) and only three have $R^2 \leq 0.95$ (red and underlined). These strong correlations support the validity of the fits as descriptions of ethanol production rate. The fluxes and their standard error are also shown in the table below (measured in the same units of μmol.min^{-1}.mg protein^{-1}).

Isolate I:		Isolate II:		Isolate III:	
[IAA] in μM =	0	[IAA] in μM =	0	[IAA] in μM =	0
R^2 =	0.9953	R^2 =	0.9931	R^2 =	0.9968
Flux (μmol.min^{-1}.mg prot^{-1}) =	0.152	Flux (μmol.min^{-1}.mg prot^{-1}) =	0.117	Flux (μmol.min^{-1}.mg prot^{-1}) =	0.122
Standard Error of flux =	0.016	Standard Error of flux =	0.011	Standard Error of flux =	0.007
[IAA] in μM =	25	[IAA] in μM =	18.75	[IAA] in μM =	15.625
R^2 =	0.9961	R^2 =	0.9944	R^2 =	0.9967
Flux (μmol.min^{-1}.mg prot^{-1}) =	0.14	Flux (μmol.min^{-1}.mg prot^{-1}) =	0.101	Flux (μmol.min^{-1}.mg prot^{-1}) =	0.136
Standard Error of flux =	0.013	Standard Error of flux =	0.009	Standard Error of flux =	0.009
[IAA] in μM =	50	[IAA] in μM =	37.5	[IAA] in μM =	31.25
R^2 =	0.9820	R^2 =	0.9801	R^2 =	0.9583
Flux (μmol.min^{-1}.mg prot^{-1}) =	0.118	Flux (μmol.min^{-1}.mg prot^{-1}) =	0.1	Flux (μmol.min^{-1}.mg prot^{-1}) =	0.083
Standard Error of flux =	0.024	Standard Error of flux =	0.016	Standard Error of flux =	0.02
[IAA] in μM =	100	[IAA] in μM =	75	[IAA] in μM =	62.5
R^2 =	0.9973	R^2 =	0.9922	R^2 =	0.9906
Flux (μmol.min^{-1}.mg prot^{-1}) =	0.096	Flux (μmol.min^{-1}.mg prot^{-1}) =	0.086	Flux (μmol.min^{-1}.mg prot^{-1}) =	0.107
Standard Error of flux =	0.008	Standard Error of flux =	0.009	Standard Error of flux =	0.012
[IAA] in μM =	200	[IAA] in μM =	150	[IAA] in μM =	125
R^2 =	0.9937	R^2 =	0.9727	R^2 =	0.9020
Flux (μmol.min^{-1}.mg prot^{-1}) =	0.07	Flux (μmol.min^{-1}.mg prot^{-1}) =	0.042	Flux (μmol.min^{-1}.mg prot^{-1}) =	0.011
Standard Error of flux =	0.009	Standard Error of flux =	0.011	Standard Error of flux =	0.005
[IAA] in μM =	400	[IAA] in μM =	300	[IAA] in μM =	250
R^2 =	0.9924	R^2 =	0.6955	R^2 =	0.8010
Flux (μmol.min^{-1}.mg prot^{-1}) =	0.063	Flux (μmol.min^{-1}.mg prot^{-1}) =	0.005	Flux (μmol.min^{-1}.mg prot^{-1}) =	0.002
Standard Error of flux =	0.008	Standard Error of flux =	0.005	Standard Error of flux =	0.001

A comparison of these data for each biological repeat showed that the rate at which ethanol concentration increases, slows down as the inhibitor concentration increases (Fig. 4.9). The rate of ethanol production could then be calculated as the first derivative of the lines in Fig. 4.9. These data were expressed as a function of IAA concentration to show the inhibitory effect.

Glycolytic flux was normalised to the mg of total protein present in each incubation. In Fig.4.10*A* the normalised ethanol production rates of the three biological repeats are compared. For the uninhibited fluxes, we found ethanol production rates between 0.1 and 0.15 μmol.min^{-1}.mg protein^{-1} (see Table 4.4), which is about a factor of five smaller than the 0.5 μmol.min^{-1}.mg protein^{-1} reported by Teusink *et al.* [1]. This scales to our $V_{max,GAPDH}$ values, that were also between a factor of two and ten smaller than the Teusink parameters. Finally, the effects of increasing IAA on the different biological repeats were clearly dose-dependent within samples but not so between samples (see Section 6.4 for more on this).

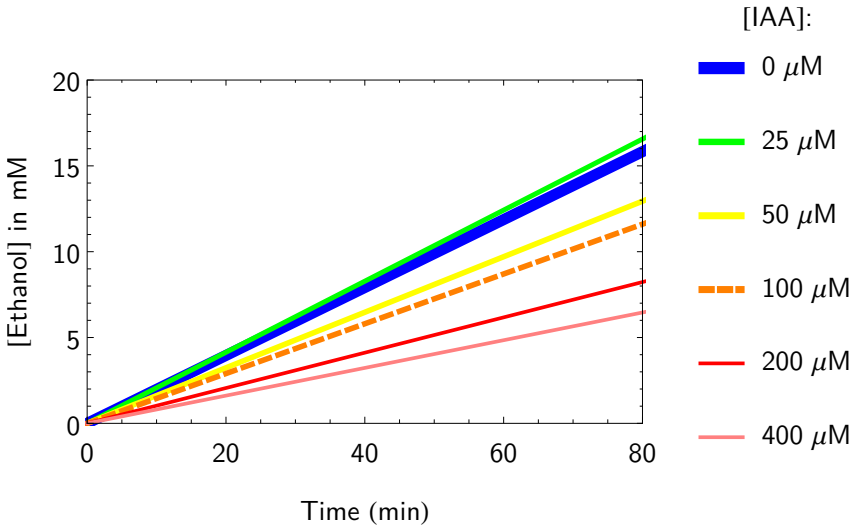

Figure 4.9: Example of a comparison of linear fits on the ethanol production rates at varying IAA concentrations (isolate I). The legend on the right-hand side indicates the IAA concentrations to which the different samples were exposed before the incubation took place. A clear IAA concentration-dependent effect was visible within each of the three biological repeats (II and III not shown).

Fig. 4.10*B* presents ethanol flux as a percentage of the wild-type flux. The normalised inhibition plots show that, for the inhibition of ethanol flux, the three biological repeats are comparable, though more disparity is observed at high IAA concentrations. Normalisation appeared to not improve the agreement between the repeats by much. This disparity was worst when comparing repeat *I* to the other two repeats (see Section 6.4).

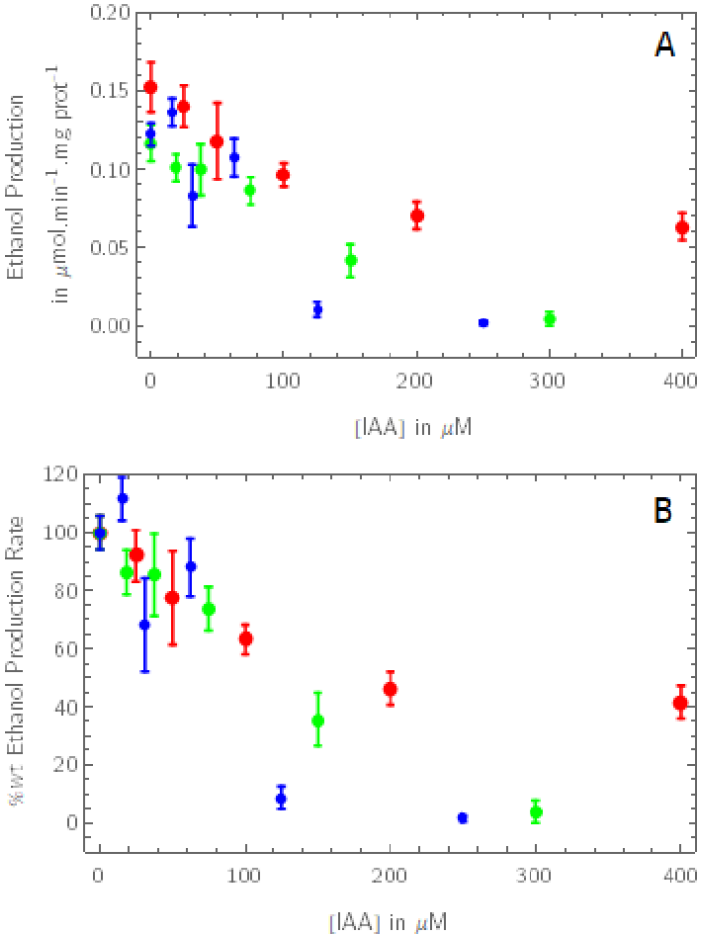

Figure 4.10: Specific and normalised ethanol production rates. *A* depicts the relationship between specific ethanol production rate and IAA concentration while *B* represents the same relationship but with ethanol production expressed as a percentage of the wild-type (uninhibited) specific flux. The different-coloured dots represent the three biological repeats (I in red, II in green, and III in blue).

4.5 Glucose Consumption Rate

Glucose consumption was also tracked by enzymatically assaying aliquots from 10-minute intervals over a 90-minute incubation. A more detailed description of the process of interpreting the raw data, is given in Appendix I.

Glucose concentrations were expressed as a function of time. Linear model fits were carried out on each of the data sets. The functions were all forced through 20 mM of glucose at 0 minutes time (the starting glucose concentration of all the incubations). In all but one of the data sets, five or more of the data points were used (40 minutes of more of the incubation). In the remaining data set, four points were used (Fig. 4.11). Only outliers and points at the plateaus of the glucose consumption curves were discarded. All of the fits had an $R^2 > 0.99$ (Table 4.5).

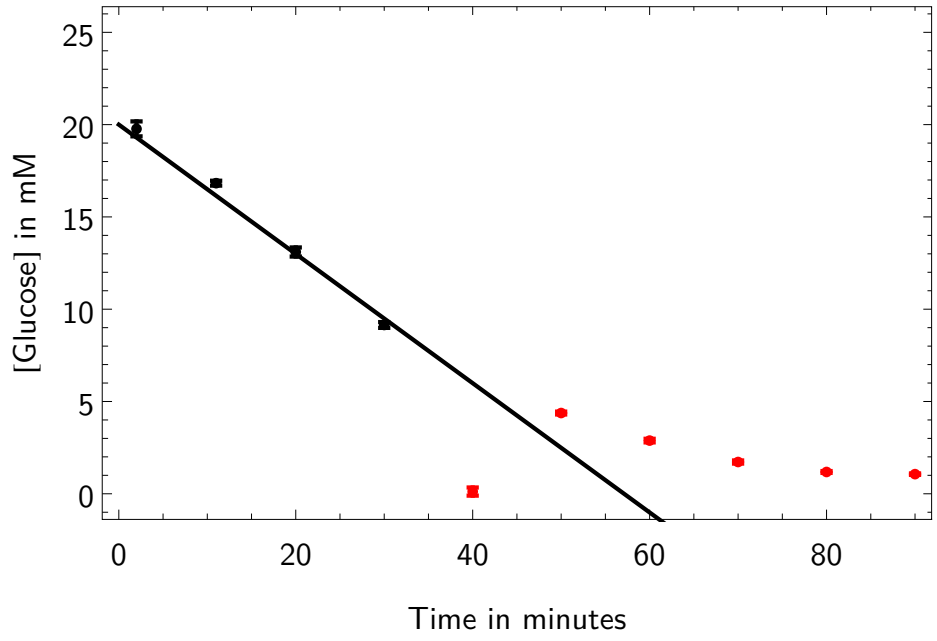

Figure 4.11: Example of glucose consumption by *S. cerevisiae* X2180. The graph shows the decrease in glucose concentration over time in the presence of yeast cells. The cells in this incubation (from isolate III) were inhibited with 15.625 μM of IAA. The black data points represent the experimentally measured glucose concentrations at each time point which were used for fitting. The red points are the points that were discarded during fitting. The black line is the linear model fit describing glucose consumption and has a function $y = 20 - 0.35x$ and an $R^2 = 0.999$.

Table 4.5: Coefficients of determination of linear model fits on glucose consumption data. All fits have $R^2 \geq 0.99$. These strong correlations support the validity of the fits as descriptions of glucose consumption rate. The fluxes and their standard error are also shown in the table below (measured in the same units of μmol.min^{-1}.mg protein^{-1}).

Isolate I:		Isolate II:		Isolate III:	
[IAA] in μM =	0	[IAA] in μM =	0	[IAA] in μM =	0
R^2 =	0.9975	R^2 =	0.9963	R^2 =	0.9992
Flux (μmol.min^{-1}.mg prot^{-1}) =	0.128	Flux (μmol.min^{-1}.mg prot^{-1}) =	0.094	Flux (μmol.min^{-1}.mg prot^{-1}) =	0.107
Standard Error of flux =	0.014	Standard Error of flux =	0.01	Standard Error of flux =	0.005
[IAA] in μM =	25	[IAA] in μM =	18.75	[IAA] in μM =	15.625
R^2 =	0.9985	R^2 =	0.9995	R^2 =	0.9991
Flux (μmol.min^{-1}.mg prot^{-1}) =	0.112	Flux (μmol.min^{-1}.mg prot^{-1}) =	0.083	Flux (μmol.min^{-1}.mg prot^{-1}) =	0.118
Standard Error of flux =	0.01	Standard Error of flux =	0.003	Standard Error of flux =	0.007
[IAA] in μM =	50	[IAA] in μM =	37.5	[IAA] in μM =	31.25
R^2 =	0.9908	R^2 =	0.9993	R^2 =	0.9997
Flux (μmol.min^{-1}.mg prot^{-1}) =	0.14	Flux (μmol.min^{-1}.mg prot^{-1}) =	0.092	Flux (μmol.min^{-1}.mg prot^{-1}) =	0.093
Standard Error of flux =	0.025	Standard Error of flux =	0.004	Standard Error of flux =	0.003
[IAA] in μM =	100	[IAA] in μM =	75	[IAA] in μM =	62.5
R^2 =	0.9970	R^2 =	0.9979	R^2 =	0.9993
Flux (μmol.min^{-1}.mg prot^{-1}) =	0.101	Flux (μmol.min^{-1}.mg prot^{-1}) =	0.09	Flux (μmol.min^{-1}.mg prot^{-1}) =	0.111
Standard Error of flux =	0.014	Standard Error of flux =	0.007	Standard Error of flux =	0.005
[IAA] in μM =	200	[IAA] in μM =	150	[IAA] in μM =	125
R^2 =	0.9976	R^2 =	0.9938	R^2 =	0.9967
Flux (μmol.min^{-1}.mg prot^{-1}) =	0.072	Flux (μmol.min^{-1}.mg prot^{-1}) =	0.04	Flux (μmol.min^{-1}.mg prot^{-1}) =	0.016
Standard Error of flux =	0.015	Standard Error of flux =	0.008	Standard Error of flux =	0.007
[IAA] in μM =	400	[IAA] in μM =	300	[IAA] in μM =	250
R^2 =	0.9994	R^2 =	0.9995	R^2 =	0.9998
Flux (μmol.min^{-1}.mg prot^{-1}) =	0.051	Flux (μmol.min^{-1}.mg prot^{-1}) =	0.003	Flux (μmol.min^{-1}.mg prot^{-1}) =	-0.001
Standard Error of flux =	0.009	Standard Error of flux =	0.004	Standard Error of flux =	0.003

Fluxes were calculated for each incubation as the first derivative of the line fitted to glucose consumption data (Fig. 4.11). Fig. 4.12*A* shows the specific rates of glucose consumption as a function of IAA concentration. Fig. 4.12*B* shows these rates as percentages of the the wild-type glucose consumption. Clear dose-dependence was seen within repeats, but not between them.

Both the ethanol and glucose fluxes measured in our study were lower than the fluxes reported by Teusink and colleagues [1]. For instance, we reported ethanol production rates ranging between 0.1 and 0.15 μmol.min^{-1}.mg protein^{-1}, while Teusink *et al.* observed an ethanol flux of 0.50μmol.min^{-1}.mg protein^{-1}. Similarly, our measured glucose flux was between 0.09 and 0.13 μmol.min^{-1}.mg protein^{-1} (see Table 4.5), while the Teusink value was 0.40 μmol.min^{-1}.mg protein^{-1}. The fact that our measured $V_{max,GAPDH}$ values were also 2 to 10 times smaller, fits with this observation.

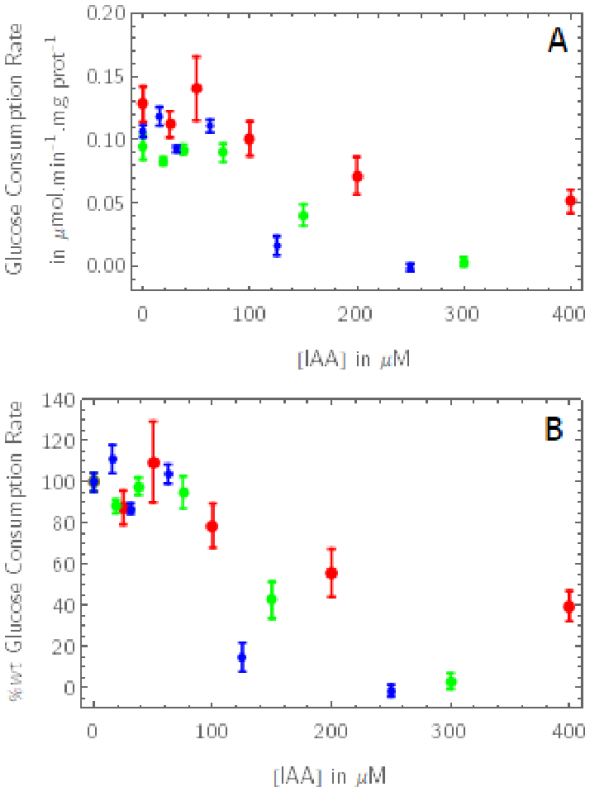

Figure 4.12: Specific and normalised glucose consumption rates exhibit dose dependence with IAA concentration. *A* depicts the relationship between specific glucose consumption rate and IAA concentration while *B* represents the same relationship but with glucose consumption expressed as a percentage of the wild-type (uninhibited) rate. The different-coloured data points represent the three biological repeats (I in red, II in green, and III in blue).

Fig. 4.13 compares the glucose consumption and ethanol production rates. The data from these assays indicate an almost 1:1 ratio of ethanol produced for glucose consumed. Presumably, carbon is lost to the branches and during pyruvate decarboxylation. Albers *et al.* [43] indicate a glucose to ethanol flux ratio of 3:4. We did not investigate the fluxes over the other metabolic branches, but it appears that flux distribution is independent of [IAA].

When the flux data were normalised to their wild-type values, the % effect of increasing IAA concentrations on glycolytic flux were obtained. Figure 4.14 shows ethanol production and glucose consumption as a function of IAA concentration. For control analysis, the relationship between glycolytic flux and IAA needed to be quantified. The effect of IAA on glycolysis is non-linear, but we only needed to describe the initial trend: it was evident in the data that a linear function could describe the initial relationship between glycolytic flux and IAA concentration. Lines were fitted to the four lowest IAA concentrations to yield R^2 values upwards of 0.97. The fits and their coefficients of determination are all presented in Fig. 4.14.

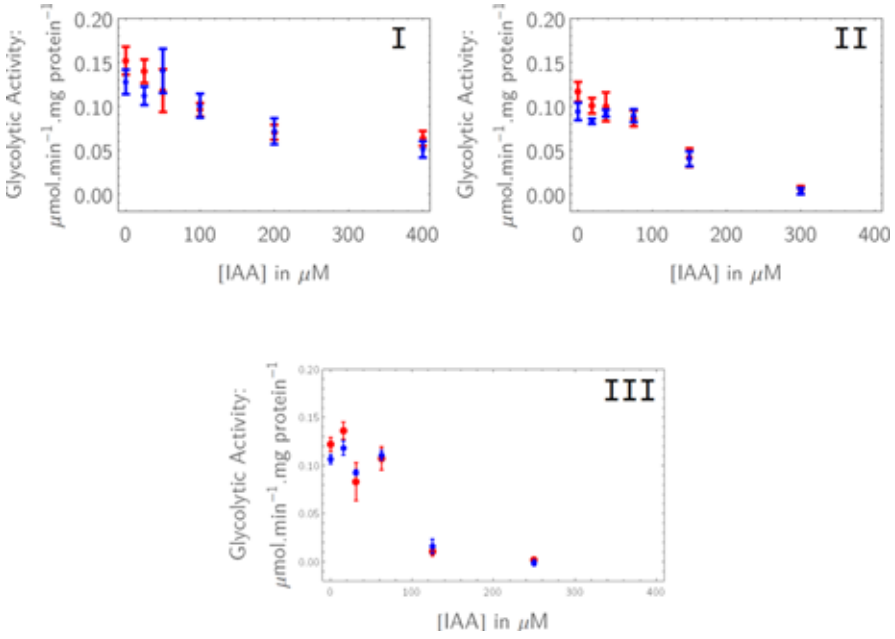

Figure 4.13: The specific ethanol production rate and the specific glucose consumption rate show similar trends within each repeats, although this rate differed between repeats. *I*, *II*, and *III* represent the different biological repeats, with different IAA ranges between 0 and 400 μM (maximum IAA concentrations of 400 μM , 300 μM , and 250 μM , respectively). It is clear from this data that a percentual expression of the glucose consumption and ethanol production rates should also correlate well with each other.

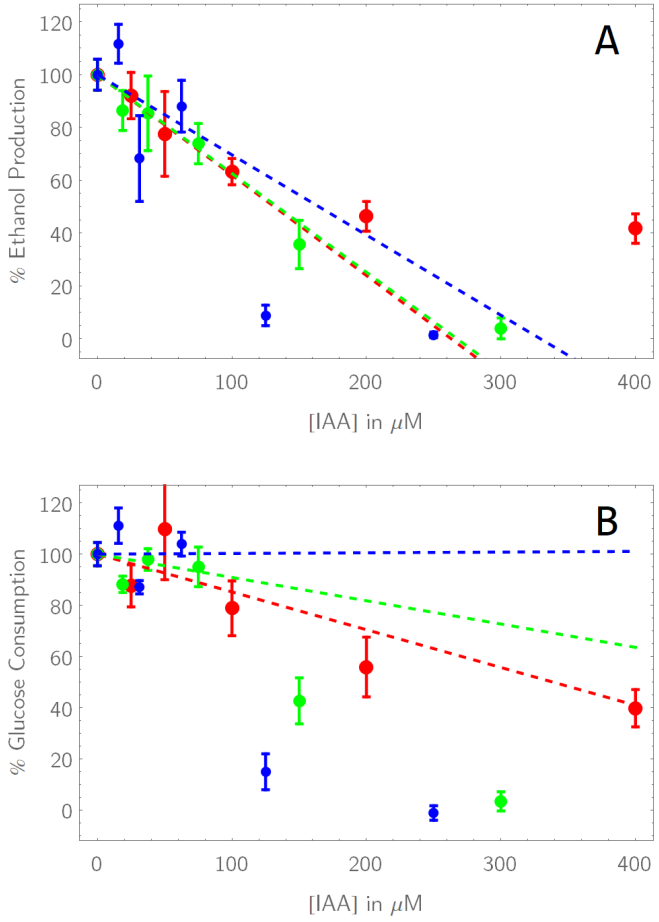

Figure 4.14: Fits obtained to low-IAA flux perturbation data for all three repeats. When the flux data were normalised to their wild-type values, the $\%wt$flux could be plotted as a function of IAA concentration. In A, the normalised ethanol production *versus* IAA concentration is shown, and, in B, the same is shown for glucose consumption. Linear fits according to the method of least squares yielded the functions that are shown as dashed lines, all with $R^2 \geq 0.97$ (red for repeat I, green for II, and blue for III). Only the first four data points (i.e. the four lowest IAA concentrations) were used for the fits, as the flux-to-IAA relation was aptly described by a linear function for the first four data points in each repeat. The fitted functions were (with R^2 in parentheses): for I, $\%Ethanol\,Flux = 100 - 0.38 \cdot [IAA]$ ($R^2 = 0.999$) and $\%Glucose\ Flux = 100 - 0.15 \cdot [IAA]$ ($R^2 = 0.99$); for II, $\%Ethanol\ Flux = 100 - 0.37 \cdot [IAA]$ ($R^2 = 0.998$) and $\%Glucose\ Flux = 100 - 0.091 \cdot [IAA]$ ($R^2 = 0.997$); and for III, $\%Ethanol\ Flux = 100 - 0.30 \cdot [IAA]$ ($R^2 = 0.98$) and $\%Glucose\ Flux = 100 - 0.0027 \cdot [IAA]$ ($R^2 = 0.992$).

4.6 Glycolytic Flux Control

Glycolytic flux was plotted against specific activity, and yielded a clear trend (Fig. 4.15). This was true regardless of the direction in which the reaction was measured or of the method by which glycolytic flux was measured (see also Fig. 4.14). Considerable scatter was visible when combining these data expressed as percentages of the uninhibited activity. Neither the chosen glycolytic flux assay (Fig. 4.16*A*) or the chosen GAPDH activity assay (Fig. 4.16*B*) deviated too strongly from the other, except perhaps for ethanol production having consistently lower % values than glucose consumption. The most significant deviation in the data was found when comparing the different biological repeats to each other.

Repeat I diverged from II and III: not only was it the only isolate in which full inhibition was not observed in the inhibitor range used (Fig. 4.6 and 4.13) but it had a much higher wild-type $V_{max,GAPDH}$ and a lower protein yield (see earlier, e.g. Fig. 4.6); finally, it was also the only one amongst the triplicate set for which the *in vitro* and prelytic methods of administering IAA yielded different results (Fig. 4.4). All of these exceptions to the behaviour of the other two isolates rendered the data from repeat *I* suspect.

GAPDH activity data (*A*), the %*wild-type* ethanol flux (*B*) and the %*wild-type* glucose flux (*C*) were separately expressed as a function of IAA concentration (Fig. 4.17 shows these plots for the combined data of repeat *II* and *III*). The exponential decay functions fitted to the GAPDH activity titration data (Fig. 4.6) and the linear fits to the initial flux inhibition data (Fig. 4.14) allowed us to calculate a glycolytic flux control coefficient for GAPDH in *S. cerevisiae*, both in terms of glucose consumption and in terms of ethanol production. The equation for the flux control coefficient of GAPDH, would be (adapted from Eq. 2.3.2):

$$C^{J}_{v_{GAPDH}} = \frac{dJ/J}{dv_{GAPDH}/v_{GAPDH}}$$

The following equations express glycolytic flux control by GAPDH at near-zero inhibition:

$$C^{J_{EtOH}}_{v_{GAPDH}} = \frac{-0.0165221 \cdot e^{4.60517-0.0165221[IAA]}}{-0.345396}$$

$$C^{J_{GLCo}}_{v_{GAPDH}} = \frac{-0.0165221 \cdot e^{4.60517-0.0165221[IAA]}}{-0.0526257}$$

The functions are solved for $[IAA] = 0$, yielding:

$$C_{v_{GAPDH}}^{J_{EtOH}} = 0.21$$

$$C_{v_{GAPDH}}^{J_{GLCo}} = 0.032$$

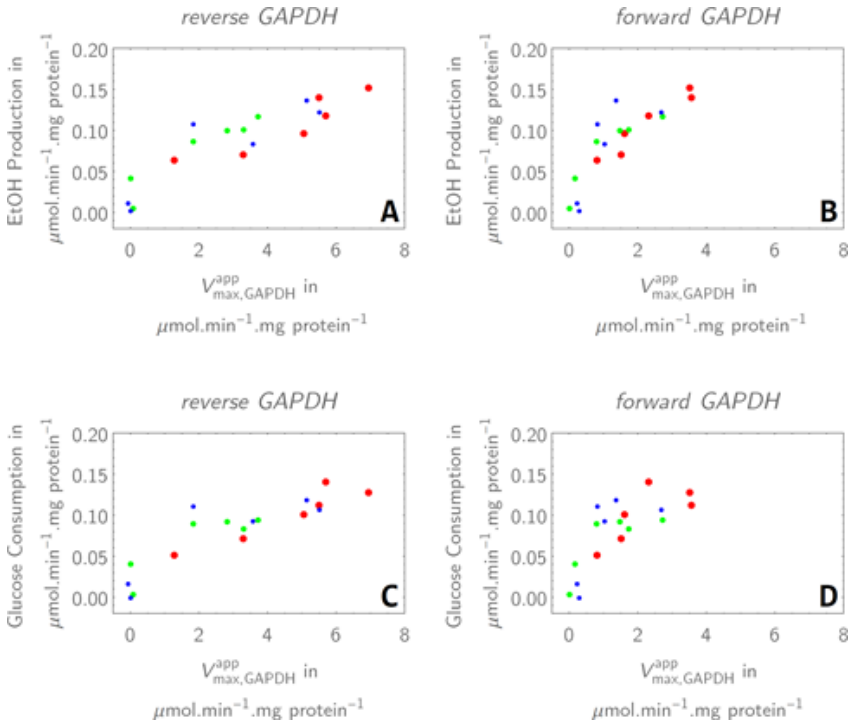

Figure 4.15: Glycolytic activity as a function of the apparent $V_{max,GAPDH}$, according to the method of Van Eunen *et al.* [3]. Various combinations of metrics show the relationship between absolute carbon flux and absolute $V_{max,GAPDH}^{app}$: A and B show ethanol production flux, while C and D track glucose consumption; A and C show reverse GAPDH activity while B and D present the forward activity. The red data points are the data from biological repeat I, green from II and blue from III. Besides for the lower $V_{max,GAPDH}^{app}$ of the forward GAPDH reaction, which is in agreement with existing biochemical knowledge, no single combination of metrics exhibited aberrant behaviour when expressed in absolute terms.

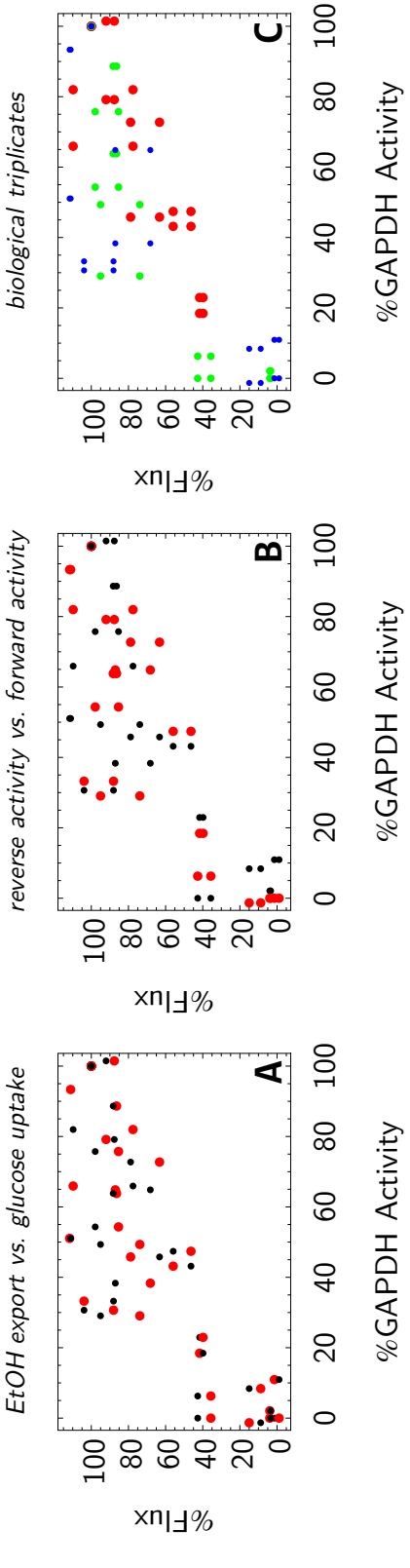

Figure 4.16: Glycolytic flux is only weakly controlled by GAPDH. All three graphs show our measured $\%wt$ glycolytic flux as a function of $\%wt$ GAPDH activity. *A* differentiates between data sets where ethanol production is the metric of glycoytic activity (red) *versus* data sets where the glycolytic activity is rendered as glucose consumption. *B* differentiates between GAPDH in the reverse (red) *versus* in the forward (black) direction. *C* distinguishes the biological repeats: I in red, II in green and III in red.

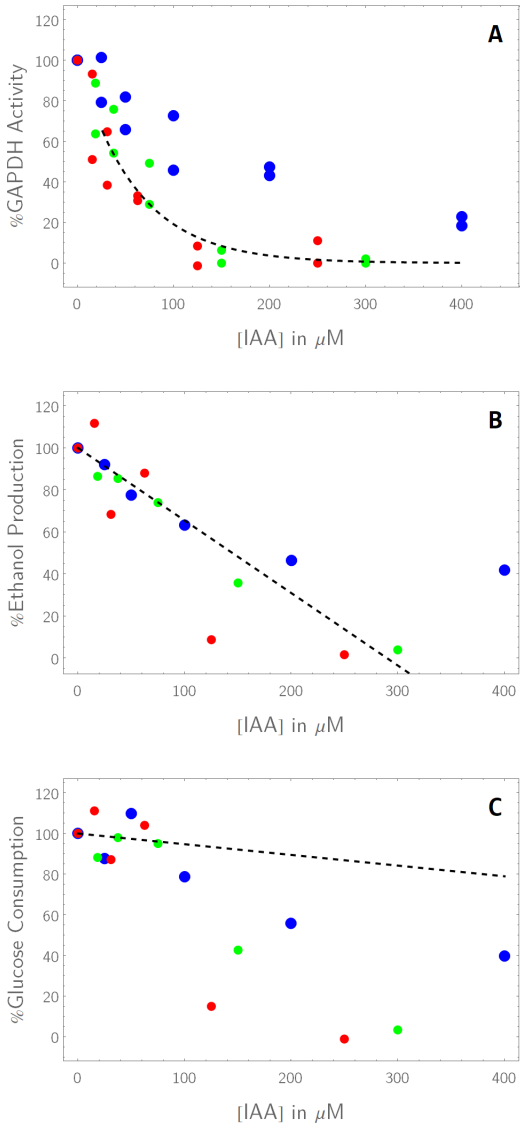

Figure 4.17: Independent fits to the flux and the GAPDH activity decrease data allows the calculation of the glycolytic flux control coefficient of GAPDH. The plots in this figure show the fits, according to the method of least squares, to the relative GAPDH activity (plot A), the relative ethanol production (B), and the relative glucose consumption data (C). In each case, the flux or enzyme activity was normalised to its wild-type value and plotted as a function of IAA concentration. Repeat I is represented in blue, II in green, and III in red. Due to the consistent outlier behaviour of repeat I, the fits were only to the data from II and II. An exponential decay function was fit to the GAPDH activity data, forward and reverse, that yielded the function $\%GAPDHActivity = 100\% \cdot e^{4.60517-0.0165221[IAA]}$, with an R^2 value of 0.96. For the ethanol and glucose fluxes, linear functions were fit to the first four points of the data, yielding functions of $\%EthanolFlux = 100 - 0.345396[IAA]$ ($R^2 = 0.99$) and $\%GlucoseFlux = 100 - 0.0526257[IAA]$ ($R^2 = 0.994$).

Chapter 5

Model Analysis

The kinetic models of glycolysis in *Saccharomyces cerevisiae* by Du Preez *et al.* [2] and Teusink *et al.* [1] were analysed for comparison to experimental GAPDH inhibition data. These models can be found on the JWS Online model repository as the teusink model and the dupreez4 models (referred to in this thesis as the Teusink and the Du Preez models, respectively).

5.1 Modelling IAA Action

The first question when comparing model predictions to experimental results is how to best simulate the experimental methods *in silico*. IAA was used to selectively perturb the activity of GAPDH, which is represented in the Teusink [1] and Du Preez [2] models in terms of reversible two-substrates, two-products Michaelis-Menten kinetics.

5.1.1 The Importance of Irreversibility

IAA is regarded as a textbook example of an irreversible enzyme inhibitor [22, 23, 93]. It covalently modifies GAPDH by alkylating an active-site cysteine residue, blocking it to inhibit the binding of substrates. Therefore, unlike reversible inhibition, which is kinetically described with a binding term, irreversible inhibition can be understood as a removal of enzymes from the pool of possible catalysts [125]:

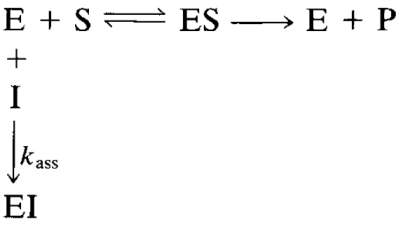

Figure 5.1: Irreversible inhibition removes enzymes from the pool of possible catalysts. In this scheme, E represents the enzyme, S and P the substrate and product, respectively, and I the inhibitor. EI and ES are enzyme-inhibitor and enzyme-substrate complexes. k_{ass} expresses the rate at which the inhibitor binds to the enzyme and captures the time dependence of irreversible inhibition.

The scheme in Fig. 5.1 shows how an irreversible inhibitor, such as IAA, sequesters enzymes in a time-dependent manner (as captured by k_{ass}). This can also be expressed in an equation representing the different states of the total enzyme concentration.

$$[E]_0 = [E]_{bi} + [E]_f \tag{5.1.1}$$

where $[E]_0$ represents total enzyme, $[E]_{bi}$ represents total inhibitor-bound enzyme, and $[E]_f$ represents total free enzyme (which includes enzymes in which the active site is occupied by a substrate). In the presence of an irreversible inhibitor some of the enzymes in the catalyst pool are occupied by the inhibitory substance and therefore inoperative. A similar equation can be constructed for the inhibitor:

$$[I]_0 = [I]_{be} + [I]_f$$

where, as before, $[I]_0$ is the total inhibitor concentration, $[I]_{be}$ the enzyme-bound inhibitor, and $[I]_f$ the total free IAA. IAA is understood to be promiscuous in its binding [96], however, and being covalently bound to other cysteine residues removes IAA from the pool of IAA molecules that can cause GAPDH inhibition. IAA concentration can therefore be expressed as the sum of free IAA ($[I]_f$), non-specifically bound IAA ($[I]^{ns}_{be}$, which includes IAA bound to GAPDH, but not to the inhibition site), and GAPDH-bound IAA ($[I]^{s}_{be}$, which includes only inhibitory binding):

$$[I]_0 = [I]^{ns}_{be} + [I]^{s}_{be} + [I]_f \tag{5.1.2}$$

IAA can only bind to a single cysteinyl thiol on GAPDH to exert its inhibitory effect, hence $[I]^{s}_{be}$ and $[E]_{bi}$ are equivalent expressions. The amount

of free enzyme, $[E]_f$, can be understood in terms of the concentration of inhibitor administered to the cell or cell-free extract:

$$[E]_f = [E]_0 - [I]_0 + [I]_f + [I]_{be}^{ns}$$

Since IAA-binding is time-dependent (Fig. 5.1), a maximal inhibition will be reached after a given amount of time, which can be interpreted as the depletion of unbound free inhibitor:

$$[E]_f = [E]_0 - [I]_0 + [I]_{be}^{ns} \tag{5.1.3}$$

Equation 5.1.3 shows that at the time of inhibitor depletion, the concentration of free enzyme depends on the starting enzyme concentration, the non-specific binding, and the concentration of inhibitor added. Two of these factors - starting enzyme concentrations and non-specific binding - are, themselves, dependent on enzyme expression in the cultures. For instance, lower proportional expression of GAPDH amongst intracellular enzymes might lead to higher levels of non-GAPDH binding and a lower proportional GAPDH-inhibitory effect of inhibitor addition to a batch of cells.

This logic can also be applied to the difference between whole-cell inhibition and cell-free extract inhibition: if, for instance, GAPDH localises in a specific part of a cell (for instance in the glycosome; see 113), the proportion of IAA that binds specifically to GAPDH will be determined not only by the relative abundance of GAPDH in the cell, but by the effective concentration of IAA that ends up reaching it before it is bound non-specifically in the greater volume of the cell. This is one mechanistic possibility of the pharmacokinetic effect posited in Eq. 3.2.1.

Though we maintain a consistent cell culturing and harvesting protocol (see Section 3.1), differences in enzyme expression can arise regardless. This can be compensated for by assuring that measurements are only compared to measurements from the same isolate and, therefore, the same inhibitor incubation. Within each biological repeat, protein expression will be assumed to be constant, so the fraction of the inhibitor that binds non-specifically will be constant and can be disregarded. This narrows any change in free enzyme concentration, hence any change in specific activity, down to the concentration of inhibitor administered.

5.1.2 IAA in Rate Equations

The question now remains how to incorporate this into an expression of the reaction rate of an enzyme. To adhere more closely to a bottom-up modelling approach, it is necessary to know not only that IAA decreases GAPDH activity but *how* this effect is achieved [26]. The effect of increasing concentrations of IAA is most usefully interpreted as a decrease in the concentration of *free GAPDH*. Enzyme concentration is not explicitly included in the Du Preez

and Teusink models, however. Rather, it is subsumed under V_{max} [26]. The Briggs-Haldane derivation of the Michaelis-Menten equation (Eq. 5.1.4, below), allows us to infer a linear relationship between enzyme concentration and reaction rate (Eq. 5.1.5):

$$v = \frac{V_{max} \cdot [S]}{K_m + [S]} \tag{5.1.4}$$

$$v = k_{cat} \cdot [ES] \tag{5.1.5}$$

In Eq. 5.1.5, $[ES]$ represents the concentration of the enzyme-substrate complex, k_{cat} represents the rate constant for the conversion from enzyme-substrate complex to enzyme and product, and v describes the specific enzyme reaction rate [6].

If assays are set up to measure maximal GAPDH activity, it can be assumed that all of the enzymes' active sites are occupied: $[ES]$ is equal to $[E]_0$, the total enzyme concentration (compare Eq. 5.1.1). Since we use the substrate-saturating assay conditions of Van Eunen and colleagues [3], we can treat the measured specific activities as equivalent to $V_{max,GAPDH}$ (for the uninhibited sample) or (*apparent*) V_{max} values ($V^{app}_{max,GAPDH}$; inhibited activity).

The distinctive contribution of thermodynamics and enzyme concentration to the V_{max} was made explicit in the work of Smallbone and colleagues [35], who separately determined protein concentration ($[E]$, by targeted proteomics) and enzyme turnover rate (k_{cat}). $[E]_0$ can then be related to $V_{max,GAPDH}$ according to the following equation:

$$V_{max} = k_{cat} \cdot [E]_0 \tag{5.1.6}$$

As part of the catalytic capacity of the cell extract is lost due to the binding of inhibitor to enzyme (Eq. 5.1.3), the maximal catalytic potential of the cell (or cell extract) can be rewritten in terms of the free enzyme:

$$V^{app}_{max} = k_{cat} \cdot [E]_f \tag{5.1.7}$$

where V^{app}_{max} refers to the apparent maximal catalytic capacity of the inhibitor pool in the presence of a given concentration of inhibitor. When substituted into Eq. 5.1.4, this gives us the following equation for the reaction rate through an inhibited, enzymatically catalysed reaction:

$$v^{app} = \frac{V^{app}_{max} \cdot [S]}{K_m + [S]} = \frac{k_{cat} \cdot [E]_f \cdot [S]}{K_m + [S]} \tag{5.1.8}$$

Eq. 5.1.8 implies that the reaction rate of the GAPDH-catalysed reaction will be proportional to the concentration of the free GAPDH, which, varies in response to changes in IAA (Eq. 5.1.3). Since component reactions form part of a network, the inhibitor's effect will manifest at a systems-level. The

inhibition of flux and enzyme activity can then be measured for the calculation of the flux control of the enzyme (Eq. 2.3.2).

The question remains on how we represent the inhibition in a model that does not explicitly contain a term for enzyme concentration. We return to this question later in this chapter (Subsection 5.2.2).

5.2 Recap: Measured $V_{max,GAPDH}$ versus Model $V_{max,GAPDH}$

As reported in Table 4.1, the unperturbed $V_{max,GAPDH}$ for the forward reaction was within a factor of two of those used by Teusink *et al.* [1] and slightly higher than what was used by Du Preez *et al.* [2]. The reverse $V_{max,GAPDH}$ however, was consistently quite a bit lower than the Teusink parameter (the Du Preez model did not include an explicit reverse $V_{max,GAPDH}$ value).

In Subsection 4.3.1, we discussed possible origins for the differences between our measured specific GAPDH activity at substrate-saturating conditions and the $V_{max,GAPDH}$ values proposed by Teusink *et al.* [1] and Du Preez *et al.* [2] and we return to these differences again in Section 6.2.

Some trends within our data were quite encouraging. For instance, in keeping with what is understood about GAPDH activity, the rates measured in reverse were always higher than those measured in the forward direction ([126]; see Subsection 4.3.4). Moreover, the effect of IAA on relative activity (percentage activity) was almost identical for the forward and reverse reactions (see Subsection 4.3.4). This is exactly the effect that is expected considering that IAA alkylates the binding site of the substrates of both directions NAD^+ and NADH [21]. This also satisfies the requirement of the Haldane relationship [6], since a change in affinity or equilibrium is not expected in response to IAA:

$$K_{eq} = \frac{V_{maxf} \cdot K_{mr}}{V_{maxr} \cdot K_{mf}} \tag{5.1}$$

Though there was disparity between the absolute V_{max} values used in the construction of the Teusink model and those measured in the present investigation, the relative responses to IAA reported here were consistent and can be regarded as credible. They also fell within the range of IAA concentrations (0 μM to 400 μM) used to inhibit $V_{max,GAPDH}$ selectively in various other cell types (e.g. 22, 24, 93, 94, 100).

5.2.1 Simulating IAA's Effect

Mechanistic descriptions of IAA-dependent GAPDH inhibition were complicated by the fact that no single, quantifiable trend related $V_{max,GAPDH}$ to IAA concentration across all data sets. Though there must, by definition, be a single mechanism responsible for inhibition, this mechanistic relationship

was not clear from the collected data. This could be ascribed to factors that are hidden from the view of the experimenter, such as differences in enzyme expression between biological isolates [15]. It was clear from this that all factors influencing the inhibition would not be accounted for in our final simulations [26].

We decided to use the relative inhibition data instead of the absolute inhibition data to generate our inhibition terms. Using fits to the absolute activity assumes that our measured $V_{max,GAPDH}$ values can be inserted directly into the models. The experimental conditions in which the parameters in the Teusink model were measured, differ from those that were used in our study [3], however. Additionally, the Teusink and Du Preez model $V_{max,GAPDH}$ parameters themselves are *in silico* adjustments of experimentally measured parameters, which indicates that model construction placed some constraints on the parameter values that could be used to begin with.

A second consideration, was that the factor difference between the literature and the measured parameters were not equal for the forward and the reverse $V_{max,GAPDH}$. Though this might be balanced out by concurrent changes in K_m [3], we did not determine the K_m and could not model this balancing. Inserting only our measured $V_{max,GAPDH}$ values would change the equilibrium of the enzyme, which would breach the Haldane relationship (see Eq. 5.1).

The percentage effect of IAA on $V_{max,GAPDH}$ in the forward and reverse directions were very similar (see Figure 4.6), which allowed us to fit a single inhibition function on the combined forward and reverse data. In so doing, the Haldane relationship was kept intact (see Eq. 5.1). Another advantage of using the relative inhibition data is that it allowed us to combine data from different isolates, so that we could do a single fit on the data from repeats *II* and *III* together.

Our modelling approach therefore assumes that there is some unaccounted-for difference between the model construction and model validation data. *A priori* assumptions like these are a deviation from a strict *bottom-up* modelling approach, though they are not uncommon, e.g. in the *post hoc* parameter adjustments by Teusink [1] and Du Preez [2] that allowed them to simulate certain behaviours. Indeed, it is common practice to depart from strict mechanistic accuracy in favour of predictive ability [37].

We conducted fits separately to the different data sets (Fig. 4.6), and then also in a single fit to the data from repeat *II* and *III* (Fig. 4.17). The fits yielded the inhibition terms that were inserted into the model (see Subsection 5.2.2).

5.2.2 IAA's Effect in Mathematics

Irreversible inhibition can be described in terms of described as a "% occupancy", with the decrease in activity expressed as an exponential decay

function [124], e.g.:

$$\begin{aligned} \%\,Total\ Occupancy &= 100\% - \%\ Remaining\ Activity \\ Fractional\ Occupancy &= 1 - Fractional\ Remaining\ Activity \\ Fractional\ Occupancy &= 1 - e^{-k_{obs} \cdot time} \end{aligned}$$

where *% Total Occupancy* is the proportion of the inhibition sites that are occupied; this can also be expressed as a *fractional occupancy*. Within the term $e^{-k_{obs} \cdot time}$, "$-k_{obs}$" is an observed first-order rate constant with units of time^{-1} (usually min^{-1}), and is converted to a time-dependent, dimensionless inhibition expression when multiplied by time. The concentration of the inhibitor is subsumed under k_{obs} in this case, and can be expressed as a *fractional remaining activity*:

$$Fractional\ Remaining\ Activity\ =\ e^{-k_{obs} \cdot time}$$

which can be used as a modifier of a wild-type $V_{max,GAPDH}$ to yield predictions of the effect of adding given concentrations of IAA. The product of the inhibition term and the wild-type $V_{max,GAPDH}$ is the expected V_{max} of the inhibited enzyme ($V^{app}_{max,GAPDH}$, referring to the apparent - or perturbed - $V_{max,GAPDH}$ value):

$$V^{app}_{max,GAPDH} = V^{wt}_{max,GAPDH} \cdot e^{-k_{obs} \cdot time} \tag{5.2}$$

For the present study, the incubation time in the inhibitor was kept constant (60 minutes) for all repeats, which - considering Eq. 5.2 - means that changes in the GAPDH activity were due to differences in k_{obs} only. k_{obs}, in turn, is defined as follows [124]:

$$k_{obs} = \frac{k_{inact} \cdot [IAA]}{K_i + [IAA]} \tag{5.3}$$

The reader might note that Eq. 5.3 has the same appearance as the Michaelis-Menten equation (Eq. 5.1.4; [6]). Similar to the V_{max} in the Michaelis-Menten equation, k_{inact} is a first-order rate constant describing the maximum potential rate of covalent bond formation, while K_i is the dissociation constant of the inhibitor, expressing the concentration of inhibitor at which half-maximal rate of inhibition is attained [124]. [IAA] is the concentration of the inhibitor.

Assuming that k_{inact} and K_i are constant for each individual data set, the IAA concentration alone is responsible for the k_{obs}, which, in turn, is entirely responsible for the *% Remaining Activity* (see Eq. 5.2). The exact determination of the parameter values involved in IAA binding, as in Eq.

5.3, are beyond the scope of this study, however. For our purposes it was sufficient to note that change in the observed % wild-type $V_{max,GAPDH}$ within each repeat was related only to differences in IAA concentration and that this change could be expressed as an exponential decay function which, if multiplied with the wild-type $V_{max,GAPDH}$, gives the perturbed parameter value ($V^{app}_{max,GAPDH}$). These fits were obtained according to the method of least squares and consistently yielded fits with $R^2 \geq 0.95$. The fitted function was an adjusted exponential decay function as in Eq. 5.2:

$$Fractional\ Remaining\ Activity\ = e^{-k_i \cdot t \cdot [IAA]} \tag{5.4}$$

in which the *fractional remaining activity* is a function of [IAA], an inhibition constant (k_i), and time.

Since incubation time was kept constant at 60 minutes, fits to the experimental data were only searches for the inhibition constant, k_i, and the time-dependence was treated as a part of this constant that was equal for all inhibitor incubations. This approach was applied to each repeat separately and to the combined data from repeats *II* and *III* (see Subsection 5.2.1). The fits to these data were all exponential decay functions and were fitted in Fig. 4.6 (for the individual repeats) and Fig. 4.17 (for repeats *II* and *III* combined):

$$\begin{aligned}
I: &\quad Fractional\ Remaining\ Activity\ = e^{-0.0044 \cdot [IAA]}; &\quad R^2 = 0.98\\
II: &\quad Fractional\ Remaining\ Activity\ = e^{-0.014 \cdot [IAA]}; &\quad R^2 = 0.98\\
III: &\quad Fractional\ Remaining\ Activity\ = e^{-0.020 \cdot [IAA]}; &\quad R^2 = 0.96\\
II\ and\ III: &\quad Fractional\ Remaining\ Activity\ = e^{-0.017 \cdot [IAA]}; &\quad R^2 = 0.96
\end{aligned}$$

These terms were then used to describe the reaction-level perturbation in the model. Eqs. 5.5 and 5.6 present the adjusted equations from the Teusink and Du Preez models, respectively. Indicated in red are the $V_{max,GAPDH}$ and the modifying term.

Some important information on the notation used:

- lower-case names refer to concentrations of metabolites;
- a lower-case "t" in square brackets indicates that a variable is time-dependent;
- an "f" or a "r" at the end of a parameter's subscript indicates whether it pertains to the forward or the reverse reaction, respectively;

The control of an enzyme over a pathway flux can be calculated as the relative change in flux in response to a perturbation, divided by the relative change in enzyme activity at constant substrate and product concentrations. This means that the exact *in vivo* conditions at which the flux was measured do

not need to be recreated to relate the flux to the GAPDH activity at constant conditions. This is captured in Equation 3.10.1, taken from Poolman *et al.* [22]:

$$C^{J}_{E_i} = \frac{(dJ/J)/(dI/I)_{ss}}{(dv_i/v_i)/(dI/I)_{S_i,P_i}}$$

Since enzyme activity is linearly related to V_{max} (see Eq. 5.1.8), the percentage change in $V_{max,GAPDH}$ is equivalent to a the percentage change in GAPDH activity, and this percentage change is taken as the relative change in GAPDH activity.

(see next page)

Adjusted equations:

Teusink *et al.* [1]:

$$v\_7 = \frac{-\frac{V^{wt}_{max,GAPDHr}\cdot e^{-k_i\cdot[IAA]}\cdot bpg[t]\cdot nadh[t]}{K_{m,GAPDH-BPG}\cdot K_{m,GAPDH-NADH}} + \frac{K_{eq,TPI}\cdot V^{wt}_{max,GAPDHf}\cdot e^{-k_i\cdot[IAA]}\cdot nad^{+}[t]\cdot trio[t]}{(1+K_{eq,TPI})\cdot K_{m,GAPDH-GAP}\cdot K_{m,GAPDH-NAD^{+}}}}{(1+\frac{nad^{+}[t]}{K_{m,GAPDH-NAD^{+}}}+\frac{nadh[t]}{K_{m,GAPDH-NADH}})\cdot(1+\frac{bpg[t]}{K_{m,GAPDH-BPG}}+\frac{K_{eq,TPI-trio[t]}}{1+K_{eq,TPI}\cdot K_{m,GAPDH-GAP}})} \tag{5.5}$$

Du Preez *et al.* [2]:

$$v\_GAPDH = \frac{-\frac{V^{wt}_{max,GAPDHf}\cdot e^{-k_i\cdot[IAA]}\cdot bpg[t]\cdot nadh[t]}{K_{eq,GAPDH}\cdot K_{m,GAPDH-GAP}\cdot K_{m,GAPDH-NAD^{+}}} + \frac{K_{eq,TPI}\cdot nad^{+}\cdot V^{wt}_{max,GAPDHf}\cdot e^{-k_i\cdot[IAA]}\cdot trio[t]}{(1+K_{eq,TPI})\cdot K_{m,GAPDH-GAP}\cdot K_{m,GAPDH-NAD+}}}{(1+\frac{nad^{+}}{K_{m,GAPDH-NAD^{+}}}+\frac{nadh[t]}{K_{m,GAPDH-NADH}})\cdot(1+\frac{bpg[t]}{K_{m,GAPDH-BPG}}+\frac{K_{eq,TPI}\cdot trio[t]}{(1+K_{eq,TPI})\cdot K_{m,GAPDH-GAP})}} \tag{5.6}$$

5.3 The *Teusink* Model

The Teusink model [1] was constructed based on *in vitro* kinetics and describes the steady-state behaviour of a yeast cell. Its kinetics pertains mostly to the intracellular events of *S. cerevisiae* glycolysis. Glucose transport was represented using kinetics that were related to the extracellular environment. Extracellular glucose concentration was fixed at 50 mM.

Efferent branches were represented as carbon "sinks": trehalose, glycogen, and succinate production were were all described as constant fluxes; ethanol production by alcohol dehydrogenase (ADH) and glycerol production by glycerol 3-phosphate dehydrogenase (G3PDH) were expressed as reversible equations. All five of these "end products" of the pathway were given fixed concentrations: succinate, trehalose, and glycogen all had concentrations of zero, whereas glycerol was fixed at 0.15 mM and ethanol at 50 mM. Importantly, the model only contains one extracellular variable (glucose) and expresses all variables in terms of their concentration per cytosolic volume - hence extracellular glucose is also expressed in terms of the intracellular volume.

5.3.1 *Teusink* Model: Glycolytic Activity in a Closed System

Mimic the measurements of glycolytic activity in the experimental set-up more precisely, the Teusink model was adjusted to reflect the conditions in a closed system with limited substrate. This meant unfixing the external glucose and the ethanol concentration and expressing them as variables. Additionally, a variable was included for extracellular glucose, as well as an ethanol export term. This ethanol export term was constructed according to Fick's Law for diffusion:

$$\frac{dETOH}{dt} = \frac{A \cdot P_{ETOH}}{V_i}(ETOH - ETOHo)$$

where the rate of ethanol export is a function of the outer area of the cell membrane (A), the permeability of the the membrane to ethanol (P_{ETOH}), the intracellular volume (V_i), and the ethanol concentration gradient between the inside and the outside of the cell *(ETOH-ETOHo)*. We followed the example of Du Preez *et al.* [2] in assuming a spherical cell with a radius of 2 μm, and used a permeability constant from existing literature ($3 \times 10^{-4} cm.s^{-1}$; 127). All of this together yielded a diffusion rate constant ($270 min^{-1}$) that - together with the cross-membrane ethanol gradient - described ethanol export as follows:

$$\frac{dETOH}{dt} = 270 min^{-1} \cdot (ETOH - ETOHo)$$

Teusink and colleagues expressed the concentrations that form a part of the *in vitro* parameter sets in terms of mmol.L-cytosol^{-1} [1]. They also suggested a ratio of 3.75 mL cytosol.g protein^{-1}, which allows the conversion of enzyme rates to specific rates (μmol.min^{-1}.mg protein^{-1}). For the flux data for which the parameters were adjusted, they state that they used 50 g.L^{-1} of cells, which amounts to between 5 and 6 g protein.mL^{-1} assay volume. Using the average of these values - 5.5 g protein.mL^{-1} - and the intracellular protein concentration mentioned above, an external volume to internal volume ratio of 48.5:1 was calculated. Following the lead of Du Preez and colleagues [2], we opted for a ratio of 50:1 (external to internal). This ratio was inserted into the model in the stoichiometry of the transport steps, allowing for the construction of ordinary differential equations for external species:

$$ETOHo'[t] = \frac{V_{internal}}{V_{external}} \cdot v_{ETOHexport}$$

$$GLCo'[t] = -\frac{V_{internal}}{V_{external}} \cdot v_{GLCimport}$$

External and internal ethanol was assigned an initial value of zero while the external glucose concentration was set to 20 mM (compare Chapter 3 for the experimental methods). All other efferent branches of the pathway were kept as in the original model.

One of the consequences of unfixing the initial substrate and final product of the pathway is that the system could no longer reach a steady state. Instead of calculating steady-state fluxes, dynamic behaviour was simulated as the change in metabolite concentration over time (Fig. 5.2). Glucose was converted almost entirely to ethanol, with only ethanol uniformly increasing for the entire duration of the simulation (see Appendix J for the time-evolution of all the variables over the simulation time). In the unperturbed model, external glucose is depleted in 13 minutes, and this period is therefore chosen as the simulation duration.

We calculated the glucose and ethanol fluxes as the rate of change over the initial slopes of the simulated glucose and ethanol concentrations (between t = 0 minutes and t = 4 minutes). The calculated values were treated as equivalent to fluxes for the purposes of this study (see also Section 4.4).

Glucose was depleted much more quickly in the model simulation than in the experiments. Teusink *et al.* [1] challenged yeast cells with 100 mM of glucose, which was depleted in 50 minutes. Considering the linear slope of glucose consumption seen in my (Fig. 4.11) and Teusink *et al.*'s data, this allows us to extrapolate that 20 mM of glucose (our initial glucose concentration) should be consumed in about 10 minutes. This is close to the model prediction but very different from what we observed experimentally. Since we compensated for the extracellular to intracellular volume ratio, the major difference between our flux measurement assays and those of Teusink

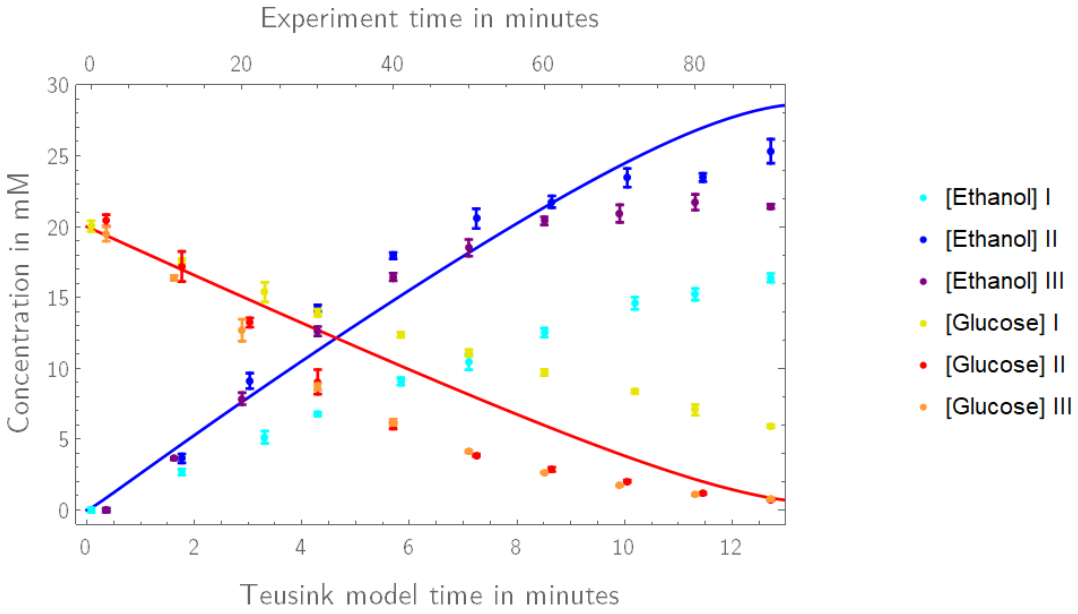

Figure 5.2: In a closed-system simulation with an adjusted version of the Teusink model, glucose is depleted in 13 minutes (bottom x-axis). The blue and red solid lines show the predicted time-dependent increase in external ethanol concentration (ETOHo) and the predicted decrease in external glucose concentration (GLCo), respectively, in an unperturbed state. The two simulated graphs mirror each other almost exactly but for a factor difference of about one glucose consumed per about one and a half molecules of ethanol produced: this is in line with Albers *et al.* [43], who found an ethanol:glucose ratio of 4:3 - carbon loss to the branches and during pyruvate decarboxylation is suspected to be responsible for glucose not being fully converted to ethanol according to the expected 1:2 stoichiometry. The wild-type data for the three biological repeats are also presented: the legend to the right of the figure identifies the data sets. The experimental data spans a much longer time frame of 90 minutes (top x-axis). This difference is mainly due to a more concentrated cell suspension being used, as can be seen when the data is normalised to protein concentration. It is also apparent that repeats *II* and *III* have higher fluxes than *I*, which did not use up its glucose in the time of the experiment. Time on both axes is measured in minutes, while concentration is measured in mM.

and colleagues was that they used a much more concentrated cell suspension than we did. Fluxes that are normalised over protein concentration are much closer to our measured fluxes, as will shortly be discussed.

For a more intuitive view of our experimental observations *versus* the model, Fig. 5.2 shows the non-normalised assays as they would be seen during the experiment. Concentrations are expressed in their non-normalised millimolar form in Fig. 5.2, and show, in addition to the differences between the model prediction and the experimental data, that there were also internal differences in the experimental data of repeat *I* compared to repeat *II* and *III*.

Using Teusink *et al.*'s factor of 3.75 mL.g protein^{-1}, the rates of concentration change in the model simulations were converted to fluxes in μmol.min^{-1}.mg protein^{-1}. The simulated ethanol production rate was 0.49 μmol.min^{-1}.mg protein^{-1} (compared to 0.50 μmol.min^{-1}.mg protein^{-1} in the Teusink paper, 1) while the glucose was consumed at at a rate of 0.32 μmol.min^{-1}.mg protein^{-1} (*versus* 0.40 μmol.min^{-1}.mg protein^{-1} in 1).

The fluxes reported by Teusink and colleagues [1] were not restored by inserting higher initial glucose in our model simulations (50 mM): very similar ethanol and glucose fluxes were calculated (0.52 μmol.min^{-1}.mg protein^{-1} and 0.33 μmol.min^{-1}.mg protein^{-1}, respectively; simulation not shown). The difference between the Teusink literature fluxes and the simulated fluxes are probably because of the structural changes that we made to the model.

5.3.2 Teusink Model Predictions: IAA Titrations

Perturbation terms were inserted in the adjusted model by generating fits that relate the percentage GAPDH activity and IAA to each other for each biological repeat (Fig. 4.6), and then also for *II* and *III* combined (Fig. 4.17).

The perturbation terms were varied by simulating the model at varying concentrations of IAA and obtaining both the % wild-type activity and the % flux for each IAA concentration. Figure 5.3 shows the results of these simulations, including the corresponding experimental data. Since the GAPDH inhibition function was derived from a fit to GAPDH activity measurements, it is not surprising that this function correlated very well with the experimental data (magenta lines in Fig. 5.3). What was striking, however, was that the resultant change in both glucose and ethanol flux - which are related to IAA only indirectly - also seemed to be predicted quite well by the perturbed model (dashed black lines in Fig. 5.3).

Repeat *I*, as has been the case throughout this study, was the outlier with the experimentally measured fluxes decreasing much faster in reaction to rising IAA concentrations than predicted by the model. For the other two repeats, flux appeared not to change very much until a critical concentration of IAA (and hence a critical level of GAPDH inhibition) was reached, after which the flux dropped precipitously, often being abrogated within one doubling of the IAA concentration.

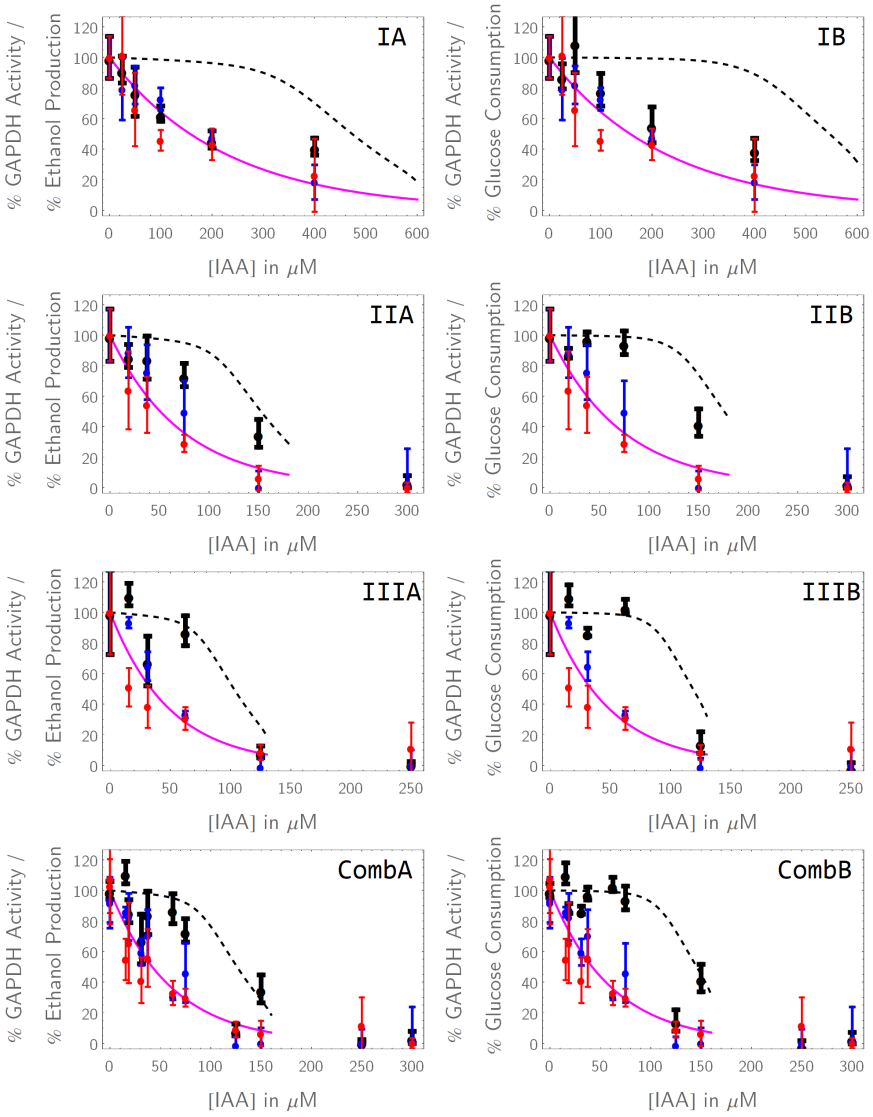

Figure 5.3: The Teusink model predicts the relationship between IAA concentration and normalised glycolytic flux well. The figure shows the change in % GAPDH activity and % glycolytic flux (the flux in terms of ethanol production and glucose consumption) as functions of increasing IAA concentrations. The effect on flux is a non-linear consequence of the local perturbation of GAPDH by IAA. The labels *I*, *II*, and *III* refer to the relevant repeat, while "*Comb*" refers to the combined data of repeats *II* and *III*. The suffix of a label indicates the metric used for flux measurements: the left-hand column (suffixed *A*) represents flux as a ethanol production rate, while the right-hand column (suffixed *B*) shows it in terms of glucose consumption. Red and blue data points represent data from forward and reverse activity measurements, respectively, and the magenta line was fitted to the data in each case and inserted as a modifier of $V_{max,GAPDH}$. The black data points represent the experimental flux measurements, while the dashed black line is the normalised Teusink model prediction of the change in flux as a function of IAA. Flux was predicted well for repeats *II* and *III*.

Interestingly, glucose consumption seemed to yield slightly better agreement between model prediction and experimental measurement. The experimental ethanol flux data showed a steeper and earlier decline in flux in response to IAA than predicted by the model.

The control coefficient can be calculated, according to Eq. 2.3.2, as the ratio between the slopes where IAA concentration is near zero in Fig. 5.3 (shown in Subsection 5.3.3).

5.3.3 Teusink Model Predictions: GAPDH Control over Glycolytic Flux

To determine the glycolytic flux control of GAPDH, % flux must be expressed as a function of % GAPDH activity at constant conditions (Subsection 3.10.1; [22]). In Subsection 2.3.3, we discuss how flux control can be calculated as a single coefficient at zero inhibition, but also as a continuous profile of relative flux as a function of relative enzyme activity. We decided to investigate the control profile as well as to calculate the flux control at near-zero IAA concentration for a single-value comparison.

Figure 5.4 reflects the changing glycolytic flux control of GAPDH, both in the models and as seen in our experimental data. The slope between the wild-type point and the point at [IAA] = 3.2 μM was used as a proxy for the flux control of GAPDH at zero inhibitor (3.2 μM IAA is the size of the inhibitor increments for the simulation). This was done by generating a fit to the flux inhibition data. As expected, the glycolytic flux control near [IAA] = 0 μM, as predicted by the Teusink model, was very close to zero. This was true for both control over glucose consumption and over ethanol production:

$$C^{J_{GLCo}}_{v_{GAPDH}} = 0.0045$$

$$C^{J_{ETOHo}}_{v_{GAPDH}} = 0.031$$

When comparing the experimental and simulated flux control plots, there was good agreement between the simulation and the measurements. It can also be seen that there is substantial agreement between the repeats, except for repeat *I*, which predicts a much stronger control of GAPDH over glycolytic flux (see Fig. 5.4).

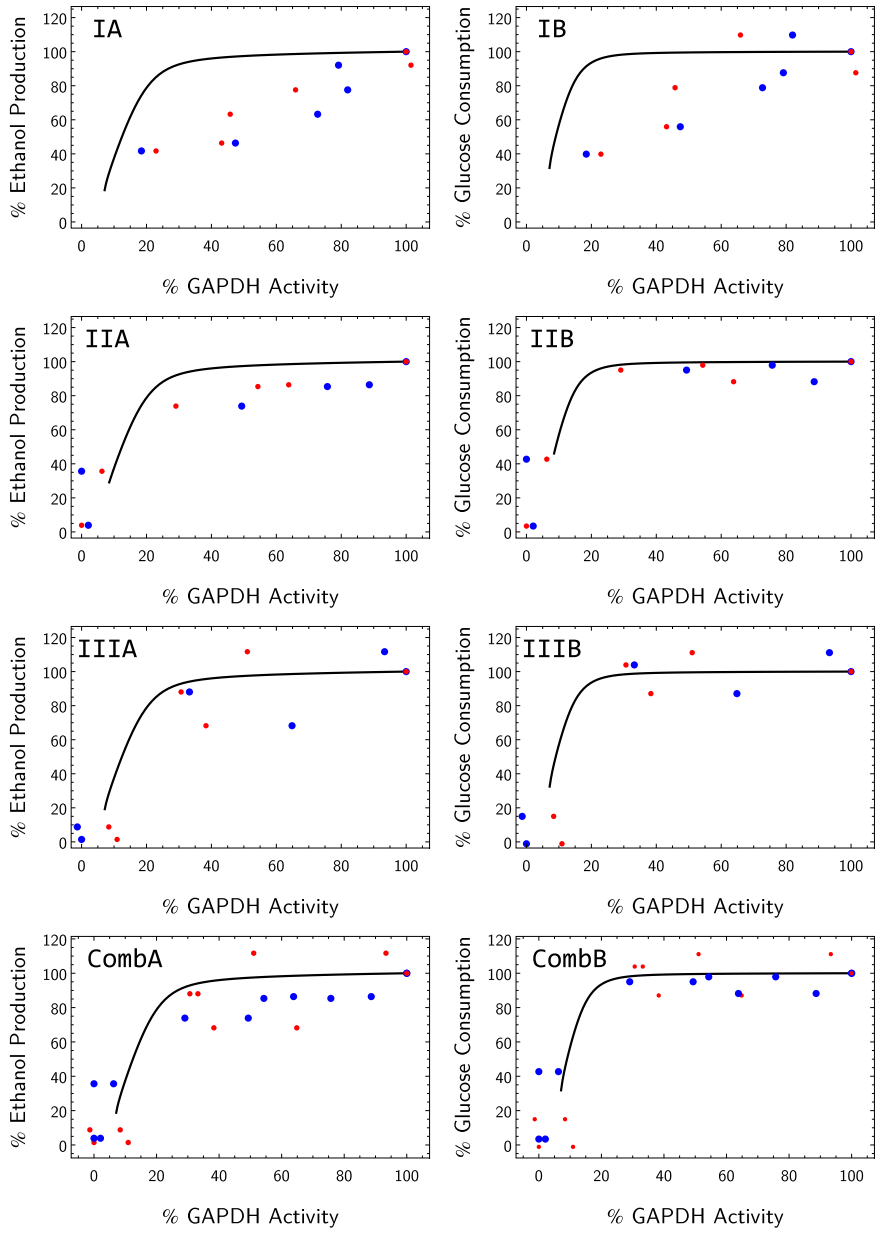

Figure 5.4: The Teusink model predicts the relationship between %GAPDH activity and % glycolytic flux well. Glycolytic flux was measured and expressed as a percentage of its wild-type value and plotted against the percentage remaining wild-type GAPDH activity at the same IAA concentration (see Eq. 5.5). GAPDH activity measured in the forward direction is presented in blue, while reverse activity is in red. *I*, *II*, and *III* refer to the individual biological repeats while "*Comb*" refers to the combined data of repeats *II* and *III*. Label suffixes indicate the metric used for flux measurements: the left-hand column (suffixed *A*) represents flux a ethanol production rate while the right-hand column (suffixed *B*) shows it as glucose consumption. The relationship between relative glycolytic flux and relative GAPDH activity was predicted well by the Teusink model for repeats *II* and *III*.

5.4 The *Du Preez* Model

The Du Preez model is an oscillating model of the glycolytic pathway of *S. cerevisiae*. Seven models were constructed and uploaded to the JWS Online model repository by Du Preez and colleagues [2, 16]. Our first task was therefore to decide which was the most appropriate for generating simulations which could be compared to our experimental data.

Out of the four Du Preez models created during the *model construction* phase of the Du Preez study [2], *dupreez4* was chosen as it was the final product of the *model construction* phase, and represents an oscillating, whole yeast cell in a population of other oscillating yeast cells, similar to what could be expected in our assays.

Du Preez *et al.* [2], for the construction of their models, made use of the Teusink model with its original parameters in its original units. Though it is not explicitly mentioned, this means that the concentrations in the Du Preez model are expressed as mmol.L cytosol^{-1}. Teusink *et al.* proposed a conversion ratio of 3.75 mL cytosol.g protein^{-1}. The concentrations and reaction rates mentioned here will therefore have been converted from the model according to this ratio. Du Preez and colleagues also include an external to internal volume ratio of 50:1 in *dupreez4*. We show in an earlier discussion (Subsection 5.3.1) that the volume ratio in the Teusink model was 48.5:1, which we rounded to 50:1.

We applied the same changes to the Du Preez model as we applied to the Teusink model to see how its ability to predict glycolytic flux control compares with its predecessor's. Having been expanded to include the ability to describe glycolytic oscillations, the ability of this model to accurately predict glycolytic flux control, as was the case with the Teusink model (see Section 5.3), would align Du Preez and colleagues' work with the iterative model expansion approach of the Silicon Cell initiative [13].

5.4.1 The *Du Preez* Model in Batch Culture Conditions

Exactly as with the Teusink model, the Du Preez model was adjusted to resemble the experimental set-up more closely by giving extracellular species concentrations of zero (cyanide, acetaldehyde, and ethanol), except for extracellular glucose, which was set to 20 mM. An ethanol transport step was also included, as explained previously, under Du Preez and colleagues' assumption [2] of a spherical cell with a radius of 2 μm and Guijarro and Lagunas' suggested permeability constant of $3 \times 10^{-4} cm.s^{-1}$ [127].

Acetaldehyde export, which is not present in the Teusink model and hence was not addressed in Section 5.3, was also removed by setting the rate constant for acetaldehyde transport to zero: this was done under the assumption that acetaldehyde is entirely converted to ethanol during aerobic fermentation at

high glucose, a phenomenon known as the Crabtree Effect [9]. Glucose is then converted mostly to ethanol (ratio 1:1.5, glucose:ethanol), according to this model (Fig. 5.5). The loss of carbon to side-branches and as CO_2 during pyruvate decarboxylation explains why full conversion (ratio of 1:2) was not obtained.

The Du Preez model has a much lower unperturbed flux than the Teusink model, owing the decrease of V_{max} values from *teusink* to construct *dupreez4*: 0.21 μmol.min^{-1}.mg protein^{-1} for ethanol production and 0.15 μmol.min^{-1}.mg protein^{-1} for glucose consumption (compared to 0.50 μmol.min^{-1}.mg protein^{-1} and 0.32 μmol.min^{-1}.mg protein^{-1} in our Teusink model simulation). This means that the Du Preez model can also be run much longer before substrate is depleted and maximal ethanol concentration is reached (Fig. 5.5). The Du Preez model, however, still shows a quicker depletion of glucose than our experimental results, owing perhaps to our incubations having contained more dilute yeast cell suspensions so that sufficiently quick sampling could be carried out by a human experimenter. In Fig. 5.5, the concentrations are given in mM instead of in protein-normalised amounts to give an intuitive view of the experimental observations *versus* the model predictions.

Repeat *I*, again, appears to be an outlier amidst the experimental data.

5.4.2 Du Preez Model Predictions: IAA Titrations

Fits that capture the relationship between IAA concentration and relative GAPDH activity were inserted in the adjusted model as explained in Subsection 5.2.2. This was done for each biological repeat, and then also for *II* and *III* together. Changes in the relative flux and the relative GAPDH activity were calculated in exactly the same way as in the case of the Teusink model (Subsection 5.3.2).

Figure 5.6 shows the results, and it can be seen that model predicts the experimental data well for repeats *II* and *III* but not for *I*. It was also the case again that the initial plateau of the response of flux to the increased IAA concentration fit better when flux was measured as glucose consumption rate rather than as ethanol production: the ethanol production rate seemed to decline more steeply at the low IAA concentrations. The gradients at zero IAA concentration for relative flux and relative GAPDH activity with respect to IAA, were again used for the calculation of the control coefficient (see next subsection).

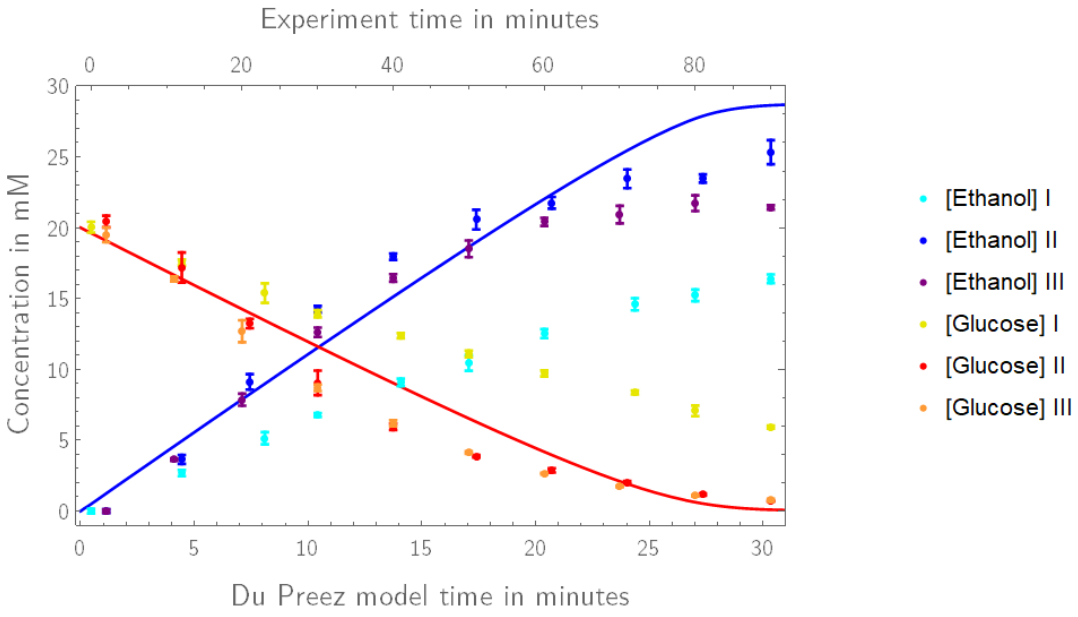

Figure 5.5: Dynamic behaviour of *Du Preez* model glucose and ethanol concentrations in a closed system shows that glucose stocks are exhausted in 30 minutes. The blue and the red solid lines represent the predicted increase in ethanol concentration and the predicted decrease in glucose concentration, respectively. Ethanol concentration eventually plateaus at about 30 mM - 1.5 times greater than the administered glucose. This agrees with the finding of Albers *et al.* [43], who noted an glucose:ethanol ratio of 3:4, instead of the expected 1:2 ratio. This is likely due to a loss of carbon to the branches, for which glycogen, succinate, and trehalose production are expressed as constant rates and not sensitive to decreasing flux through the pathway, and due to carbon loss during pyruvate decarboxylation. We did no investigate the activity of the branches further. The wild-type data for the three biological repeats are also presented: the legend to the right of the figure identifies the data sets. The experimental data spans a much longer time frame of 90 minutes (top x-axis). It is also apparent that repeats *II* and *III* have higher fluxes than *I*, which did not use up its glucose during the experiment. Time on both axes is measured in minutes, while concentration is measured in mM. Ethanol in the experimental data appears to be produced at a stoichiometry of 1:1 to glucose molecules consumed.

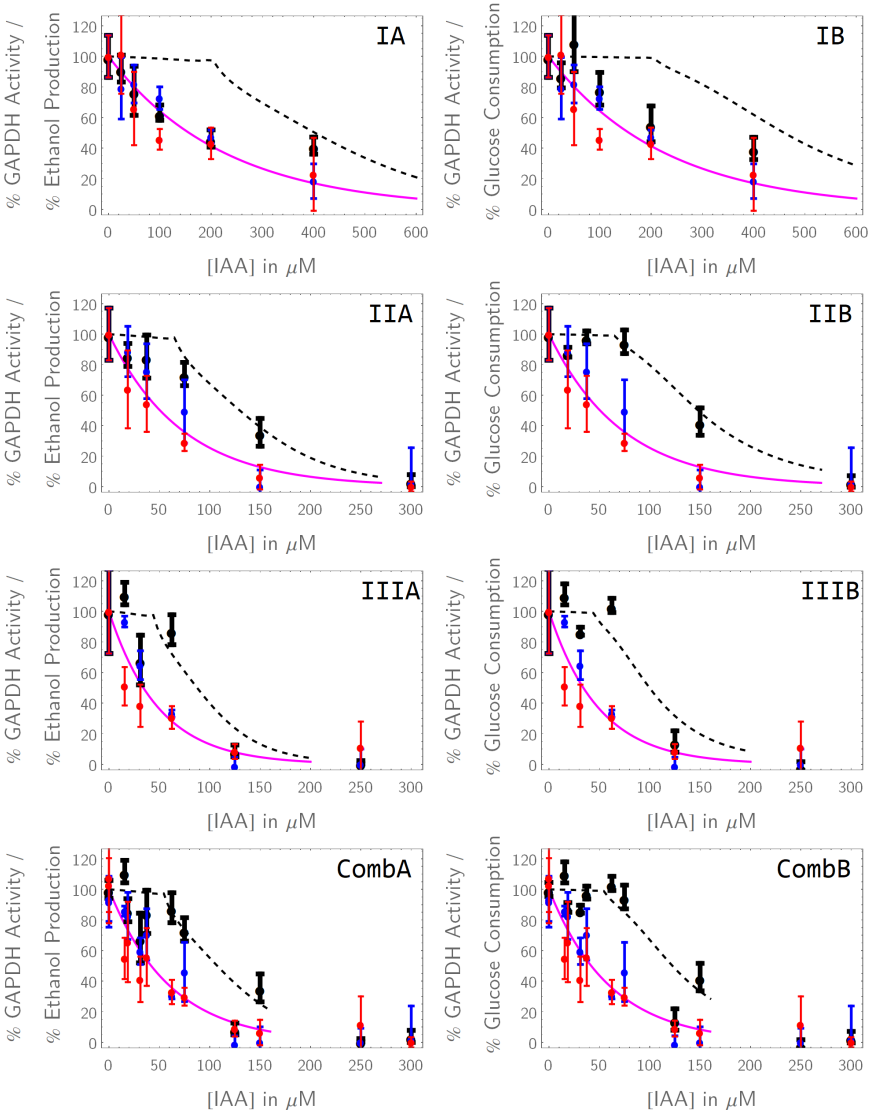

Figure 5.6: The Du Preez model predicts the relationship between IAA concentration and normalised glycolytic flux well. The figure shows the change in GAPDH activity and glycolytic flux (in terms of ethanol production and glucose consumption) as functions of increasing IAA concentrations. The effect on flux is a non-linear systemic effect. The labels *I*, *II*, and *III* refer to the relevant repeat, while "*Comb*" refers to the combined data of repeats *II* and *III*. The suffix of a label indicates the metric used for flux measurements: the left-hand column (suffixed *A*) represents flux as a ethanol production rate while the right-hand column (suffixed *B*) shows it in terms of glucose consumption. Red and blue data points represent data from forward and reverse activity measurements, respectively, and the magenta line was fitted to the data in each case and inserted as a modifier of $V_{max,GAPDH}$ in the model. The black data points represent the experimental flux measurements, while the dashed black line is the normalised Du Preez model prediction of the change in flux as a function of IAA. Flux was predicted well for repeats *II* and *III*, bit not so well for repeat *I*.

5.4.3 Du Preez Model Predictions: GAPDH Control over Glycolytic Flux

Exactly as with Teusink model, we created a flux control plot by presenting % glycolytic flux as a function of the % GAPDH activity at the same IAA concentrations (Fig. 5.7). The model predictions, again, to matched up well with the experimental data from repeats *II* and *III*.

The glycolytic flux control coefficient at near-zero IAA concentration (in our case, between the predicted points of zero inhibition and the first simulated increment, at [IAA] = 3.2 μM) were then calculated for both ethanol production and glucose consumption. As with the Teusink model predictions, the control of GAPDH was very close to zero:

$$C^{J_{GLCo}}_{v_{GAPDH}} = 0.0068$$

$$C^{J_{ETOHo}}_{v_{GAPDH}} = 0.024$$

Control increases very sharply when GAPDH is inhibited further below about 40% wild-type activity. The model also predicts this behaviour well.

5.5 Du Preez *versus* Teusink

Both models predicted the change in glycolytic flux in response to the inhibition of GAPDH well. This is clearest in Fig. 5.8, where the models are compared to each other, and also to the experimental data. The model predictions are quite similar. For yeast isolate *I*, the measured glycolytic flux control of GAPDH is consistently different from the model predictions, but also from the other two biological repeats. This data set was regarded as an outlier, as the combination of the other two data sets showed strong correlation with the model predictions.

Both the model predictions and the experimental determination of glycolytic flux control suggest a higher control over ethanol production rate for GAPDH (the factor difference for the Teusink model, the Du Preez model, and the experimental data being about 7, 3.5, and 6.5). In this sense, there seems to be agreement between the models and the experimental data that glucose consumption rate is affected less strongly by GAPDH inhibition: one could speculate that this might be due to carbon flux being redirected to the branches in upper glycolysis (which would be the case in the model, where there is a fixed flux in some of the branches).

The ratio between GAPDH control over glucose consumption and ethanol production might be deceptive, however, as they do not reveal that the control exerted over both fluxes are very small (3% and lower) in the model

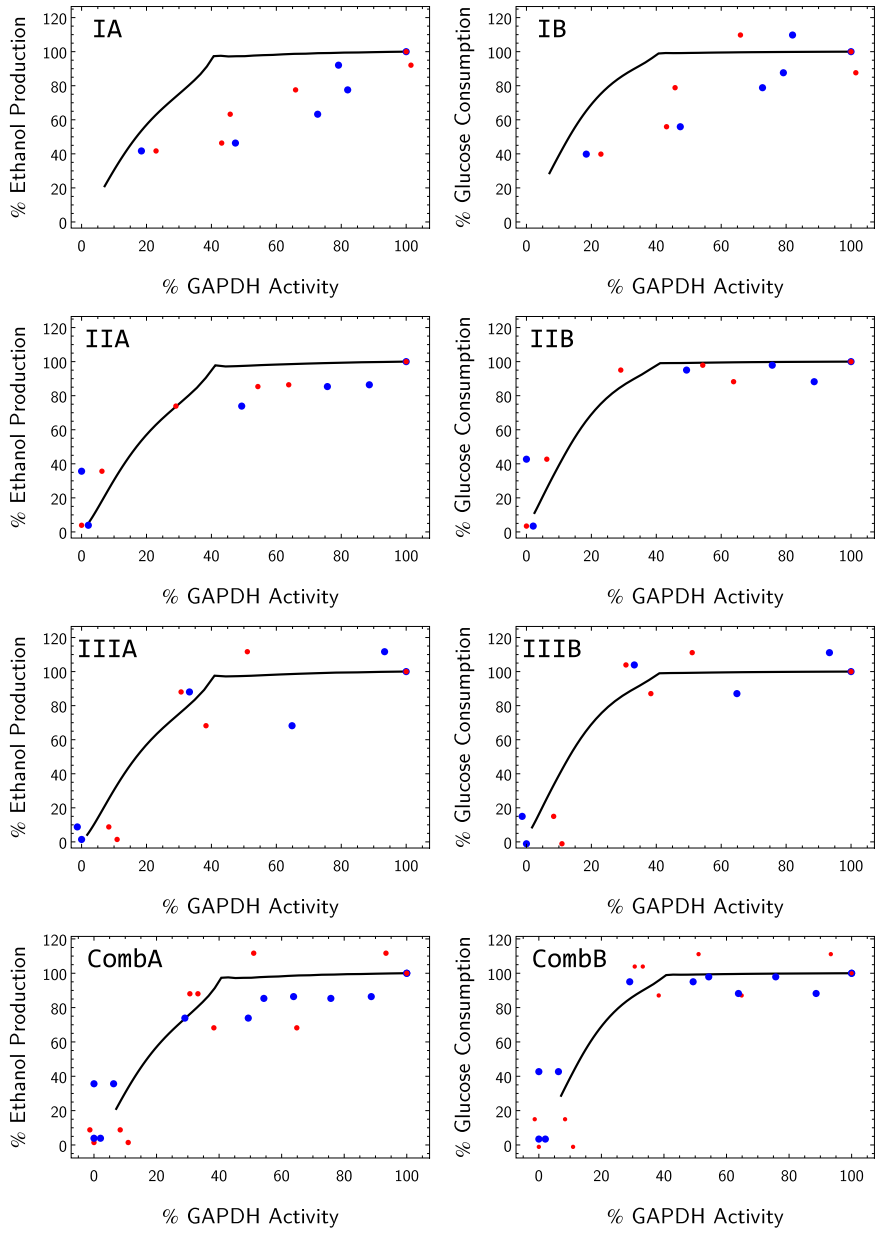

Figure 5.7: The Du Preez model predicts the relationship between % GAPDH activity and % glycolytic flux well. Glycolytic flux was measured and expressed as a percentage of its wild-type value and plotted against the percentage remaining wild-type GAPDH activity preincubated at the same IAA concentrations (see Eq. 5.6). GAPDH activity data measured in the forward direction are presented in blue, while reverse activity is in red. *I*, *II*, and *III* refer to the individual biological repeats while "*Comb*" refers to the combined data of repeats *II* and *III*. Label suffixes the metric used for flux measurements: the left-hand column (suffixed *A*) represents flux an ethanol production rate while the right-hand column (suffixed *B*) shows is as glucose consumption. The relationship between relative glycolytic flux and relative GAPDH activity was predicted well by the Du Preez model for repeats *II* and *III*.

simulations, and also for the experimentally observed control over glucose consumption. The only significant control exerted over any flux at near-zero IAA concentrations was the experimentally observed control over ethanol production (Fig. 5.8*C* shows this most clearly). The combined ethanol production data from repeat *II* and *III* are also affected by a large amount of scatter.

However, if the plots of flux to GAPDH activity are inspected (Fig. 5.8), a different picture can be seen: both models appear to exhibit extremely low flux control by GAPDH over both production and consumption. The ethanol production fluxes seem just as flat at first, except that they are generally lower than the glucose consumption fluxes. One might speculate that the wild-type ethanol flux is an overestimation and leads to this high apparent ethanol production control at zero IAA.

We posit that the experimentally observed control of GAPDH over glucose consumption is a validation of the model predictions, but that the ethanol production flux data are inconclusive, owing to the high level of scatter. The agreement between the model predictions and the experimental data is actually striking when one inspects the relationship of relative flux and relative $V^{app}_{max,GAPDH}$ to IAA, and to each other (Figs. 5.3, 5.6, and 5.8).

The control coefficients, both calculated from the models and determined experimentally, are:

Teusink:

$$C^{J_{GLCo}}_{v_{GAPDH}} = 0.0045$$

$$C^{J_{ETOHo}}_{v_{GAPDH}} = 0.031$$

Du Preez:

$$C^{J_{GLCo}}_{v_{GAPDH}} = 0.0068$$

$$C^{J_{ETOHo}}_{v_{GAPDH}} = 0.024$$

versus the experimental data, which yielded the flux control coefficients:

$$C^{J_{GLCo}}_{v_{GAPDH}} = 0.032$$

$$C^{J_{ETOHo}}_{v_{GAPDH}} = 0.21$$

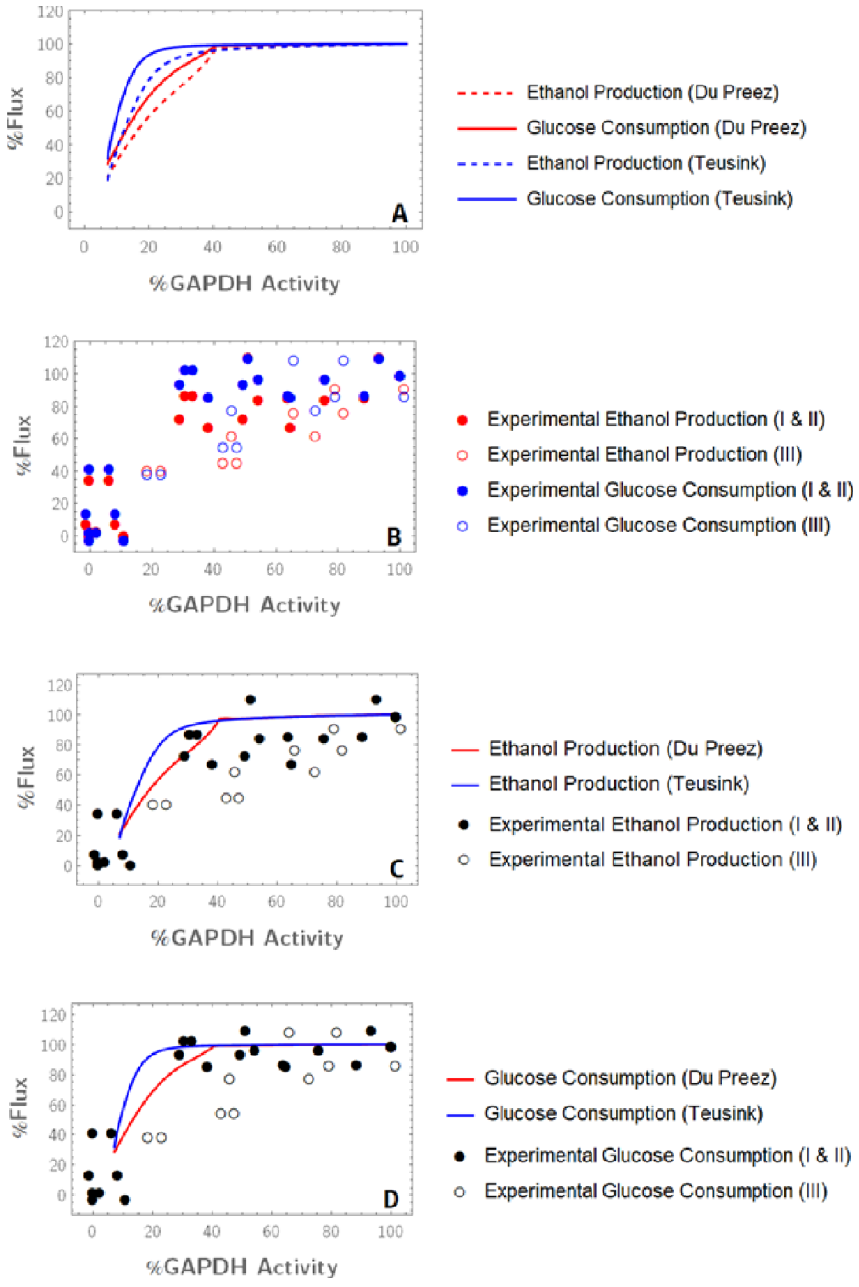

Figure 5.8: Both models predict the change of glucose consumption rate as a function of GAPDH inhibition better than ethanol production rate. In *A*, the model predictions for the Teusink and the Du Preez models using the inhibition equation for data sets *II* and *III* combined, are both presented. In *B*, glucose consumption appears to have a higher rate than ethanol production for most of the GAPDH perturbations, and ethanol also declines earlier in response to GAPDH inhibition. The empty circles indicate the data arising from biological isolate *I*, which consistently diverged from the other two members of the biological triplicate set. Ethanol production data (*C*) deviate slightly from the trend of the model predictions, however. In *D*, glucose consumption is highly correlated for both the Teusink and Du Preez models, and for the experimental data. Legends to the right of each figure contain full information about its contents.

Chapter 6

Discussion

Limits in experimental time and resources make it necessary to investigate metabolic pathways in a piecemeal way: larger models are often difficult to validate, and are more easily studied by linking smaller, validated models [13]. Adherence to the modular approach would eliminate much duplicative work.

Another benefit of metabolic modelling lies in fact that a network-level view of a pathway can illuminate useful metabolic characteristics, like drug targets [18, 28], and deepen our understanding of metabolic behaviour. Metabolic Control Analysis (MCA) is a very useful tool for the investigation of systemic properties in metabolism [19]. Within MCA, flux control coefficients can be experimentally determined [25] as well as predicted [20]. These metabolic flux control coefficients are not only useful tools for interpreting metabolic models, but also constitute core predictions for model validation [4, 20, 54]. Model validation is of cardinal importance, as model application and model expansion often presuppose models that are correctly parameterised at their current level of detail [15, 36, 47].

In this study, we experimentally determined the glycolytic flux control coefficient of GAPDH in *S. cerevisiae* cells that were grown to diauxic shift and then challenged with excess glucose. We did this to test the validity of two related, kinetic models of *S. cerevisiae* glycolysis by Du Preez *et al.* [2] and Teusink *et al.* [1]. This validation serves both as a validation of the two models and also sheds light on how the computational adaptation of the Teusink model by Du Preez and affected the original model's ability to predict the glycolytic control of GAPDH. For this, credible ways of perturbing and measuring the rate enzyme activity and glycolytic flux needed to be established.

6.1 Iodoacetic Acid

One of the restrictions of applying MCA to an experimental context stems from the difficulty of perturbing individual enzymatic steps in an isolated fashion [25]. IAA was suggested by Fell [128] as a way of experimentally

determining the flux control of GAPDH. Before evaluating the Teusink and Du Preez models for their ability to predict the glycolytic flux control of GAPDH, we investigated some aspects of GAPDH inhibition by IAA to confirm the appropriateness of the compound for our purposes.

Authors had used this inhibitor in a variety of organisms as an alkylating agent that targets the active thiol group of GAPDH (e.g. 22, 86, 93, 101, 103). We performed time-course assays on lysate incubated in IAA and found - in accordance with what is understood in the literature - that GAPDH activity is not recovered when the concentration of IAA is lowered (Appendix B). If the inhibitor bound reversibly, a decreased inhibitory effect would have been seen when the volume of the sample increased.

In Subsection 6.1.1, we discuss prelytic inhibitor incubation as a way to circumvent possible differences in pharmacokinetics and inhibitor affinity that might arise when comparing kinetic measurements in cell-free extract to whole-cell fluxes (see also Subsection 2.3.3). This technique is by no means novel: for instance, Poolman *et al.* [22] exposed *Streptococcus lactis* and *Streptococcus cremoris* cells to IAA before lysis, after which cell-free extract was produced. Though the technique has been used before, previous authors have not made explicit the benefit of prelytic inhibitor administration. Ours is the first study of which we are aware in which the potential of IAA for MCA is discussed specifically with regard to overcoming *in vitro-in vivo* differences in the laboratory (see Subsection 6.1.1).

Though we gathered evidence for irreversibility over a two-hour incubation in cell-free extract, one can reasonably ask the question whether this irreversible bond survives the mechanic stresses of our glass-bead extraction (see Section 3.5). This was not directly tested in our study, but evidence of the inhibition withstanding the lytic steps was forthcoming from the comparison of samples that were exposed to IAA prelytically and samples that were subjected to glass-bead extraction before inhibition. In Fig. 4.3.3, it can be seen that the IAA titrations of GAPDH activity yielded very similar measurements of $V^{app}_{max,GAPDH}$ (according to the method of 3) irrespective of the method of IAA addition. This was the case for biological repeat *II* and *III*, but not for *I*, which was a consistent outlier to the other two isolates (see Section 6.4). The measured $V^{app}_{max,GAPDH}$ of the prelytically inhibited cells could only match that of the directly inhibited cell-free extract if IAA diffused over the cell envelope, then evenly into the cytosol, and then did not dissociate from the target thiol during the glass bead extraction.

Unlike irreversibility, specificity of IAA was not investigated in this study. It was concluded from literature that IAA could be used as a specific inhibitor of GAPDH activity. In his "Handbook of Enzyme Inhibitors", Zollner [96] cites over 100 targets for IAA in various metabolic pathways across species, which is unsurprising, considering its chemistry: a small-molecule thiol-alkyating agent with no specific structural affinity for a given enzyme [92]. Despite the known promiscuity of IAA, it has been reported to act on glycolysis

via GAPDH since the 1930s [21]. IAA has subsequently been used as a selective inhibitor of GAPDH in multiple organisms, including *S. cremoris* and *S. lactis* [22], *Trypsonoma cruzi* [23], and human lung carcinoma cells [105]. According to what was reported by Campbell-Burk *et al.* [101], we kept to IAA concentrations that were below 500 μM so that we could assume specific GAPDH inhibition.

Finally, we also collected data on the effect of the redox state on IAA inhibition. The findings by Brodie and Reed [105] show that the an oxidated state of the cysteinyl thiolate can protect GAPDH from IAA binding. An oxidised state reduces the affinity of the cysteine residue for the electrophilic inhibitor [124]. The addition of DTT to our assay cocktails did not to a change in the % inhibition (Fig. 4.2).

Accounting for all of these factors allowed us to directly link the decrease in GAPDH activity to the specific and irreversible action of IAA. The rest of the discussion will elaborate on how this knowledge was applied.

6.1.1 Prelytic Inhibition

Beyond its GAPDH specificity, the fact that IAA acts irreversibly makes it doubly useful as a model validation tool. The reason for this was discussed in detail in Section 3.2: a major concern with inhibiting flux in whole cells, and then doing the same in cell-free extract for the measurement of its local effect, lies in the differences in the composition of the two environments - the whole cell *versus* cell-free extract. These differences can often lead to quite substantial disparities between enzyme activity measurements *in vitro* and *in vivo* [26]. We captured this idea in Eq. 3.2.1, an adaptation of a selectivity equation by Haanstra *et al.* [80], with which we explained how differences in the ambient conditions in which the IAA alkylates the active-site cysteine of GAPDH can lead to unaccounted-for differences in pharmacokinetic availability of the IAA and the affinity of the enzyme for the IAA (see Section 3.2).

The irreversibility of IAA allowed us to incubate cells in set concentrations of IAA before lysis, and only to split them after the incubation into the cells that would be lysed for GAPDH activity determination and the cells that would be kept intact and incubated in a glucose-containing medium to measure flux (Section 3.4). We found that the % inhibition seen when administering IAA prelytically *versus* administering it directly to the cell-free yeast extract yielded nearly identical results in two out of the three biological repeats (see Figure 4.3.3). This suggests that the inhibitor permeates the cell envelope and that equilibrium is reached within the hour incubation of the cells in the inhibitor, contrary to what was reported by Hansen and Winther [102].

For *S. cerevisiae*, therefore, it appeared that the method of IAA administration did not make a difference, hence the differences in the ambient conditions were unimportant. However, this does not necessarily mean that

the same will be the case for other organisms. Yeast glycolytic enzymes are all located in the cytosol [3], whereas in some other organisms they are localised inside organelles that might more effectively restrict the access of IAA to these enzymes (e.g. the glycosome, which has a membrane that is known to be impermeable to small molecules 61). Beyond extra barriers, compartmentalisation or localisation of certain enzymes might also lead to different binding conditions for inhibitors *in vivo* and *in vitro* that are not present in the cytosolic distribution of GAPDH in *S. cerevisiae*. Differences in redox conditions [105] or macromolecular crowding conditions [44] are examples of intracellular conditions that might be heterogeneous inside a cell and lead to poorer IAA access to GAPDH in the whole cell.

Our results show, at least in principle, that prelytic inhibition of GAPDH with IAA can be a work-around when differences in ambient conditions are suspected to lead to different inhibitory profiles between whole cells and cell-free extract: this by exposing cells to IAA prelytically and then measuring the flux and GAPDH inhibition by assaying the same cells (or extract from these same cells). Though we saw no such disparity in binding between whole cells and cell extract, we did confirm that IAA can be administered prelytically and that GAPDH does not recover activity upon lysis or dilution. However, these results would have to be revisited if the inhibitor is used on organisms that house GAPDH in an intracellular compartment (like *T. brucei*; [113]) to see if the inhibitor reaches GAPDH at all. Typical cell-lysis techniques like the application of mechanical force or sonication have been known to lead to the breakage of covalent bonds [129], and though it might not have been the case in the current study, future work making use of prelytic IAA incubations should investigate whether their extraction method leads to IAA dissociation or not.

There are two other potential advantages of the prelytic inhibition method that, though they did not make a difference in our work, are important to note. First, that the experimenter has more precise control over the incubation time: by washing external IAA away, the IAA concentration gradient is reversed from the inside to the outside of the cell, which will lead to an abrogation of further inhibition. Second, since the cell extract on which GAPDH activity is measured and the whole cells on which flux is measured, come from the same IAA-exposed cell suspension, the effect of experimental error between flux inhibition and GAPDH inhibition is eliminated.

Note that, for the sake of brevity, all GAPDH activities discussed in the rest of this chapter (unless explicitly stated otherwise) were measured in the presence of DTT and were exposed to IAA before lysis. We choose to focus on prelytic inhibition as it is the main focus of this study, and also prefer the presence of DTT, as it is common in literature to add a moderate reducing agent like DTT to reverse the effects of oxidative damage (e.g. during the construction of the Teusink model [1]).

6.2 GAPDH Activity Measurements

The GAPDH activities measured in this study were all measured in the *in vivo*-like buffer proposed by Van Eunen *et al.* [3]. Their buffer was designed to have an ionic composition and pH that is as close as possible to what they determined for the *S. cerevisiae* CEN.PK113-7D strain, while still being practical in a laboratory environment. In spite of the strain difference, the buffer that they proposed should be a good approximation of the cytosolic conditions in most *S. cerevisiae* cells.

The approximate $V_{max,GAPDH}$ that we measured in the buffer by Van Eunen *et al.* was smaller than the same parameter in the Teusink model regardless of the assay buffer of method of IAA administration: the forward $V_{max,GAPDH}$ reported by Teusink *et al.* was 4.4 μmol.min^{-1}.mg protein^{-1}, compared to our measurements of 4.15, 2.56, and 2.54 μmol.min^{-1}.mg protein^{-1} for the repeats *I*, *II*, and *III*; in the reverse direction, their $V_{max,GAPDH}$ of 24.3 μmol.min^{-1}.mg protein^{-1} was considerably higher than our 6.96, 4.5, and 4.69 μmol.min^{-1}.mg protein^{-1} (*I*, *II*, and *III*, respectively).

Repeat *I*, which yielded the highest flux measurements, was a consistent outlier to the other data in this study and to what was expected, so the true flux probably lies closer to the measurements of *II* and *III*: a forward $V_{max,GAPDH}$ of about 2.5 μmol.min^{-1}.mg protein^{-1} and a reverse $V_{max,GAPDH}$ of about 4.5 μmol.min^{-1}.mg protein^{-1}.

Higher literature V_{max} values are not unexpected, as experimentally measured V_{max} values are never truly substrate-saturating, and parameters are typically determined using fits that are extrapolated to infinitely high substrate conditions [26]. This technicality, though important, cannot account for the factor two (in the case of the forward $V_{max,GAPDH}$) or factor six (in the case of the reverse $V_{max,GAPDH}$) difference between the literature values and our measured values.

One contributing factor to the differences between our measured, approximate $V_{max,GAPDH}$ values and those from Teusink and colleagues [1], could be the different strains (Koningsgist *versus* X2180). Du Preez *et al.* [2], however, used X2180, as did we. We adjusted the parameter in the *dupreez4* model upwards to yield 2.08 μmol.min^{-1}.mg protein^{-1}, according to the temperature difference and Q10 value suggested by Du Preez *et al.* [2] themselves (Subsection 4.3.1). This is much closer to our measured forward $V_{max,GAPDH}$ of about 2.5 μmol.min^{-1}.mg protein^{-1}.

In light of this, strain differences do seem to partially account for the disparity between our measured forward $V_{max,GAPDH}$ and what was reported by Teusink *et al.* [1]. The disparity between the reverse $V_{max,GAPDH}$ is more puzzling, however, as the Du Preez model has no expicit reverse $V_{max,GAPDH}$, and the difference between our and Teusink *et al.*'s values is much larger (about a factor of six): it would be a breach of the Haldane relationship if the K_m values did not concurrently change to conserve the K_{eq} (see Eq. 5.1).

Since we did not determine the K_m values, however, we could not confirm that the Haldane relationship remains in tact. What is interesting to note, are the differences between the buffer proposed by Van Eunen and colleagues [3] and what they called "optimised" conditions. The composition of the different buffers were:

- *Van Hoek*: 100 mM triethanolamine, 1 mM EDTA, 1.5 mM $MgSO_4$, pH = 7.6;
- *Teusink*: 50 mM Pipes, 100 mM KCl, 5 mM $MgSO_4$, pH = 7.0;
- *Van Eunen*: 300 mM K^+, 20 mM Na^+, 1.0 mM Ca^{2+}, 1.0 mM Cl^-, 245 mM glutamate, 50 mM phosphate, 10 mM $MgSO_4$, pH = 6.8;

What is most striking about the buffers, is that the Van Eunen buffer contains more different solutes than the buffers used by Van Hoek *et al.* [118] and Teusink *et al.* [1], for instance the amino acid glutamate and a larger variety of ions (specifically calcium, potassium, sodium, and free phosphates). Van Eunen and colleagues [3] report that the GAPDH activity that they measured in the reverse direction in the *in vivo* buffer is two times smaller than what they measured in the Van Hoek buffer. They do not measure the activity of GAPDH in the forward direction, so it is not clear from their work whether the V_{max} is affected similarly in both directions.

García-Contreras and colleagues [46] reported a similar finding when comparing measured enzyme capacity in an optimised *versus* an *in vivo*-like medium: eight out of twelve assayed glycolytic and nitrogen assimilation enzymes in an *Escherichia coli* cell extract had significantly different V_{max}. Specifically, they found *E. coli* GAPDH to have an almost 80% lower activity in an *in vivo*-like buffer than in an optimised buffer; they also found that potassium ions and inorganic phosphates can account for almost all of this activity loss, while glutamate had no or only a moderate effect on the activity of glycolytic enzymes. If the inhibitory effect of potassium and free phosphates also applies to *S. cerevisiae* enzymes, the absence of both potassium and inorganic phosphate in the Van Hoek and Teusink buffers might account for the comparatively lower GAPDH activity measured in the Van Eunen buffer.

Under the assumptions that the disparity in measured enzyme activity is equal for the forward and the reverse reactions, and that the expected difference between the measured values in the Van Eunen [3] and Teusink [1] buffers will be similar to what was seen when comparing the Van Eunen [3] and the Van Hoek [118] buffers, one could reduce the Teusink parameters by a factor of two for comparison. The hypothetical values that would be measured in the Van Eunen buffer on the Koningsgist (DSM Bakery Ingredients, Heerlen, The Netherlands) enzymes used by Teusink *et al.* would be: 2.2 μmol.min^{-1}.mg protein^{-1} in the forward direction and 12.15 μmol.min^{-1}.mg protein^{-1} in the

reverse direction. In the following paragraphs, we refer to them simply as the *hypothetical* parameters.

For the forward parameter, the experimental values (2.5 μmol.min^{-1}.mg protein^{-1}) are now very close to the hypothetical value of from the Teusink model (2.2 μmol.min^{-1}.mg protein^{-1}). When one compares the reverse parameter to the experimental result, however, the measured $V_{max,GAPDH}$ of about 4.5 μmol.min^{-1}.mg protein^{-1} is still up to a factor of three smaller than the hypothetical parameter of 12.15 μmol.min^{-1}.mg protein^{-1}.

It is, then, not just the measured V_{max} values that change, but the ratio between the two. Since we did not perturb the substrate concentrations, we could not fit a V_{max} parameter to see whether the ratio between the parameters are restored when a true V_{max} is calculated, but we followed the method of Van Eunen *et al.* [3] for the measurement of the reverse $V_{max,GAPDH}$ and the method of Ferdinand [120], in Van Eunen *et al.*'s buffer, for the measurement of the forward $V_{max,GAPDH}$. These measurements are therefore expected to be at least close to substrate-saturating and not at arbitrary conditions.

An asymmetric change in the V_{max} values of a reversible enzymatic step means, according to the Haldane relationship (Eq. 5.1), that the equilibrium constant (K_{eq}) or the enzyme's affinity for its substrate (K_m) must also change. In our case - assuming the K_{eq} does not change - the K_m ratio ($\frac{K_{m,BPG}}{K_{m,GAP}}$) would need to increase by a factor of between two and three to compensate for the change in V_{max} ratios. This is not unrealistic, as "other kinetic parameters, such as affinity constants, are also likely to be affected by the composition of the assay medium" [3]. We did not measure the K_m values of GAPDH to confirm that this was, indeed, the case. However, the combination of strain differences and buffer differences offer two testable hypotheses for future studies to validate our work.

6.2.1 Percentage Response of GAPDH to IAA

Encouragingly, the relative effect of IAA was almost identical for the forward and the reverse GAPDH activity titrations (see Fig. 4.6). This means that the Haldane relationship was perfectly obeyed in terms of relative activity decrease. IAA sequesters individual GAPDH enzymes by binding to their NADH/NAD$^+$ site [93]. The relative inhibitory effect should therefore be identical in the forward and reverse direction, as the substrates of both reactions are prevented from interacting with the active site of the enzyme. That this was what we saw, was confirmation that we could proceed with the relative activity inhibition functions as descriptions of IAA action.

We inserted the inhibition term as a modifier of $V_{max,GAPDH}$ (see Eqs. 5.5 and 5.6), since IAA is irreversible in its action and permanently decrease the catalytic capacity in a given cell/extract (Subsection 5.1.1).

6.3 Glycolytic Flux Measurements

By incubating *S. cerevisiae* cells in high glucose concentrations, we could assume that the Crabtree effect would cause nearly all glucose to be converted to ethanol, instead of being diverted to the branches of glycolysis or being further oxidised in the tricarboxylic acid (TCA) cycle [9]. For the purposes of this study, therefore, our assumption was that glucose consumption and ethanol production should be equivalent, albeit stoichiometrically different.

We measured the glucose consumption and the ethanol production rates as expressions of glycolytic flux. The measured glucose consumption rate was 0.1 to 0.13 μmol.min^{-1}.mg protein^{-1} and the ethanol production rate was measured to be 0.11 to 0.15 μmol.min^{-1}.mg protein^{-1}. If the mean of repeats *II* and *III* are taken, glucose flux was 0.12 μmol.min^{-1}.mg protein^{-1} and ethanol flux 0.13 μmol.min^{-1}.mg protein^{-1}: a ratio of about 1:1 (see Fig. 4.13). The models predicted a glucose:ethanol ratio closer to 1:1.5 (see Section 6.5.1): the Teusink model predicted a glucose flux of about 0.32 μmol.min^{-1}.mg protein^{-1} and an ethanol flux of 0.50 μmol.min^{-1}.mg protein^{-1} (ratio 3:5), while the Du Preez model predicted the glucose and ethanol fluxes to be 0.15 μmol.min^{-1}.mg protein^{-1} and 0.21 μmol.min^{-1}.mg protein^{-1} (3:4), respectively.

We reproducibly measured flux values that were within a factor of two from each other (Fig. 4.13). Moreover, our forward $V_{max,GAPDH}$ approximations were all much larger than our measured flux values. This shows that our measured approximate $V_{max,GAPDH}$ values can realistically support our measured flux, which is a requirement for experimentally determined flux and enzyme activities to be acceptable [35]. What remained unexplained, however, was why our fluxes were so much lower and, in a different ratio, than the literature values.

Albers *et al.* [43] experimentally measured glucose consumption and ethanol production in *S. cerevisiae* X2180 cells that were grown to diauxic shift and then challenged with 50 mM of glucose: they found a glucose flux of about 0.3 μmol.min^{-1}.mg protein^{-1} and an ethanol flux of about 0.40 μmol.min^{-1}.mg protein^{-1}; glycerol and acetate fluxes were comparatively very small, as expected in high-glucose conditions [82]. Unlike the Teusink and the Du Preez models, Albers and colleagues used the same strain at the same temperature (30°C) as we did. In their and our experiments, the yeast cells were grown to diauxic shift and challenged with an excess of glucose. That they also found a lower glucose to ethanol flux ratio (3:4) is good support of the validity of our experimental results. However, Albers *et al.* [43] still measured glycolytic fluxes that were quite a bit higher than ours.

One possible explanation could be the he Pasteur effect - the inhibition of fermentation by oxygen. This effect is known to slow glycolysis by diverting some of the traffic of glycolysis to the slower, higher energy-yielding respiratory pathway downstream from pyruvate kinase [130]. The repression of fermentation is avoided in *S. cerevisiae* culturing by partially sealing culture

flasks and filling them to half or more of their total volume, making the environment in the flask less aerobic, hence curbing the Pasteur effect (e.g. in 43). Our culturing was done in this way, but during our flux measurements the incubating cell suspensions were redistributed to 1.5 mL Eppendorf tubes where the aliquots of $\leq$ 200 μL occupied not even 10% of the volume. It is feasible that an increased oxygen to sample volume allowed inhibition of glycolysis by the up-regulation of respiration. Davies and Brindle [130] showed that aeration can lower both glucose consumption and ethanol production rates. This might be a partial explanation of why were measured lower fluxes. We did not measure the rate of respiration, however, for instance by measuring oxygen consumption, so we do not have evidence for this effect. But it does provide a hypothesis for suture studies in a similar manner.

That leaves the question of the disparity between the ratio of glucose:ethanol between our experimental data and what was reported in literature. A first instinct is to ascribe it to the branches of glycolysis. Neither the a computational interrogation of the Teusink model [33], nor our experimental results suggested that flux is redistributed to the branches in any significant way, however. One can also see this in the fact that the % flux only diverges for glucose consumption and ethanol production at very low GAPDH activity (Fig. 5.8: only when flux is very low (40%), do the branches between glucose import and ethanol export significantly impact the relative flux of carbon so what goes in and what comes out starts to look different in relative terms.

Interestingly, the idea of the Pasteur effect also fits with our observation of a lower ethanol to glucose ratio than was seen by Teusink *et al.* [1]: exposure to oxygen lowered the ethanol to glucose ratio to close to 1:1 in the study by Davies and Brindle [130], which was similar to our results. This could be a consequence of some part of the carbon flux not ending up as ethanol but being further metabolised in the TCA cycle. This hypothesis could be confirmed by measuring the rate of respiration, as mentioned earlier.

6.4 Disparity between Repeats

One of the recurring findings of this study was the outlier behaviour of biological repeat *I*. A number of considerations led us to believe that repeats *II* and *III* are more credible data sets.

The considerably lower protein yield of *I* (1.0, 7.8, and 7.6 mg.mL^{-1} for *I*, *II*, and *III*, respectively; see Section 4.2), despite the similar growth conditions (Fig. 4.1) was puzzling. This disparity between the cultures might be explained by an incomplete cell extraction for repeat *I*. This difference was considerably lower when the protein concentrations were determined for the preincubated lysate (0.22, 0.64, and 0.55 mg.mL^{-1}, respectively, for *I*, *II*, and *III*).

Under the assumption of an incomplete glass-bead protein extraction, we considered insufficient lytic cycles (see Section 3.5; "Lysis") as a potential cause of the extraction inefficiency. All of the samples (prelytic and otherwise) were subjected to the extraction protocol concurrently and for the same length of time within each biological repeat. There were a minimum number of lytic cycles for each biological repeat, but we judged by eye when the lysis protocol had been completed in the case of incomplete lysis after the minimum number of cycles. It might well be that not enough time was given for the full lysis of the yeast cells in isolate *I*, which was done first (hence when the experimenter was at his most inexperienced): in this situation, a more dilute cell suspension would see a larger percentage of its cells successfully lysed, compared to more concentrated cell suspensions. The fact that the difference in protein yield is less pronounced for the prelytically inhibited cells (*preinh-batch*, which were more dilute during extraction) than for the larger batch (*in-vitro-batch*), is in line with this hypothesis.

If a lower protein extraction efficiency is assumed, much of the disparity in the data begins to make sense. Since equal concentrations of IAA were added to equal volumes of the general lysate batch for the *in vitro* inhibition assays, an equal inhibitor concentration would have been exposed to a lower enzyme concentration in *I*. The understanding of IAA as reducing the free enzyme concentration (Eq. 5.1.7) implies that equal concentrations of IAA will have a much greater effect if the enzyme concentration is lower to begin with. This might be compensated for by normalising the data to protein yield, unless the protein concentration is so low as to yield full or nearly full inhibition at all IAA concentrations - as was, indeed, the case (Fig. 4.3.3). In contrast to this, the prelytic inhibitor incubations take place before lysis: the prelytically incubating enzyme concentration is therefore not yet affected by poor extraction efficiency. Assuming that the lytic procedure does not somehow select for cells that have been more or less strongly inhibited, the fractional inhibition of GAPDH should not be increased by low protein extraction efficiency (as is seen in Fig. 4.3.3).

Poor protein extraction could therefore be responsible for some aberrant observations of repeat *I*. This was, however, not the full story: since the protein concentrations determined in Section 4.2 were used to normalise the measured fluxes as well (which are measured on whole cells), one would expect a seven times less effective protein extraction to suggest a seven times higher normalised flux. This was not the case - rather, the flux in *I* was about two times higher than in *II* and *III* (see Fig. 4.13). This suggests that the trouble with repeat *I* is more than just poor protein extraction efficiency. We could not identify the cause of this discrepancy, and that - together with the fact that IAA did not elicit full GAPDH inhibition at 400 μM of IAA in repeat *I* even when the other repeats were fully inhibited at IAA concentrations below 200 μM - was the big consideration for treating repeat *I* as an outlier when comparing the data sets.

6.5 Model *versus* Experiment

6.5.1 Du Preez *versus* Teusink: Glycolytic Flux

One of the main aims of this study was to test the validity of two models in their prediction of the the glycolytic flux control of GAPDH in yeast. Cvijovic and colleagues [37] refer to the challenge of maintaining the consistency of integrated models with respect to the original models. If the model adjustment of Du Preez *et al.* [2] is regarded as an attempt to expand the predictive capacity of the Teusink model [1], then it would be interesting to know whether that improvement required a rebalancing of the relations between the enzymes. In light of the asymmetry of the parameter changes made by Du Preez *et al.* (for instance, the V_{max} glucokinase being adjusted to 101% of its Teusink size while $V_{max,GAPDH}$ was decreased all the way to 23.6% of its original size; [2]) it seems intuitively possible that flux control might be redistributed by the model adjustment.

Both models were adapted to simulate the conditions of our assays: batch culture and glucose excess, with the addition of an ethanol export step. Under the assumption that all acetaldehyde is quickly converted to ethanol (Crabtree effect; [9]) we set the rate constant of the acetaldehyde export step to zero. The fluxes predicted by the adjusted models with an initial external glucose concentration of 20 mM, were:

Table 6.1: Simulated glycolytic flux in two adapted kinetic models of yeast glycolysis. The fluxes are measured in μmol.min^{-1}.mg protein^{-1}.

	Glucose consumption	Ethanol production
Teusink model	0.32	0.50
Du Preez model	0.15	0.21

The Teusink model simulated fluxes that were about two times larger than the Du Preez simulations. The mean downwards adjustment of the V_{max} values by to 50% of their original sizes during the algorithmic adaptation of the Teusink model to the Du Preez model are accounted for by an assumed Q10 value of 2, as explained in [2]. The effect was also seen in the flux, where the 20 mM of initial glucose was depleted by the Teusink model in 13 minutes, and by the Du Preez model in 30 minutes.

6.6 Glycolytic Flux Control

To simulate GAPDH inhibition by IAA, we modified the $V_{max,GAPDH}$ values of the original models by multiplying them with an exponential decay function (see Fig. 4.6; [124]). Repeats *II* and *III* combined yielded the fit:

$$Fractional\ Remaining\ Activity\ = e^{-0.017\cdot[IAA]} \tag{6.6.1}$$

with an R^2 value of 0.96. [IAA] was varied over the concentration range 0 μM to 200 μM to simulate a GAPDH activity titration.

The predicted control coefficients were very similar for the two models (see below). Calculating the control over ethanol production and glucose consumption, both models predicted almost zero control for GAPDH:

Teusink:

$$\begin{aligned} C^{J_{GLCo}}_{v_{GAPDH}} &= 0.0045 \\ C^{J_{ETOHo}}_{v_{GAPDH}} &= 0.031 \end{aligned}$$

Du Preez:

$$\begin{aligned} C^{J_{GLCo}}_{v_{GAPDH}} &= 0.0068 \\ C^{J_{ETOHo}}_{v_{GAPDH}} &= 0.024 \end{aligned}$$

From these calculated control coefficients, we could conclude that Du Preez and colleagues' computational adjustment of the Teusink model [2] did not significantly redistribute flux control. This is in agreement with the parameter scan by Pritchard and Kell [33]: they varied the V_{max} values of the Teusink model in different combinations and found flux control not be significantly redistributed by these changes. We compared the models not just for their control coefficient at zero IAA, however, but over a range of intermediate GAPDH activity: the models were good predictors of the experimental results (Fig. 5.8). Together with the control coefficients, these graphs were good evidence that the parameter adjustment by Du Preez *et al.* did not change the control distribution of the original Teusink model significantly.

The slopes of the experimentally measured relative GAPDH activity and relative glycolytic flux as functions of IAA near $[IAA] = 0\,\mu M$, could be used to calculate glycolytic flux control (Figs. 5.3 and 5.6):

$$C^{J_{EtOH}}_{v_{GAPDH}} = 0.21$$

$$C^{J_{GLCo}}_{v_{GAPDH}} = 0.032$$

It is striking how different the control over production and consumption appears to be: the excess glucose in the flux incubations was expected to initiate aerobic fermentation, during which flux through glycolysis is quick and fermentative, and flux to the branches is limited [9]. In this case, one would expect control over the flux of ethanol production and glucose consumption to be very similar. Interestingly, Poolman and colleagues [22] found that GAPDH

in *S. lactis* and *S. cremoris* had a glycolytic flux control of almost unity ($C^J_{v_{GAPDH}} = 0.9$). These organisms are also both fermentative, like yeast, and Poolman *et al.* [22] measured glycolytic activity as H^+ increase (pH decrease): this is a product formation rate and hence agrees more closely to our measured ethanol production flux rather than glucose consumption flux.

Poolman and colleagues noted that flux control is additive and that other enzymes might have negative control that allows flux control to be more distributed through glycolysis. The difference in control over production and consumption must be due to branching pathways diverting some of the glycolytic flux away from the main chain - otherwise flux through glycolysis would be the same everywhere in the pathway [131].

Considering our application of glucose excess conditions, we did not expect glycolytic flux to be strongly influenced by branching pathways. However, the Pasteur effect (Section 6.3; [130]) might have contributed to a redistribution of flux control by slowing down main-chain glycolysis and leading to proportionally larger branch fluxes and incomplete conversion of glucose to ethanol. This might then also contribute to a difference in the amount of control that GAPDH can exert over the two enzymes: the presence of significant branch fluxes will mean that carbon flux can be redirected to the branches and kept constant at the import step, while ethanol production slows down due to GAPDH inhibition. That the parameter scan by Pritchard and Kell [33] did not suggest this redistribution of flux, might be due to the fact that it was performed on the Teusink model, which has limited detail in its branch kinetics. It might therefore be that the Teusink model cannot be simulate this effect. The same could be true for the Du Preez model, which also lacks some detail in its branches.

Despite this possible explanation for the higher experimental flux control of GAPDH over ethanol production than over glucose consumption, the possibility also exists that the experimentally determined flux control coefficient over ethanol production is not accurate. Figure 5.8 shows both experimental and simulated results for relative flux as a function of relative GAPDH activity. The relative ethanol production flux lies lower than at a given relative GAPDH activity, but the slope is not obviously steeper. It looks plausible that the wild-type ethanol production flux is an overestimation, which yields a high control when moving from the wild-type flux value to the low-IAA flux values: this might, however, be an artefact and might be corrected by simply generating more data. It is worth noting, also, that the ethanol production curves that were fitted to the data were consistently worse fits than the glucose consumption curves (Table 4.4 *versus* Table 4.5). Ethanol is very volatile and evaporation during sampling and analysis might be responsible for some artefacts in the data.

A repeat of the experiments and the independent measurement of respiratory and branch flux would be able to confirm the significance of the Pasteur effect and the contributions of the side-chains, and shed light

on whether the higher experimentally measured control is an experimental artefact or a true result.

6.6.1 Glycolytic Flux Control at High [IAA]

Between 40% and 20% remaining activity of GAPDH, there is sudden precipitous decline in glycolytic flux in the model simulations and the experimental data (Fig.5.8). This is reminiscent of the *tps1*Δ phenotype, where lower glycolysis fails to keep up with upper glycolysis, leading to toxic accumulation of the metabolites of upper glycolysis [132]. This makes sense considering that inhibition of GAPDH, which is located directly after the branch point of the pathway, effectively limits the maximum rate at which lower glycolysis can use the triose phosphates coming from upper glycolysis.

If the glucose and ethanol concentrations of the models are fixed at 20 mM and 20 mM, respectively (as in the original models), the gradual increase in the glycolytic flux control of GAPDH seen in Fig.5.8 is replaced by a sudden and precipitous collapse of glycolytic activity (from close to 100% flux to effectively 0% without any intermediate points; data not shown) at between 20% and 40% GAPDH activity. If the glucose and ethanol concentrations change (as in our simulations), intermediate flux control is seen since the flux through upper glycolysis slows down as the external glucose concentration decreases, alleviating some of the pressure that causes upper glycolysis to be so much more active than lower glycolysis [82]. If the organism is at very high glucose concentrations that do not significantly decrease due to its activity (similar to glucose clamped at high concentrations) the *tps1*Δ phenotype is especially deadly, as the pressure from the oversupply of glucose remains constant.

For the batch culture conditions, the Du Preez and Teusink model predictions and the experimental data seemed to agree in their description of a sudden and strong increase in glycolytic flux control by GAPDH when the enzyme is inhibited below a certain threshold point (between 20% and 40% of its wild-type activity). This is evidence that the models are, indeed, credible representations of steady state *S. cerevisiae* aerobic fermentation behaviour.

6.7 Conclusions and Future Prospects

The models by Teusink *et al.* [1] and Du Preez *et al.* [2] predicted the glycolytic control of GAPDH as measured experimentally in this study quite well. Unexplained differences between our experimental data and the literature still exist: the difference of a factor three between our measured fluxes and those measured by Albers *et al.* [43] on the same strain as ours; the fact that we observed ethanol to be produced in a 1:1 ratio for every glucose molecule consumed, as opposed to the higher ethanol yields seen by Teusink and colleagues [1] and by Albers and colleagues [43]; and, finally, that ethanol

production flux was calculated to be more strongly controlled by GAPDH than glucose consumption flux. We have presented multiple possible explanations for these findings, but in the absence of confirmatory evidence, we cannot decisively ascribe our observations to any of them.

Despite these remaining questions, the agreement between the model predictions and the experimentally predicted behaviour was remarkable, particularly what is seen in Fig. 5.8. The initially weak response of glycolytic flux to the decrease in GAPDH activity gives way to a sudden, precipitous decline in both ethanol and glucose flux between 40% and 20% remaining GAPDH activity. It is not unreasonable to speculate that more data might well get rid of the discrepancy between ethanol production and glucose consumption control, as the flux *versus* IAA plots are in shape very similar for production and consumption (Figs. 4.13 and 5.8).

Measuring the glycerol and O_2 production in replications of these experiments should also shed some light on the question of whether a higher oxygen-to-sample volume-ratio during the flux incubations elicited the Pasteur effect [130]. This would have partially repressed fermentation and activated respiration, hence slowing glycolysis and changing the glucose to ethanol ratio. Measurement of the fluxes through branching pathways can illuminate whether this was the case.

A control for the evaporation of ethanol from the flux measurement samples should also reveal whether the volatility of ethanol had much to do with the differences seen between glucose and ethanol flux.

The Teusink and Du Preez models are related, and benefit from almost twenty years of investigation and validation (e.g. [16, 33, 43, 47]). The accuracy of their predictions in this study, adds to a large accumulation of evidence that the models are good descriptions of the steady-state glycolytic activity of yeast cells in excess glucose conditions. It also shows that a consistency in the relation between GAPDH and its pathway was maintained during the model adaptation by Du Preez *et al.* [2]: the summation theorem of glycolytic flux control [20] implies that this is also a partial and indirect validation of the flux control distribution through the rest of the pathway.

IAA itself appears to have good *bona fides* as an experimental tool for metabolic control analysis [128]: exposing whole cells to this irreversible, GAPDH specific inhibitor can allow systems biologists to partially circumvent the problem of differences in *in vitro* and *in vivo* conditions during inhibition titration. Along with the glucose transporter, which is situated on the outside of a cell and can be perturbed and assayed without lysing the cells, the flux control of GAPDH can be used as a standard check for glycolytic model validity. IAA has been used on a wide variety of organisms and can be appropriate for any number of glycolytic models [22, 93, 101].

GAPDH, being the first enzyme of lower glycolysis, has been reported to be involved in a number of metabolic behaviours. IAA can be used to investigate these behaviours without the need for cell lysis before inhibitor administration.

Production of NADH by alcohol dehydrogenase, fuelled by the capture of acetaldehyde by cyanide, leads to a build-up in fructose-1,6-bisphosphate (FBP) by inhibiting GAPDH activity - this FBP build-up then hypothetically causes the increased ATP sensitivity of PFK, manifesting in glycolytic oscillations [67]. Wolf *et al.* [111], also argue that NADH-ATP coupling via the GAPDH-PGK module transduces extracellular acetaldehyde to glycolytic oscillations, which lead to the synchronisation of oscillations. These claims can be investigated using IAA as an inhibitor of GAPDH in whole-cells.

Most importantly of all, perhaps, IAA offers the opportunity to directly measure the glycolytic flux control of human pathogens for which GAPDH has been reported to be a major controlling enzyme. The glycolysis of *Plasmodium falciparum* and *Trypsonoma brucei*, the causal agents of malaria and African sleeping sickness, have both been suggested to be strongly controlled by GAPDH in their blood-borne stages [10, 59], while red-blood cells have been shown to lack clinical symptoms even upon a 95% reduction in their GAPDH function [133]. The application of IAA to validating the predictions of high flux control by GAPDH, can be a potentially fruitful route to rational drug design according to the principles of network-based selectivity [79].

Appendices

Appendix A

Protein Concentration

Table A.1: Protein yield varied considerably between different biological repeats but not within them. Protein concentrations, determined from assaying multiple dilutions of the protein extract, sometimes had high standard deviations (up to 20% of value itself). 80% accuracy was accepted as sufficiently precise for the purposes of this study.

I

[IAA] in μM	[Protein] mg.mL^{-1}	Standard Deviation	%Standard Deviation
(*in vitro* inhibition)	0.996774	0.080416	8.06763
0	0.216716	0.00151323	0.698256
25	0.234271	0.0112211	4.78981
50	0.218027	0.0228457	10.4784
100	0.25113	0.0204845	8.15693
200	0.235686	0.00133999	0.568551
400	0.212086	0.0245517	11.5763

II

[IAA] in μM	[Protein] mg.mL^{-1}	Standard Deviation	%Standard Deviation
(*in vitro* inhibition)	7.75881	0.066928	0.862606
0	0.610336	0.06618	10.8432
18.75	0.70613	0.0838657	11.8768
37.5	0.640606	0.11821	18.4529
75	0.628163	0.0952763	15.1675
150	0.636711	0.132906	20.8739
300	0.6018	0.0956056	15.8866

III

[IAA] in μM	[Protein] mg.mL^{-1}	Standard Deviation	%Standard Deviation
(*in vitro* inhibition)	7.57461	0.232738	3.07261
0	0.557252	0.0897569	16.1071
15.625	0.492936	0.0458401	9.29941
31.25	0.625021	0.0633688	10.1387
62.5	0.470016	0.0775217	16.4934
125	0.641863	0.0691127	10.7675
250	0.475908	0.0508479	10.6844

Appendix B

Inhibitor Irreversibility

To confirm the purported irreversibility of IAA's binding [21, 22, 95], cell-free extract was incubated at 30°C in a physiological buffer according to Van Eunen *et al.* [3]: one sample was incubated without any IAA and another with 400 μM . Periodic measurements of GAPDH reaction rates, both forward and reverse, were then taken over two hours (the *inhibition* incubation). This cell-free yeast extract was then diluted to five times its original volume, and an identical 120 minute time-course assay performed (the *dilution* incubation). A recovery of activity after dilution would be indicative of a reversible inhibition mechanism.

In the case of reversible binding, however, the speed of the adjustment of the binding upon dilution might exceed the sampling rate in the assay and prevent us from seeing the dynamics. Therefore it was considered insufficient to merely observe the absence of an increase in activity during *dilution*. Preliminary results showed 400 μM of IAA to fully abrogate GAPDH activity, while its five-times dilution (80 μM) does not. The presence of activity (even if its recovery is much faster than our sampling speed) would therefore be evidence of binding reversibility.

Fig. B.1 shows the measured reaction rates as a function of time during *inhibition* and *dilution* phase, respectively. There was a time-dependent loss of specific activity upon IAA addition, and activity was effectively abrogated after 60 minutes of incubation (Fig. B.1 *A* and *C*). Fig. B.1*C* contains significant scatter: this scatter - which is troublesome when trends are sought - arose from high levels of noise in the initial readings of the activity assays that are often unavoidable when high concentrations of cell-free extract are used. For the purposes of this assay, however, it was necessary only to ascertain that high levels of activity remain when IAA is not added: the stark contrast between the low-noise, low-activity data of the inhibited extract and the highly active, very noisy data from the positive control confirmed this.

After the *inhibition* phase, a 5 times dilution of the extract was made: no recovery of activity was seen over 120 minutes in the inhibitor-containing samples, though a constant level of activity was observable in the positive controls throughout (Fig. B.1 *B* and *D*). It followed from these results that

IAA acted irreversibly over the time-scales that were implemented in this study, and subsequent data are treated as such.

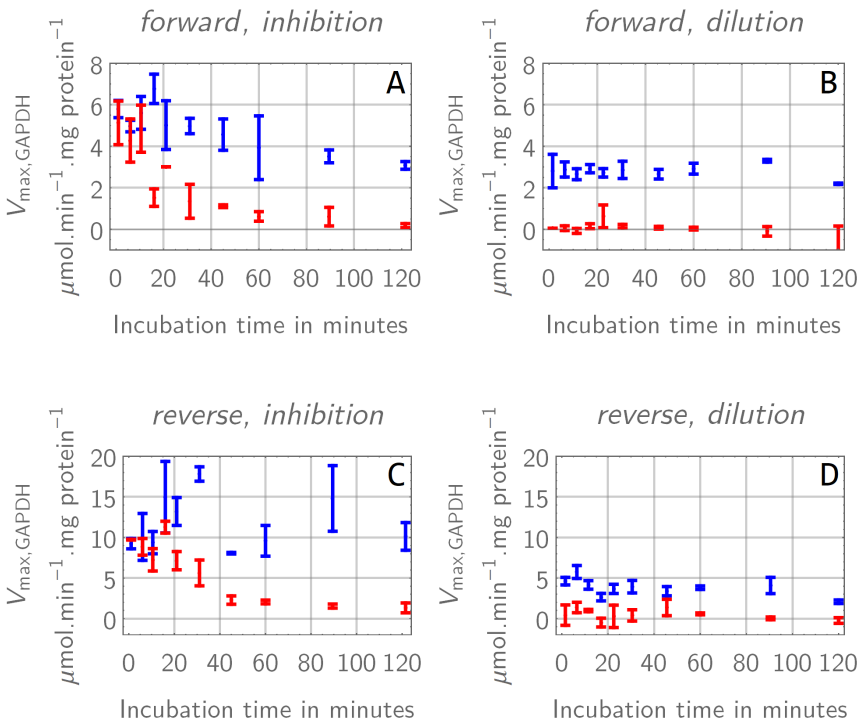

Figure B.1: Dilution of an inhibited cell-free extract does not reduce the effects of IAA on GAPDH activity. GAPDH activities, both forward and reverse, are shown as a function of incubation time after the cells were first exposed to 400 μM of the inhibitor (*A* and *C*), and then again after the same extract was diluted 5 times (*B* and *D*). The red data points were administered with IAA while the blue data points were positive controls and were incubated for the same length of time, but in the absence of IAA. It can be seen that there is a time dependence in the effect of IAA on the measured specific activity values. After the maximal effect has been reached, however, dilution does not lead to a recovery in activity. The y-axis expresses specific GAPDH activity in units of μmol.min^{-1}.mg protein^{-1}

.

Appendix C

Non-specific NADH Oxidation

To control for residual NADH oxidation, a range of lysate dilutions was put in the presence of a fully prepared reverse GAPDH activity assay, save for the starting metabolite, 3-PG. Fig. C.1 shows that background activity accounted for no more than 3% of the observed activity in an activated assay. The influence of this background activity would henceforward be disregarded.

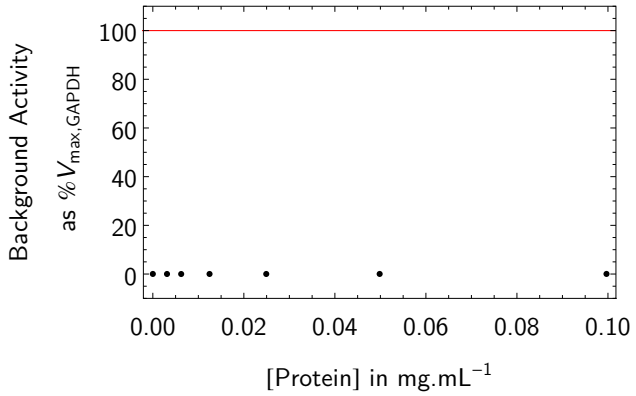

Figure C.1: Non-specific NADH oxidation accounts for only a negligible background absorbance change. Negative controls were tested at varying cell-extract concentrations, with only the starting metabolite (PGA) omitted. The points represent the protein concentrations that were assayed for background activity, normalised over the same measured specific activity (approximate $V_{max,GAPDH}$, horizontal red line). The $V_{max,GAPDH}$ was calculated to be 0.39μmol.min^{-1}.mg protein^{-1} - it was measured at a protein concentration of 0.003 mM.mL^{-1}. Background activity at various protein concentrations contribute no more than 3% of the specific activity visible in an initiated assay.

Appendix D

V_{max} Segment Selection

In both the forward and the reverse directions, the segments which would be used to calculate the reaction rate were selected manually (Figure D.1 shows some examples to illustrate this process).

The criteria that were applied for segment selection were:

1. selected segments were all at least 30 seconds (four readings) to a minute (seven readings) long;
2. the same segments were used within each technical replicate in the same direction (e.g. B and C) for consistency (see 4.3.2);
3. to avoid underestimation of V_{max} , the segments all started at the first time point, unless there was a clear initial lag in the reaction (e.g. at 31.25 μM and 62.5 μM in C);
4. if the standard deviation of the data was unstable or large, the members of a triplicate were inspected and the member with the higher error dropped (*cleaning*) - no more than one member of each triplicate was dropped(E is an example data before discarding and F is an example of the same data after *cleaning*);

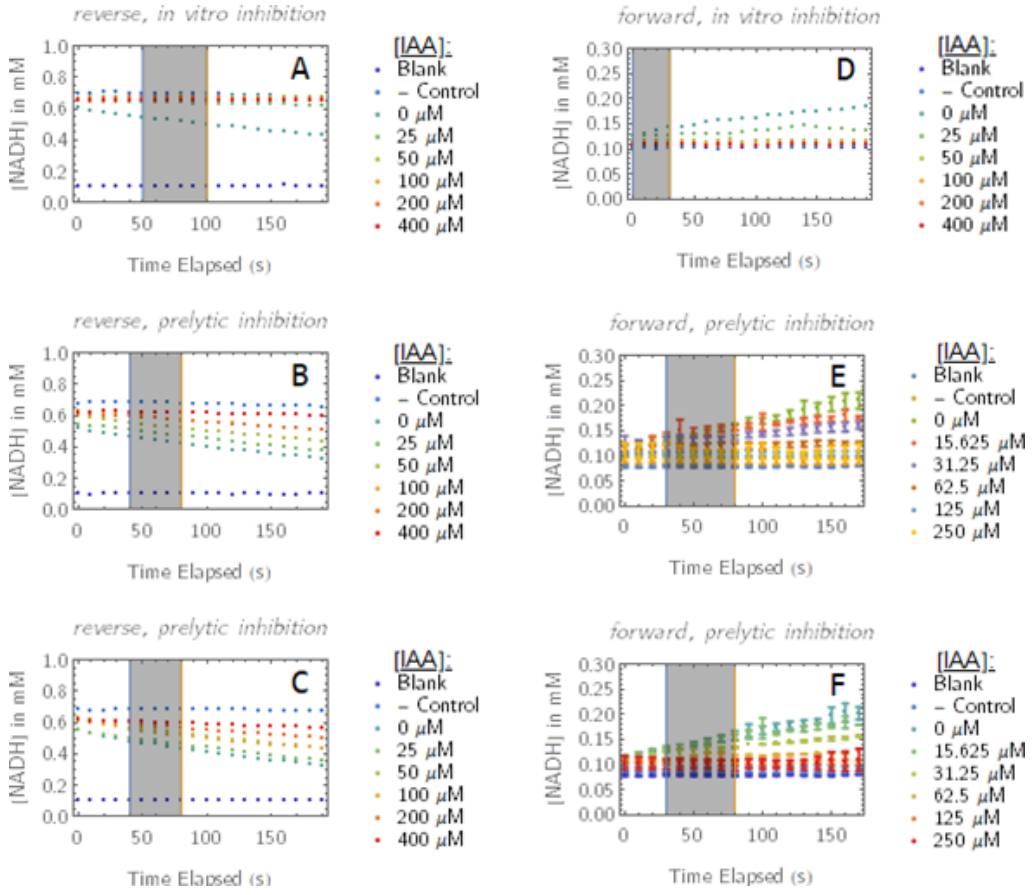

Figure D.1: Examples of selections of V_{max} segments. The data in these plots are the means of the absorbance measurements at $\lambda = 340nm$ as a function of time. The segments from which reactions rates would be calculated were selected by hand. A to C are examples of this for reverse activity assays, while D to F are examples of forward V_{max} segment selections.

Appendix E

NADH Calibration Curve

The function relating NADH concentration to absorbance at 340 nm ($y = 1.30801x$ ($R^2 = 999855$); from Fig. E.1 below) was used to convert absorbance measurements to NADH concentrations.

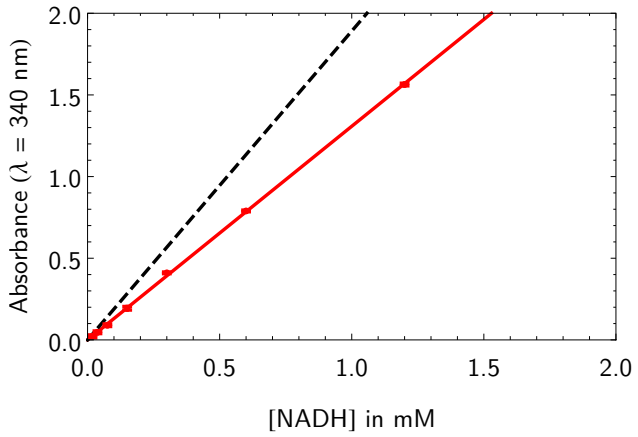

Figure E.1: A good correlation exists between measured absorbance values at $\lambda = 340nm$ and NADH concentration. Varying NADH concentrations were visualised spectrophotometrically in the buffer of [3]. The experimentally constructed calibration curve is shown in red, both the data and the linear model fit. The fitted function was $y = 1.30801x$ ($R^2 = 999855$). The dashed black line was created by calculating the expected absorbance reading from the NADH concentrations of the standards, the extinction coefficient of NADH, and the light path length through 100 μL of contents in a well of a Greiner F-bottom mictrotitre plate (specification sheet available here); it has a function $y = 1.89088x$. The disparity between the theoretical trend and the measured trend is not worrisome, however, since a very reliable fit through the experimental data can be obtained.

Appendix F

Inspection Error in Rate Data

Table F.1 shows the standard deviation within technical triplicates for each reaction condition as a percentage of the the wild-type ([IAA] = 0 μM) rate for the same reaction condition. Data represented in red are standard deviations more than 20% the size of the wild-type and those that are both underlined and red are more than 30% the size of the wild-type rate. These % standard deviations guided decisions on data that might have to be discarded due to large error.

Using the normalised standard deviations from Table F.1 as a guide, graphic representations of reaction rate (in μmol.min^{-1}.mg protein^{-1}) as function of IAA concentration were inspected. In Fig. F.1, examples are presented to illustrate the considerations when deciding whether to discard data points with large standard deviations or not. No more than one point was dropped for each set of conditions and care was taken not to obscure or suggest trends that are not suggested by the data.

Table F.1: Normalised standard deviations at various assay conditions suggest possible outliers. The standard deviations of the GAPDH activity rates within triplicates were normalised over the wild-type rate for each reaction condition. Points with a standard deviation 20% the size of the wild-type rate are presented in red, while points with a standard deviation 30% the size of the wild-type rate are presented in red and underlined. The three tables - *I*, *II*, and *III* - represent the three biological repeats.

I

[IAA] in μM	*In vitro* inhibition				Prelytic inhibition			
	Reverse		Forward		Reverse		Forward	
	-DTT	+DTT	-DTT	+DTT	-DTT	+DTT	-DTT	+DTT
0	12.4101	8.40857	34.0731	7.17816	4.70395	31.6076	22.597	13.7408
25	19.1673	7.73177	17.174	16.0554	7.66804	20.0952	23.9782	25.9027
50	16.5403	19.1315	33.2751	10.7025	15.2707	12.4101	31.5026	23.9735
100	33.6728	18.0383	6.36614	9.29175	13.7571	7.34975	110.854	6.7447
200	9.61424	13.0122	23.9292	2.74594	12.0537	4.3784	9.97059	10.2783
400	6.58229	2.30321	24.7897	13.9837	3.28767	11.3295	19.4634	23.8377

II

[IAA] in μM	*In vitro* inhibition				Prelytic inhibition			
	Reverse		Forward		Reverse		Forward	
	-DTT	+DTT	-DTT	+DTT	-DTT	+DTT	-DTT	+DTT
0	5.04376	12.0088	29.7585	19.4022	8.81658	15.1665	17.6312	17.1311
18.75	11.1028	3.73498	15.4151	15.7761	19.3073	16.5295	45.1655	25.5319
37.5	10.8492	10.0457	7.19012	9.91708	10.6228	17.9829	20.4339	18.3619
75	14.5537	15.8214	5.09146	11.1913	5.37284	20.7764	21.1222	5.67081
150	23.4239	7.6292	69.7682	19.2824	15.0974	10.9037	12.1111	8.06279
300	7.33392	6.14992	9.3739	3.89385	9.00714	23.437	10.1833	3.2834

III

[IAA] in μM	*In vitro* inhibition				Prelytic inhibition			
	Reverse		Forward		Reverse		Forward	
	-DTT	+DTT	-DTT	+DTT	-DTT	+DTT	-DTT	+DTT
0	7.33822	16.6066	19.7802	20.5597	15.3876	18.0869	22.0054	27.5265
15.625	26.4731	15.0976	11.1805	29.8319	51.3415	3.56556	21.1085	12.5504
31.25	3.66181	13.6827	17.6355	17.3443	11.4009	9.42386	21.276	13.8178
62.5	5.82845	15.6641	11.5556	30.6097	29.4168	2.3191	31.0455	7.38692
125	4.75573	8.2952	7.30742	10.7895	13.4729	5.97999	14.0909	4.83815
250	10.2262	11.1424	20.9069	11.9336	14.9731	10.036	14.5758	17.0412

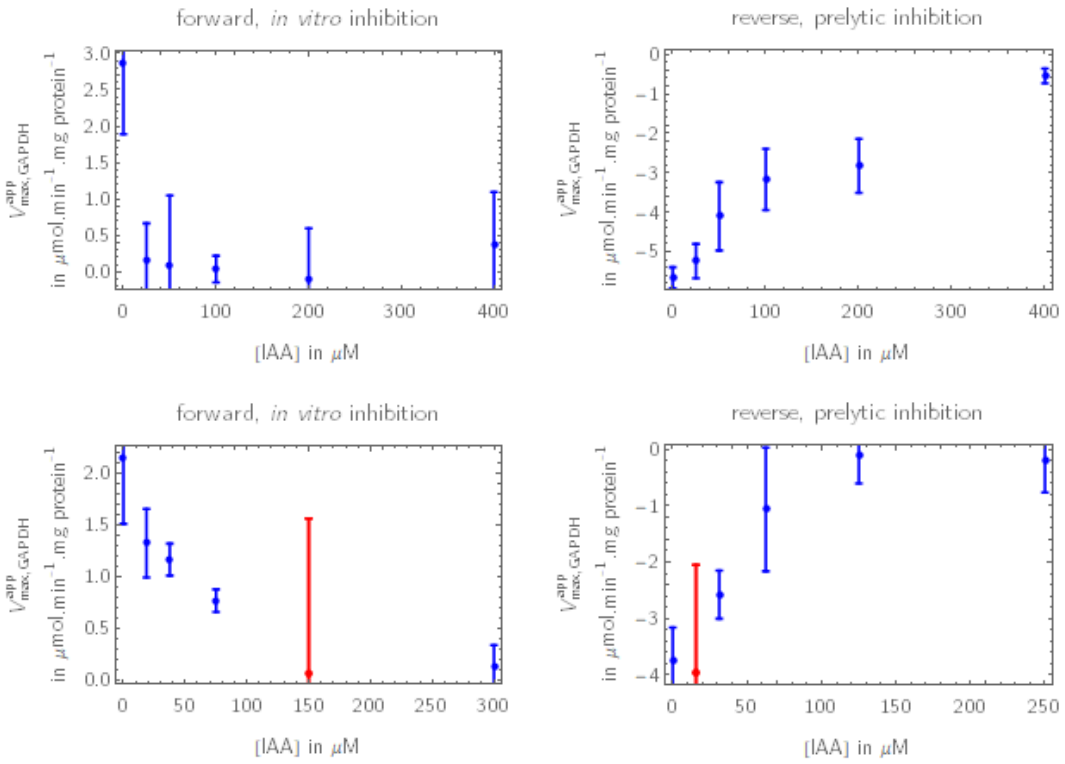

Figure F.1: Examples of inspected plots of GAPDH activity as a function of IAA concentration. These examples illustrate the approach taken to discarding or retaining data with large error. The red data points were dropped after inspection - no more than one point was dropped for each set of conditions (e.g. from the assay that was DTT-containing, measured in the forward direction, and from biological repeat *I*). *A* (see Table F.1A) showed standard deviations that were more than 30% of the wild-type activity, but the data point with the large error fell exactly into the trend created by the other points. *B* had a very clear trend encompassing all the data points and had standard deviations lower than 20% of the wild-type activity in all cases. The points dropped from *C* and *D* were dropped from their respective sets because they had standard deviations which were greater than 30% of their respective wild-type rates and they would suggest trends that might not be suggested in their absence.

Appendix G

Ethanol Detection: Calibration Curve Construction

Absorbance measurements (see Appendix H) were converted to ethanol concentrations using a calibration curve (Fig. G.1). The linearity of the experimental calibration curve and its consistency over multiple iterations with the same concentration range (complete data not shown) confirmed that ethanol concentration is predicted reliably by this method, though it does not strictly correspond to the Beer-Lambert equation. It was concluded that any under-detection of ethanol concentrations is uniform for a given set of experimental conditions. This would imply that possible under-sensitivity to sample ethanol concentrations would be compensated for by equivalent under-sensitivity to known standard ethanol concentrations.

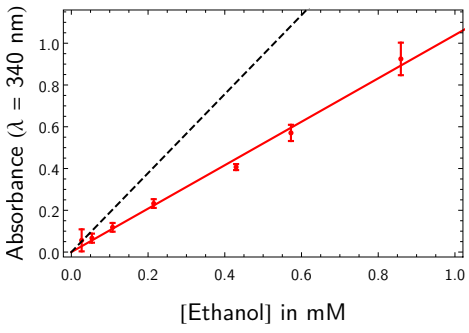

Figure G.1: An ethanol determination calibration curve shows high agreement with experimental data. End-point absorption values, at 340 nm, of ADH-catalysed conversion of ethanol and NAD^+ to pyruvate and NADH. The ADH is from *S. cerevisiae* . The red points indicate the means and standard error of triplicate reads of a set of standards. The solid red line represents the best-fitting linear function ($y = 1.04x$, $R^2 = 0.997$) on the experimental means. The dashed black line indicates the function which would be expected if the Beer-Lambert law were perfectly obeyed ($y = 1.9x$).

Appendix H

Ethanol Determination - Plateau Selection

Theoretically, only end-point reads should be required for ADH-dependent ethanol determination. The plateaus after full conversion, however, exhibited some instability which could cause misestimations if only single end points were read. Hence, absorbance reads at 340 nm were taken over time until a plateau was observed and then for another 30 minutes to an hour. A segment of this plateau which is sufficiently flat was then selected by inspection: the average absorbance reading over this segment was taken as the end point for the read (Fig. H.1). This segment was kept constant over all ethanol determinations within each technical replicate.

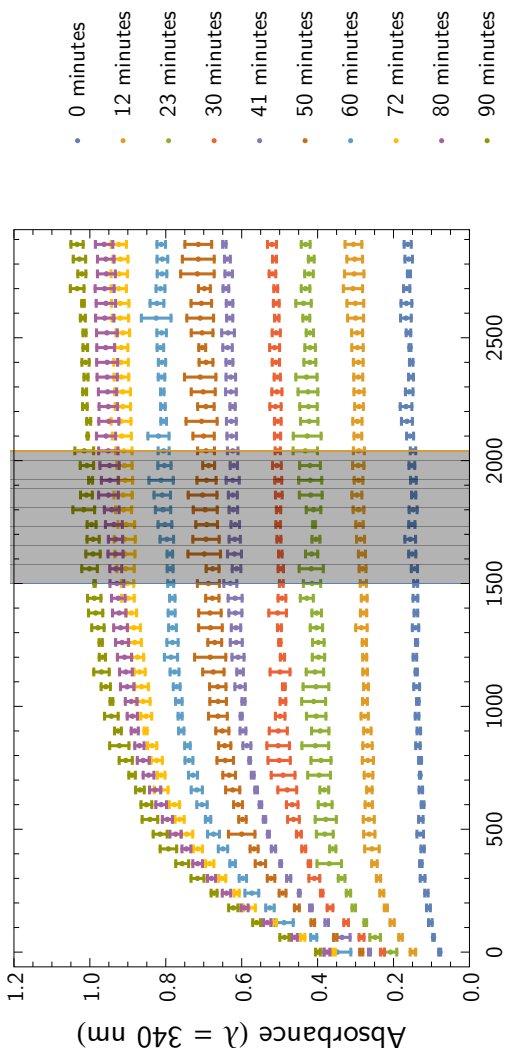

Figure H.1: Example of the selection of an end-point segment. This set of absorbance curves is from the time-course aliquots of a single incubation at one IAA concentration; in this case, the IAA concentration was 0 μM . By inspection, a suitable segment of 500 to 1000 seconds long was selected for each of the technical replicate. In this figure, a shaded section indicates the selected plateaus. The mean absorbance value across this segment was taken as the end-point value.

Appendix I

Glucose Detection: Calibration Curve Construction

The absorbance measurements that were used for glucose determination had very little error. This supports the validity of the concentrations determinations very stongly. In Fig. I.1*A*, one of these sets of absorbance data is presented. Figure I.1*B* shows the calibration curve that was used to convert absorbance readings into glucose concentrations. Though the gradient of the calibration curve does not correspond to the theoretical function according to the Beer-Lambert Law, multiple iterations of this curve (data not shown) consistently showed very similar gradients, confirming the method as a reproducible concentration determination assay.

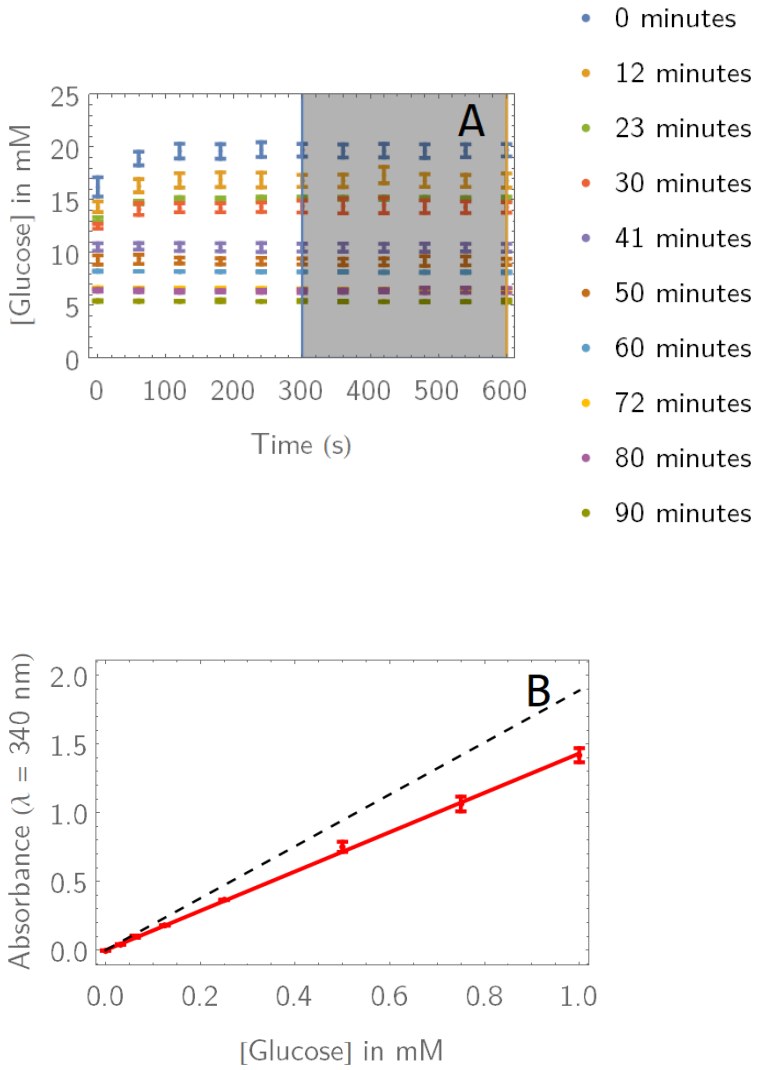

Figure I.1: Glucose determination. *A* shows an example of raw absorbance data as a function of time and the selection of a linear segment (shaded area) of which the average will be used as the end-point value. The time-course data in *A* come from yeast cells inhibited with 50 μM IAA. *B* is a comparison between a experimentally generated calibration curve ($y = 1.43x; R^2 = 0.9996$) and the theoretical curve according to the detection assay's stoichiometry and the Beer-Lambert law ($y = 1.89x$). The experimentally constructed curve has a different gradient than what was calculated using the extinction coefficient of NADH, the concentrations of glucose added (assuming full conversion of glucose), and the path length of 100 μL of liquid in a well of a Greiner F-bottom plate (specification sheet available here). The experimentally constructed calibration curves were consistent and had very little error in all cases, however, and are considered reliable.

Appendix J

Model Predictions: GAPDH Metabolite Changes

Fig. J.1 shows the time evolution of the model variables (metabolite concentrations) for the duration of the simulation. The simulation is the final simulation as we used it for the prediction of metabolic flux control, but at a IAA concentration of 0 μM. The ratio between the internal and external volumes is 1:50 and concentrations were adjusted accordingly.

This time evolution serves to show how the changes in external glucose and external ethanol concentrations were the products of changing internal metabolite concentrations. A peculiarity of the simulation appears to be the fact that the ethanol concentrations inside and outside the cell are the same. This can be understood in terms of the diffusion rate of ethanol across the yeast cell envelope being so free and quick that the trans-envelope ethanol concentration is constantly in equilibrium [127].

APPENDIX J. MODEL PREDICTIONS: GAPDH METABOLITE CHANGES

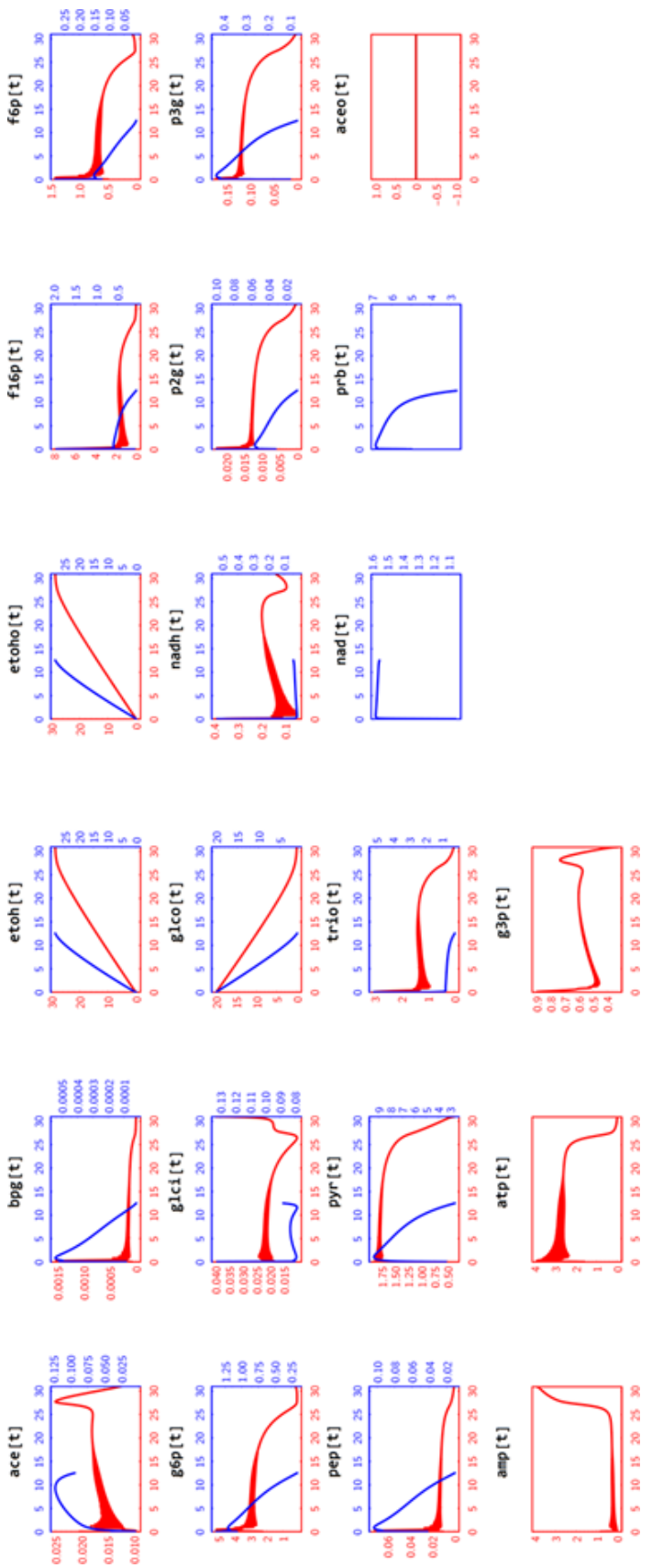

Figure J.1: Simulated change in metolite concentrations over time for both models. In both cases the glucose concentration was unfixed and set to 20 mM, while the ethanol concentration and external acetaldehyde concentration (in the case of 2) were unfixed and set to 0 mM. An external ethanol concentration and an ethanol export term were included, based on passive diffusion kinetics from [127]; the acetaldehyde efflux term was also removed from the Du Preez model, assuming that all acetaldehyde is converted to ethanol as is observed during the Crabtree effect [9]. All other parameters were kept the same. In blue, the right-hand y-axis ($mM.min^{-1}$) and the top x-axis (time in minutes) show the change in metabolite concentration as a function of time according to the Teusink model. In red, the left-hand y-axis ($mM.min^{-1}$) and the bottom x-axis (time in minutes) show the evolution of metabolite concentrations according to the Du Preez model: the Du Preez model shows transient oscillations that last for about the first fifteen minutes of the simulation (thickness of the red lines show the oscillation amplitudes. The metabolites tracked are the following: ethanol (etoh),external ethanol (etoho), fructose 1,6-bisphosphate (f16p), fructose 6-phosphate (f6p), glucose 6-phosphate (g6p), internal glucose (glci), external glucose (glco), nad, 2-phosphoglycerate (p2g), 3-phosphoglycerate (p3g), phosphoenol pyruvate (pep), pyruvate (pyr), and triose-phiosphates (trio). In the second to last row, the Teusink model (blue) is alone is its explicit expression of NAD^+ concentration (nad) and in the grouping of adenosine phosphates into a single term (prb). The Du Preez model, on the other hand, uniquely includes explicit variables for external acetaldehyde (aceo), adenosine monophosphate (amp), ATP (atp), and glycerol 3-phosphate (g3p).

Bibliography

[1] Teusink, B., Passarge, J., Reijenga, C.a., Eshalgado, E., van der Weijden, C.C., Schepper, M., Walsh, M., Bakker, B., van Dam, K., Westerhoff, H. and Snoep, J.: Can yeast glycolysis be understood in terms of in vitro kientics of the constitutent enzyme? Testing biochemnistry. *European Journal of Biochemnistry*, vol. 267, no. February, pp. 5313–5329, 2000. ISSN 00142956.

[2] Du Preez, F.B., Van Niekerk, D.D., Kooi, B., Rohwer, J.M. and Snoep, J.L.: From steady-state to synchronized yeast glycolytic oscillations I: Model construction. *FEBS Journal*, vol. 279, no. 2012, pp. 2810–2822, 2012.

[3] Van Eunen, K., Bouwman, J., Daran-Lapujade, P., Postmus, J., Canelas, A.B., Mensonides, F.I., Orij, R., Tuzun, I., Van Den Brink, J., Smits, G.J., Van Gulik, W.M., Brul, S., Heijnen, J.J., De Winde, J.H., Teixeira De Mattos, M.J., Kettner, C., Nielsen, J., Westerhoff, H.V. and Bakker, B.M.: Measuring enzyme activities under standardized in vivo-like conditions for systems biology. *FEBS Journal*, vol. 277, no. 3, pp. 749–760, 2010. ISSN 1742464X.

[4] Westerhoff, H.V. and Palsson, B.O.: The evolution of molecular biology into systems biology. *Nature Biotechnology*, vol. 22, no. 10, pp. 1249–1252, 2004. ISSN 10870156. arXiv:1408.1149.

[5] Snoep, J.L.: The Silicon Cell initiative: Working towards a detailed kinetic description at the cellular level. *Current Opinion in Biotechnology*, vol. 16, no. 3 SPEC. ISS., pp. 336–343, 2005. ISSN 09581669.

[6] Mathews, C.K., van Holde, K. and Ahern, K.G.: *Biochemistry*. 3rd edn. Addison Wesley Longman, San Francisco, 2000.

[7] Chance, B., Gafinkel, D., Higgens, J. and Hess, B.: Metabolic Control Mechanisms V. A Solution for the Equations Representing Interaction Between Glycolysis and Respiration in Ascites Tumor Cells. *Journal of Biological Chemistry*, vol. 235, no. 8, 1960.

[8] Heinrich, R., Rapoport, S. and Rapoport, T.: Metabolic regulation and mathematical models. *Progress in Biophysics and Molecular Biology*, vol. 32, pp. 1–82, jan 1978. ISSN 0079-6107.

[9] Piškur, J., Rozpędowska, E., Polakova, S., Merico, A. and Compagno, C.: How did Saccharomyces evolve to become a good brewer? *Trends in Genetics*, vol. 22, no. 4, pp. 183–186, apr 2006. ISSN 0168-9525.

[10] Penkler, G., Du Toit, F., Adams, W., Rautenbach, M., Palm, D.C., Van Niekerk, D.D. and Snoep, J.L.: Construction and validation of a detailed kinetic model of glycolysis in Plasmodium falciparum. *FEBS Journal*, vol. 282, no. 8, pp. 1481–1511, 2015. ISSN 17424658. 0510054.

[11] Bakker, B.M., Michels, P.A.M., Opperdoes, F.R. and Westerhoff, H.V.: Glycolysis in bloodstream form Trypanosoma brucei can be understood in terms of the kinetics of the glycolytic enzymes. *Journal of Biological Chemistry*, vol. 272, no. 6, pp. 3207–3215, 1997. ISSN 00219258. NIHMS150003.

[12] Cascante, M., Boros, L.G., Comin-Anduix, B., De Atauri, P., Centelles, J.J. and Lee, P.W.: Metabolic control analysis in drug discovery and disease. *Nature Biotechnology*, vol. 20, no. 3, pp. 243–249, 2002. ISSN 10870156.

[13] Snoep, J.L., Bruggeman, F., Olivier, B.G. and Westerhoff, H.V.: Towards building the silicon cell: A modular approach. *BioSystems*, vol. 83, no. 2-3 SPEC. ISS., pp. 207–216, 2006. ISSN 03032647.

[14] Bates, D. and Cosentino, C.: Validation and invalidation of systems biology models using robustness analysis. *IET Systems Biology*, vol. 5, no. 4, pp. 229–244, 2011. ISSN 1751-8849.

[15] Bruggeman, F.J. and Westerhoff, H.V.: The nature of systems biology. *Trends in Microbiology*, vol. 15, no. 1, pp. 45–50, 2007. ISSN 0966842X.

[16] Du Preez, F.B., Van Niekerk, D.D. and Snoep, J.L.: From steady-state to synchronized yeast glycolytic oscillations II: Model validation. *FEBS Journal*, vol. 279, no. 16, pp. 2823–2836, 2012. ISSN 1742464X.

[17] Nyman, E., Cedersund, G. and Strålfors, P.: Insulin signaling - mathematical modeling comes of age. *Trends in Endocrinology and Metabolism*, vol. 23, no. 3, pp. 107–115, 2012. ISSN 10432760.

[18] Anderson, J. and Papachristodoulou, A.: On validation and invalidation of biological models. *BMC Bioinformatics*, vol. 10, no. 132, 2009. ISSN 14712105.

[19] Hofmeyr, J.: Metabolic control analysis in a nutshell. In: *Proceedings of the 2nd International Conference on Systems Biology*, ii, pp. 291–300. 2001.

[20] Kholodenko, B.N. and Westerhoff, H.V.: Metabolic channelling and control of the flux. *FEBS Letters*, vol. 320, no. 1, pp. 71–74, 1993. ISSN 00145793.

[21] Webb, J.L.: Iodoacetate and Iodoacetamide. In: *Enzyme and Metabolic Inhibitors*, 1st edn, chap. I, pp. 1 – 270. Academic Press, New York, 1963.

[22] Poolman, B., Bosman, B., Kiers, J. and Konings, W.N.: Control of glycolysis by glyceraldehyde-3-phosphate dehydrogenase in Streptococcus cremoris and Streptococcus lactis. *Journal of Bacteriology*, vol. 169, no. 12, pp. 5887–5890, 1987. ISSN 00219193.

[23] Carneiro, A.S., Lameira, J. and Alves, C.N.: A theoretical study of the molecular mechanism of the GAPDH Trypanosoma cruzi enzyme involving iodoacetate inhibitor. *Chemical Physics Letters*, vol. 514, no. 4-6, pp. 336–340, 2011. ISSN 00092614.

[24] Liao, S.L., Ou, Y.C., Chang, C.Y., Chen, W.Y., Kuan, Y.H., Wang, W.Y., Pan, H.C. and Chen, C.J.: Diethylmaleate and iodoacetate in combination caused profound cell death in astrocytes. *Journal of Neurochemistry*, vol. 127, no. 2, pp. 271–282, 2013. ISSN 00223042.

[25] Moreno-Sánchez, R., Saavedra, E., Rodríguez-Enríquez, S. and Olín-Sandoval, V.: Metabolic Control Analysis: A tool for designing strategies to manipulate metabolic pathways. *Journal of Biomedicine and Biotechnology*, vol. 2008, no. 1, 2008. ISSN 11107243.

[26] Westerhoff, H.V., Kolodkin, A., Conradie, R., Wilkinson, S.J., Bruggeman, F.J., Krab, K., van Schuppen, J.H., Hardin, H., Bakker, B.M., Moné, M.J., Rybakova, K.N., Eijken, M., van Leeuwen, H.J. and Snoep, J.L.: Systems biology towards life in silico: Mathematics of the control of living cells. *Journal of Mathematical Biology*, vol. 58, no. 1-2, pp. 7–34, 2009. ISSN 03036812.

[27] Bakker, B.M., Krauth-Siegel, R.L., Clayton, C., Matthews, K., Girolami, M., Westerhoff, H.V., Michels, P.A., Breitling, R. and Barrett, M.P.: The silicon trypanosome. *Parasitology*, vol. 137, no. 9, pp. 1333–1341, 2010. ISSN 00311820.

[28] Aon, M. and Cortassa, S.: Systems Biology of the Fluxome. *Processes*, vol. 3, no. 3, pp. 607–618, 2015. ISSN 2227-9717.

[29] Fleischmann, R.D., Adams, M.D., White, O., Clayton, R.A., Kirkness, E.F., Kerlavage, A.R., Bult, C.J., Tomb, J.F., Dougherty, B.A., Merrick, J.M., McKenney, K., Sutton, G., FitzHugh, W., Fields, C., Gocayne, J.D., Scott, J., Shirley, R., Liu, L.I., Glodek, A., Kelley, J.M., Weidman, J.F., Phillips, C.A., Spriggs, T., Hedblom, E., Cotton, M.D., Utterback, T.R., Hanna, M.C., Nguyen, D.T., Saudek, D.M., Brandon, R.C., Fine, L.D., Fritchman, J.L., Fuhrmann, J.L., Geoghagen, N.S., Gnehm, C.L., McDonald, L.A., Small, K.V., Fraser, C.M., Smith, H.O. and Venter, J.C.: Whole-genome random sequencing and assembly of Haemophilus influenzae Rd. *Science*, vol. 269, no. 5223, pp. 496–512, 1995. ISSN 00368075. 20.

[30] Venter, J.C., Adams, M.D., Myers, E.W., Li, P.W., Mural, R.J., Sutton, G.G., Smith, H.O., Yandell, M., Evans, C.A., Holt, R.A., Gocayne, J.D., Amanatides, P., Ballew, R.M., Huson, D.H., Wortman, J.R., Zhang, Q., Kodira, C.D., Zheng, X.H., Chen, L., Skupski, M., Subramanian, G., Thomas, P.D., Zhang, J., Gabor Miklos, G.L., Nelson, C., Broder, S., Clark, A.G., Nadeau, J., McKusick, V.A., Zinder, N., Levine, A.J., Roberts, R.J., Simon, M., Slayman, C., Hunkapiller, M., Bolanos, R., Delcher, A., Dew, I., Fasulo, D., Flanigan, M., Florea, L., Halpern, A., Hannenhalli, S., Kravitz, S., Levy, S., Mobarry, C., Reinert, K., Remington, K., Abu-Threideh, J., Beasley, E., Biddick, K., Bonazzi, V., Brandon, R., Cargill, M., Chandramouliswaran, I., Charlab, R., Chaturvedi, K., Deng, Z., Di Francesco, V., Dunn, P., Eilbeck, K., Evangelista, C., Gabrielian, A.E., Gan, W., Ge, W., Gong, F., Gu, Z., Guan, P., Heiman, T.J., Higgins, M.E., Ji, R.R., Ke, Z., Ketchum, K.A., Lai, Z., Lei, Y., Li, Z., Li, J., Liang, Y., Lin, X., Lu, F., Merkulov, G.V., Milshina, N., Moore, H.M., Naik, A.K., Narayan, V.A., Neelam, B., Nusskern, D., Rusch, D.B., Salzberg, S., Shao, W., Shue, B., Sun, J., Wang, Z., Wang, A., Wang, X., Wang, J., Wei, M., Wides, R., Xiao, C., Yan, C., Yao, A., Ye, J., Zhan, M., Zhang, W., Zhang, H., Zhao, Q., Zheng, L., Zhong, F., Zhong, W., Zhu, S., Zhao, S., Gilbert, D., Baumhueter, S., Spier, G., Carter, C., Cravchik, A., Woodage, T., Ali, F., An, H., Awe, A., Baldwin, D.: The sequence of the human genome. *Science (New York, N.Y.)*, vol. 291, no. 5507, pp. 1304–51, feb 2001. ISSN 0036-8075.

[31] Uetz, P., Glot, L., Cagney, G., Mansfield, T.A., Judson, R.S., Knight, J.R., Lockshon, D., Narayan, V., Srinivasan, M., Pochart, P., Qureshi-Emlli, A., Li, Y., Godwin, B., Conover, D., Kalbfleisch, T., Vijayadamodar, G., Yang, M., Johnston, M., Fields, S. and Rothberg, J.M.: A comprehensive analysis of protein-protein interactions in Saccharomyces cerevisiae. *Nature*, vol. 403, no. 6770, pp. 623–627, 2000. ISSN 00280836. R49.

[32] Mendes, P.: Emerging bioinformatics for the metabolome. *Briefings in Bioinformatics*, vol. 3, no. 2, pp. 134–145, 2002.

[33] Pritchard, L. and Kell, D.B.: Schemes of flux control in a model of Saccharomyces cerevisiae glycolysis. *European Journal of Biochemistry*, vol. 269, no. 16, pp. 3894–3904, 2002. ISSN 00142956.

[34] Bakker, B.M., van Eunen, K., Jeneson, J.A., van Riel, N.A., Bruggeman, F.J. and Teusink, B.: Systems biology from micro-organisms to human metabolic diseases: the role of detailed kinetic models. *Biochemical Society Transactions*, vol. 38, no. 5, pp. 1294–1301, 2010. ISSN 0300-5127. NIHMS150003.

[35] Smallbone, K., Messiha, H.L., Carroll, K.M., Winder, C.L., Malys, N., Dunn, W.B., Murabito, E., Swainston, N., Dada, J.O., Hayes, N.W., Jameson, D., Broomhead, D.S., Weichart, D., Oliver, S.G., Gaskell, S.J., Mccarthy, J.E.G., Paton, N.W., Westerhoff, H.V., Kell, D.B. and Mendes, P.: A model of yeast glycolysis based on a consistent kinetic characterisation of all its enzymes. *FEBS Letters*, vol. 587, pp. 2832–2841, 2013.

[36] Westerhoff, H.V.: The silicon cell, not dead but live! *Metabolic Engineering*, vol. 3, no. 3, pp. 207–210, 2001. ISSN 10967176.

[37] Cvijovic, M., Almquist, J., Hagmar, J., Hohmann, S., Kaltenbach, H., Klipp, E., Krantz, M., Mendes, P., Nelander, S., Nielsen, J., Paganini, A., Przulj, N., Raue, A., Stelling, J., Stoma, S., Tobin, F., Wodke, J., Zecchina, R. and Jirstrand, M.: Bridging the gaps in systems biology. *Molecular and General Genomics*, vol. 289, no. 5, pp. 727–734, 2014.

[38] Wiley, H.S., Shvartsman, S.Y. and Lauffenburger, D.A.: Computational modeling of the EGF-receptor system: A paradigm for systems biology. *Trends in Cell Biology*, vol. 13, no. 1, pp. 43–50, 2003. ISSN 09628924.

[39] Morohashi, M., Winn, A.E., Borisuk, M.T., Bolouri, H., Doyle, J. and Kitano, H.: Robustness as a measure of plausibility in models of biochemical networks. *Journal of Theoretical Biology*, vol. 216, no. 1, pp. 19–30, 2002. ISSN 00225193.

[40] Liebermeister, W. and Klipp, E.: Bringing metabolic networks to life: Convenience rate law and thermodynamic constraints. *Theoretical Biology and Medical Modelling*, vol. 3, no. 41, 2006. ISSN 17424682.

[41] Rohwer, J., Hanekom, A., Crous, C., Snoep, J. and Hofmeyr, J.: Evaluation of a simplified generic bi-substrate rate equation for computational systems biology. *IEE Proceedings-Systems Biology*, vol. 153, no. 5, pp. 338–341, 2006.

[42] Hoops, S., Sahle, S., Gauges, R., Lee, C., Simus, N., Singhal, M., Xu, L., Mendes, P. and Kummer, U.: COPASI - A COmplex PAthway SImulator. *Bioinformatics*, vol. 22, no. 24, pp. 3067–3074, 2006.

[43] Albers, E., Larsson, C., Andlid, T., Walsh, M.C. and Gustafsson, L.: Effect of nutrient starvation on the cellular composition and metabolic capacity of Saccharomyces cerevisiae. *Applied and Environmental Microbiology*, vol. 73, no. 15, pp. 4839–4848, 2007. ISSN 00992240.

[44] Ellis, R.J.: TRENDS in Biochemical Sciences. *Duden*, vol. 26, no. 10, pp. 597–604, 2001. ISSN 0968-0004.

[45] Schilling, M., Pfeifer, A.C., Bohl, S. and Klingmüller, U.: Standardizing experimental protocols. *Current Opinion in Biotechnology*, vol. 19, no. 4, pp. 354–359, aug 2008. ISSN 0958-1669.

[46] García-Contreras, R., Vos, P., Westerhoff, H.V. and Boogerd, F.C.: Why in vivo may not equal in vitro - New effectors revealed by measurement of enzymatic activities under the same in vivo-like assay conditions. *FEBS Journal*, vol. 279, no. 22, pp. 4145–4159, 2012.

[47] Bruck, J., Liebermeister, W. and Klipp, E.: Exploring the effect of variable enzyme concentrations in a kinetic model of yeast glycolysis. *Genome informatics International Conference on Genome Informatics*, vol. 20, pp. 1–14, 2008. ISSN 0919-9454.

[48] Miller, A.K., Marsh, J., Reeve, A., Garny, A., Britten, R., Halstead, M., Cooper, J., Nickerson, D.P. and Nielsen, P.F.: An overview of the CellML API and its implementation. *BMC Bioinformatics*, vol. 11, no. 178, 2010. ISSN 14712105.

[49] Hucka, M., Finney, A., Bornstein, B., Keating, S., Shapiro, J., Matthews, J., Kovitz, B., Schilstra, M., Funahashi, A., Doyle, J. and Kitano, H.: Evolving a lingua franca and associated software infrastructure for computational systems biology - the Systems Biology Markup Language (SBML) project. *Systems Biology*, vol. 1, no. 1, pp. 41–53, 2004.

[50] Le Novere, N., Bornstein, B., Broicher, A., Courtot, M., Donizelli, M., Dharuri, H., Li, L., Sauro, H., Schilstra, M., Shapiro, B., Snoep, J.L. and Hucka, M.: BioModels Database: a free, centralized database of curated, published, quantitative kinetic models of biochemical and cellular systems. *Nucleic Acids Research*, vol. 34, no. 90001, pp. D689–D691, jan 2006. ISSN 0305-1048.

[51] Snoep, J.L. and Olivier, B.G.: JWS Online Cellular Systems Modelling and Microbiology. *Microbiology*, vol. 149, no. 11, pp. 3045–3047, 2003.

[52] Wiebe, M.G., Rintala, E., Tamminen, A., Simolin, H., Salusjärvi, L., Toivari, M., Kokkonen, J.T., Kiuru, J., Ketola, R.A., Jouhten, P., Huuskonen, A., Maaheimo, H., Ruohonen, L. and Penttilä, M.: Central carbon metabolism of Saccharomyces cerevisiae in anaerobic, oxygen-limited and fully aerobic steady-state conditions and following a shift to anaerobic conditions. *FEMS Yeast Research*, vol. 8, no. 1, pp. 140–154, feb 2008. ISSN 15671356.

[53] Herrgård, M.J., Swainston, N., Dobson, P., Dunn, W.B., Arga, K.Y., Arvas, M., Blüthgen, N., Borger, S., Costenoble, R., Heinemann, M., Hucka, M., Le Novère, N., Li, P., Liebermeister, W., Mo, M.L., Oliveira, A.P., Petranovic, D., Pettifer, S., Simeonidis, E., Smallbone, K., Spasić, I., Weichart, D., Brent, R., Broomhead, D.S., Westerhoff, H.V., Kirdar, B., Penttilä, M., Klipp, E., Palsson, B.O., Sauer, U., Oliver, S.G., Mendes, P., Nielsen, J. and Kell: A consensus yeast metabolic network reconstruction obtained from a community approach to systems biology. *Nature Biotechnology*, vol. 26, no. 10, pp. 1155–1160, 2008.

[54] Oreskes, N., Shrader-frechette, K. and Belitz, K.: Verification, validation, and confirmation of numerical models in the earth sciences. *Science*, vol. 263, no. 5147, pp. 641–646, 1994.

[55] Kolch, W., Halasz, M., Granovskaya, M. and Kholodenko, B.N.: The dynamic control of signal transduction networks in cancer cells. *Nature Reviews Cancer*, vol. 15, no. 9, pp. 515–527, sep 2015. ISSN 1474-175X.

[56] Loos, B., Du Toit, A. and Hofmeyr, J.H.S.: Defining and measuring autophagosome flux - Concept and reality. *Autophagy*, vol. 10, no. 11, pp. 2087–2096, 2014. ISSN 15548635.

[57] Locasale, J.W.: New concepts in feedback regulation of glucose metabolism. *Current Opinion in Systems Biology*, vol. 8, pp. 32–38, 2017. ISSN 24523100.

[58] Wang, L., Birol, I. and Hatzimanikatis, V.: Metabolic control analysis under uncertainty: Framework development and case studies. *Biophysical Journal*, vol. 87, no. 6, pp. 3750–3763, 2004. ISSN 00063495.

[59] Bakker, B.M., Michels, P.a.M., Opperdoes, F., Westerhoff, H.V. and Opperdoes, F.R.: What Controls Glycolysis in Bloodstream Form Trypanosoma brucei? *The Journal of biological chemistry*, vol. 274, no. 21, pp. 14551–14559, 1999.

[60] Albert, M.A., Haanstra, J.R., Hannaert, V., Van Roy, J., Opperdoes, F.R., Bakker, B.M. and Michels, P.A.: Experimental and in silico analyses of glycolytic flux control in bloodstream form Trypanosoma

brucei. *Journal of Biological Chemistry*, vol. 280, no. 31, pp. 28306–28315, 2005. ISSN 00219258.

[61] Haanstra, J.R., van Tuijl, A., Kessler, P., Reijnders, W., Michels, P.A.M., Westerhoff, H.V., Parsons, M. and Bakker, B.M.: Compartmentation prevents a lethal turbo-explosion of glycolysis in trypanosomes. *Proceedings of the National Academy of Sciences*, vol. 105, no. 46, pp. 17718–17723, 2008. ISSN 0027-8424.

[62] Pattanaik, P., Raman, J. and Balaram, H.: Perspectives in Drug Design Against Malaria. *Current Topics in Medicinal Chemistry*, vol. 2, no. 5, pp. 483–505, may 2002. ISSN 15680266.

[63] Sherman, I.W.: Biochemistry of Plasmodium (Malarial Parasites). *Microbiological reviews*, vol. 43, no. 4, pp. 453–495, 1979. ISSN 0146-0749.

[64] Van Niekerk, D.D., Penkler, G.P., Du Toit, F. and Snoep, J.L.: Targeting glycolysis in the malaria parasite Plasmodium falciparum. *FEBS Journal*, vol. 283, no. 4, pp. 634–646, 2016. ISSN 17424658.

[65] Hynne, F., Danø, S. and Sørensen, P.G.: *Full-scale model of glycolysis in Saccharomyces cerevisiae*, vol. 94. 2001. ISBN 0301-4622.

[66] Richard, P.: The rhythm of yeast. *FEMS Microbiology Reviews*, vol. 27, no. 4, pp. 547–557, oct 2003. ISSN 1574-6976.

[67] Gustavsson, A.K., Van Niekerk, D.D., Adiels, C.B., Du Preez, F.B., Goksör, M. and Snoep, J.L.: Sustained glycolytic oscillations in individual isolated yeast cells. *FEBS Journal*, vol. 279, no. 16, pp. 2837–2847, 2012. ISSN 1742464X.

[68] Clifton, D., Weinstock, S.B. and Fraenkel, D.G.: Glycolysis mutants in Saccharomyces cerevisiae. *Genetics*, vol. 88, no. 1, pp. 1–11, 1978. ISSN 00166731.

[69] Kascer, H. and Burns, J.: Rate control of biological processes. *Symposia of the Society for Experimental Biology*, vol. 27, pp. 65–104, 1973.

[70] Heinrich, R. and Rapoport, T.A.: A Linear Steady-State Treatment of Enzymatic Chains. General Properties, Control and Effector Strength. *European Journal of Biochemistry*, vol. 42, no. 1, pp. 89–95, feb 1974. ISSN 0014-2956.

[71] Reder, C.: Metabolic control theory: A structural approach. *Journal of Theoretical Biology*, vol. 135, no. 2, pp. 175–201, 1988. ISSN 10958541. arXiv:1011.1669v3.

[72] Visser, D. and Heijnen, J.J.: The mathematics of Metabolic Control Analysis revisited. *Metabolic Engineering*, vol. 4, no. 2, pp. 114–123, 2002. ISSN 10967176.

[73] Brand, M.D.: Top down metabolic control analysis. *Journal of Theoretical Biology*, vol. 182, no. 3, pp. 351–360, 1996. ISSN 00225193.

[74] Groen, A.K., Wanders, R.J., Westerhoff, H.V., van der Meer, R. and Tager, J.M.: Quantification of the contribution of various steps to the control of mitochondrial respiration. *The Journal of biological chemistry*, vol. 257, no. 6, pp. 2754–7, mar 1982. ISSN 0021-9258.

[75] Haanstra, J.R. and Bakker, B.M.: Drug target identification through systems biology. *Drug Discovery Today: Technologies*, vol. 15, no. 259, pp. 17–22, 2015. ISSN 17406749.

[76] Brand, M.D., D'Alessandri, L., Reis, H.M. and Hafner, R.P.: Stimulation of the electron transport chain in mitochondria isolated from rats treated with mannoheptulose or glucagon. *Archives of Biochemistry and Biophysics*, vol. 283, no. 2, pp. 278–284, dec 1990. ISSN 0003-9861.

[77] Brand, M.D., Couture, P., Else, P.L., Withers, K.W. and Hulbert, A.J.: Evolution of Energy Metabolism. *Biochemical Journal*, vol. 1991, no. 275, pp. 81–86, 1991.

[78] Brand, M.D., Chien, L.-F. and Rolfe, D.F.S.: Control of oxidative phosphorylation in liver mitochondria and hepatocytes. *Biochemical Society Transactions*, vol. 21, no. 3, pp. 757–762, aug 1993. ISSN 0300-5127.

[79] Bakker, B.M., Assmus, H.E., Bruggeman, F., Haanstra, J.R., Klipp, E. and Westerhoff, H.: Network-Based Selectivity of Antiparasitic Inhibitors. *Molecular Biology Reports*, vol. 29, no. 1/2, pp. 1–5, 2002. ISSN 03014851.

[80] Haanstra, J.R., Gerding, A., Dolga, A.M., Sorgdrager, F.J., Buist-Homan, M., Du Toit, F., Faber, K.N., Holzhütter, H.G., Szöör, B., Matthews, K.R., Snoep, J.L., Westerhoff, H.V. and Bakker, B.M.: Targeting pathogen metabolism without collateral damage to the host. *Scientific Reports*, vol. 7, no. August 2016, pp. 1–15, 2017. ISSN 20452322.

[81] Penkler, G.P.: *A kinetic model of glucose catabolism in Plasmodium falciparum*. Ph.D., Stellenbosch University, 2013.

[82] Van Heerden, J.H., Wortel, M.T., Bruggeman, F.J., Heijnen, J.J., Bollen, Y.J., Planqué, R., Hulshof, J., O'Toole, T.G., Wahl, S.A.

and Teusink, B.: Lost in transition: Start-up of glycolysis yields subpopulations of nongrowing cells. *Science*, vol. 343, no. 6174, 2014. ISSN 10959203.

[83] Boren, J., Montoya, A.R., de Atauri, P., Comin-Anduix, B., Cortes, A., Centelles, J.J., Frederiks, W.M., Van Noorden, C.J.F. and Cascante, M.: Metabolic control analysis aimed at the ribose synthesis pathways of tumor cells: a new strategy for antitumor drug development. *Molecular biology reports*, vol. 29, no. 1-2, pp. 7–12, 2002. ISSN 0301-4851.

[84] Frederiks, W.M., Vizan, P., Bosch, K.S., Vreeling-Sindelárová, H., Boren, J. and Cascante, M.: Elevated activity of the oxidative and non-oxidative pentose phosphate pathway in (pre)neoplastic lesions in rat liver. *International Journal of Experimental Pathology*, vol. 89, no. 4, pp. 232–240, apr 2008. ISSN 09599673.

[85] Ovádi, J. and Srere, P.A.: Metabolic consequences of enzyme interactions. *Cell Biochemistry and Function*, vol. 14, no. 4, pp. 249–258, dec 1996. ISSN 02636484.

[86] Shestov, A.A., Liu, X., Ser, Z., Cluntun, A.A., Hung, Y.P., Huang, L., Kim, D., Le, A., Yellen, G., Albeck, J.G. and Locasale, J.W.: Quantitative determinants of aerobic glycolysis identify flux through the enzyme GAPDH as a limiting step. *eLife*, vol. 3, no. July2014, pp. 1–18, 2014. ISSN 2050084X.

[87] Warburg, O., Wind, F. and Negelein, E.: THE METABOLISM OF TUMORS IN THE BODY. *The Journal of general physiology*, vol. 8, no. 6, pp. 519–30, mar 1927. ISSN 0022-1295.

[88] Locasale, J.W. and Cantley, L.C.: Metabolic Flux and the Regulation of Mammalian Cell Growth. *Cell Metabolism*, vol. 14, no. 4, pp. 443–451, oct 2011. ISSN 1550-4131.

[89] Martyniuk, C.J., Fang, B., Koomen, J.M., Gavin, T., Zhang, L., Barber, D.S. and Lopachin, R.M.: Molecular mechanism of glyceraldehyde-3-phosphate dehydrogenase inactivation by ??,??-unsaturated carbonyl derivatives. *Chemical Research in Toxicology*, vol. 24, no. 12, pp. 2302–2311, 2011. ISSN 0893228X.

[90] Marino, S.M. and Gladyshev, V.N.: Cysteine Function Governs Its Conservation and Degeneration and Restricts Its Utilization on Protein Surfaces. *Journal of Molecular Biology*, vol. 404, no. 5, pp. 902–916, 2010. ISSN 00222836. NIHMS150003.

[91] Go, Y.M., Chandler, J.D. and Jones, D.P.: The cysteine proteome. *Free Radical Biology and Medicine*, vol. 84, pp. 227–245, 2015. ISSN 18734596.

[92] Winther, J.R. and Thorpe, C.: Quantification of thiols and disulfides. *Biochimica et Biophysica Acta (BBA) - General Subjects*, vol. 1840, no. 2, pp. 838–846, feb 2014. ISSN 0304-4165.

[93] Schmidt, M.M.: Differential effects of iodoacetamide and iodoacetate on glycolysis and glutathione metabolism of cultured astrocytes. *Frontiers in Neuroenergetics*, vol. 1, no. March, pp. 1–10, 2009. ISSN 16626427.

[94] Thompson, J.: Lactose metabolism in Streptococcus lactis: Phosphorylation of galactose and glucose moieties in vivo. *Journal of Bacteriology*, vol. 140, no. 3, pp. 774–785, 1979. ISSN 00219193.

[95] Sabri, M.I. and Ochs, S.: Inhibition of glyceraldehyde-3-phosphate dehydrogenase in mammalian nerve by iodoacetic acid. *Journal of Neurochemistry*, vol. 18, no. 8, pp. 1509–1514, aug 1971. ISSN 0022-3042.

[96] Zollner, H.: *Handbook of enzyme inhibitors*. VCH, 1989. ISBN 3527269940.

[97] Wong, H.L. and Liebler, D.C.: Mitochondrial Protein Targets of Thiol-Reactive Electrophiles. *Chemical Research in Toxicology*, pp. 796–804, 2008.

[98] Jones, J.G., Otieno, S., Barnard, E.A. and Bhargava, A.K.: Essential and Nonessential Thiols of Yeast Hexokinase. Reactions with Iodoacetate and Iodoacetamide. *Biochemistry*, vol. 14, no. 11, pp. 2396–2403, 1975. ISSN 15204995.

[99] Whitehead, E.P. and Rabin, B.R.: The thiol groups of yeast alcohol dehydrogenase. *The Biochemical journal*, vol. 90, no. 3, pp. 532–9, 1964. ISSN 0264-6021.

[100] Corcoran, B.M., Stanton, C., Fitzgerald, G.F. and Ross, R.P.: Survival of Probiotic Lactobacilli in Acidic Environments Is Enhanced.pdf. *Applied and Environmental Microbiology*, vol. 71, no. 6, pp. 3060–3067, 2005.

[101] Campbell-Burk, S.L., Shulman, R.G. and Jones, K.A.: 31P NMR Saturation-Transfer Measurements in Saccharomyces cerevisiae: Characterization of Phosphate Exchange Reactions by Iodoacetate and Antimycin A Inhibition. *Biochemistry*, vol. 26, no. 23, pp. 7483–7492, 1987. ISSN 15204995.

[102] Hansen, R.E. and Winther, J.R.: An introduction to methods for analyzing thiols and disulfides : Reactions , reagents , and practical considerations. *Analytical Biochemistry*, vol. 394, no. 2, pp. 147–158, 2009. ISSN 0003-2697.

[103] Aldous, B.Y.J.G.: THE EFFECT OF pH UPON THE TOXICITY OF IODOACETIC ACID TO YEAST CELLS. *Journal of Biological Chemistry*, vol. 176, no. 1, pp. 83–89, 1948.

[104] Even, S., Garrigues, C., Loubiere, P., Lindley, N.D. and Cocaign-Bousquet, M.: Pyruvate metabolism in Lactococcus lactis is dependent upon glyceraldehyde-3-phosphate dehydrogenase activity. *Metabolic engineering*, vol. 1, no. 3, pp. 198–205, 1999. ISSN 1096-7176.

[105] Brodie, A.E. and Reed, D.J.: Reversible oxidation of glyceraldehyde 3-phosphate dehydrogenase thiols in human lung carcinoma cells by hydrogen peroxide. *Biochemical and Biophysical Research Communications*, vol. 148, no. 1, pp. 120–125, 1987. ISSN 10902104.

[106] Cleland, W.W.: Dithiothreitol, a New Protective Reagent for SH Groups. *Biochemistry*, vol. 3, no. 4, pp. 480–482, 1964. ISSN 15204995.

[107] Le Moan, N., Clement, G., Le Maout, S., Tacnet, F. and Toledano, M.B.: The Saccharomyces cerevisiae proteome of oxidized protein thiols: Contrasted functions for the thioredoxin and glutathione pathways. *Journal of Biological Chemistry*, vol. 281, no. 15, pp. 10420–10430, 2006. ISSN 00219258.

[108] Jones, D.P.: Redox sensing: Orthogonal control in cell cycle and apoptosis signalling. *Journal of Internal Medicine*, vol. 268, no. 5, pp. 432–448, 2010. ISSN 09546820.

[109] Go, Y.M. and Jones, D.P.: The redox proteome. *Journal of Biological Chemistry*, vol. 288, no. 37, pp. 26512–26520, 2013. ISSN 00219258.

[110] Segal, H. and Boyer, P.: The role of sylfhydryl groups in the activity of D-glyceraldehyde 3-phosphate dehydrogenase. *Journal of Biological Chemistry*, vol. 1953, no. 204, pp. 25 – 281, 1953.

[111] Wolf, J., Passarge, J., Somsen, O.J.G., Snoep, J.L., Heinrich, R. and Westerhoff, H.V.: Transduction of Intracellular and Intercellular Dynamics in Yeast Glycolytic Oscillations. *Biophysical Journal*, vol. 78, no. 3, pp. 1145–53, 2000.

[112] Rüegg, U.T. and Rudinger, J.: [10] Reductive cleavage of cystine disulfides with tributylphosphine. *Methods in Enzymology*, vol. 47, pp. 111–116, jan 1977. ISSN 0076-6879.

[113] Bakker, B.M., Westerhoff, H.V. and Michels, P.A.: Regulation and control of compartmentalized glycolysis in bloodstream form Trypanosoma brucei. *Journal of bioenergetics and biomembranes*, vol. 27, no. 5, pp. 513–25, oct 1995. ISSN 0145-479X.

[114] Bergmeyer, H.U.: *Methods of enzymatic analysis. Volume 2.* Academic Press, 1974. ISBN 9780120913022.

[115] Ogawa, Z., Kanashima, M. and Nishioka, H.: Improvement of the quantitative method for glucose determination using hexokinase and glucose 6-phosphate dehydrogenase. *Clinical Chemistry and Laboratory Medicine*, vol. 39, no. 5, pp. 396–400, 2001. ISSN 14346621.

[116] Bradford, M.M.: A rapid and sensitive method for the quantitation of microgram quantities of protein utilizing the principle of protein-dye binding. *Analytical Biochemistry*, vol. 72, no. 1-2, pp. 248–254, 1976. ISSN 0003-2697. arXiv:1011.1669v3.

[117] Ernst, O. and Zor, T.: Linearization of the Bradford Assay. *Journal of Visualized Experiments*, vol. 38, no. 1918, pp. 1–6, 2010. ISSN 1940-087X.

[118] Van Hoek, P., Van Dijken, J.P. and Pronk, J.T.: Effect of Specific Growth Rate on Fermentative Capacity of Baker ' s Yeast. *Applied and Environmental Microbiology*, vol. 64, no. 11, pp. 4226–4233, 1998.

[119] Byers, L.D.: Glyceraldehyde 3-Phosphate Dehydrogenase from Yeast. In: *Methods in Enzymology*, vol. 89, pp. 326–335. Academic Press, 1982. ISBN 0121819892.

[120] Ferdinand, W.: The isolation and specific activity of rabbit-muscle glyceraldehyde phosphate dehydrogenase. *The Biochemical journal*, vol. 92, no. 1957, pp. 578–585, 1964. ISSN 02646021.

[121] Leichert, L.I., Gehrke, F., Gudiseva, H.V., Blackwell, T., Ilbert, M., Walker, A.K., Strahler, J.R., Andrews, P.C. and Jakob, U.: Quantifying changes in the thiol redox proteome upon oxidative stress in vivo. *Proceedings of the National Academy of Sciences*, vol. 105, no. 24, pp. 8197–8202, 2008. ISSN 0027-8424.

[122] Ziegler, D.M.: Role of Reversible Oxidation-Reduction of Enzyme Thiols-Disulfides in Metabolic Regulation. *Annual Review of Biochemistry*, vol. 54, no. 1, pp. 305–329, 1985.

[123] Lopes De Almeida, J.P. and Saldanha, C.: Dithiothreitol revisited in red cells: A new head for an old hat. *Clinical Hemorheology and Microcirculation*, vol. 46, no. 1, pp. 51–56, 2010. ISSN 13860291.

[124] Strelow, J.M.: A Perspective on the Kinetics of Covalent and Irreversible Inhibition. *SLAS DISCOVERY*, vol. 22, no. 1, pp. 3–20, jan 2017. ISSN 2472-5552.

[125] Bieth, J.G.: [5] Theoretical and practical aspects of proteinase inhibition kinetics. *Methods in Enzymology*, vol. 248, pp. 59–84, jan 1995. ISSN 0076-6879.

[126] Byers, L.D., She, H.S. and Alayoff, A.: Interaction of Phosphate Analogues with Glyceraldehyde-3-phosphate Dehydrogenase. *Biochemistry*, vol. 18, no. 12, pp. 2471–2480, 1979. ISSN 15204995.

[127] Guijarro, J.M. and Lagunas, R.: Saccharomyces cerevisiae does not accumulate ethanol against a concentration gradient. *Journal of Bacteriology*, vol. 160, no. 3, pp. 874–878, 1984. ISSN 00219193.

[128] Fell, D.A.: *Understanding the Control of Metabolism*. Portland Press Limited, London, UK, 1997.

[129] Kaupp, G.: Mechanochemistry : the varied applications of mechanical bond-breaking. *Royal Society for Chemistry*, vol. 11, no. 3, pp. 388 – 403, 2009.

[130] Davies, S. and Brindle, K.: Effects of Overexpression of Phosphofructokinase on Glycolysis in the Yeast Saccharomyces cerevisiaet of. *Biochemistry*, vol. 31, pp. 4729–4735, 1992.

[131] Heinrich, R., Holzhütter, H.G. and Schuster, S.: A theoretical approach to the evolution and structural enzymatic networks; Lnear enzymatic chains, branched pathways and glycolysis of erythrocytes. *Bulletin of Mathematical Biology*, vol. 49, no. 5, pp. 539 – 595, 1987.

[132] Thevelein, M. and Hohmann, S.: Trehalose synthase: guard to the gate of glycolysis in yeast ? *Science*, vol. 95, no. 4, pp. 3–10, 1995.

[133] Schuster, R. and Holzhütter, H.G.: Use of Mathematical Models for Predicting the Metabolic Effect of Large-Scale Enzyme Activity Alterations: Application to Enzyme Deficiencies of Red Blood Cells. *European Journal of Biochemistry*, vol. 229, no. 2, pp. 403–418, 1995. ISSN 14321033.